Universidad de Valladolid

PROGRAMA DE DOCTORADO EN FÍSICAS

TESIS DOCTORAL:

Formación de Defectos Topológicos en la Transición de Fase de Manganitas Hexagonales

Presentada por

Marcos Tello Fraile

para optar al grado de
Doctor/a por la Universidad de Valladolid

Dirigida por:
Manuel Donaire del Yerro
Luis Miguel Nieto Calzada

Formation of Topological Defects in a Phase Transition of Hexagonal Manganites

Marcos Tello-Fraile

February 15, 2022

Acknowledgments

I would like to start by thanking my supervisor Manuel Donaire for his support and teaching during all my PhD studies. I am deeply grateful for his helpful comments and the enlightening discussions with him. I would also like to acknowledge Luismi for his help and guidance throughout these years. Many thanks also to all the people in the department of Física Atómica, Teórica y Óptica of the University of Valladolid. Specially to my peers: César, Lucía, Julio, Carlos and Sergio. I am grateful to professor Andrés Cano for his collaboration on the publication of the paper included in this thesis. I also appreciate his hospitality during my stay in the Institute Néel in Grenoble, as well as the kindness of all the people at the Institute.

This work could not have been done without the support of my friends and family. Many thanks to my parents and to all the friends of the Chaminade, the Scouts, the Physics Faculty of the Complutense University... You are too many to name all of you, but you know who you are. Thank you very much. Finally, I would like to specially thank three people who have helped me in the final stages of this journey: Eva, Raquel, Jordi, I am very grateful to you.

This work has been financially supported by the European Social Fund, the Operational Programme of Junta de Castilla y León, and the regional Ministry of Education. The simulations to obtain the results of this thesis have been performed thanks to the strong performance computing resources of the Castilla y León Supercomputing Center (SCAYLE), financed by the European Regional Development Fund (ERDF).

Contents

Introduction 9

Introducción 15

I State of the art 21

1 Phase transitions. Phase transitions of the second kind and criticality. 23

2 Topological defects 32

3 Kibble-Zurek mechanism 36

4 Hexagonal manganites 45

II Thermal vortices in Hexagonal Manganites 49

5 The model 55

5.1 Correlation lengths and relaxation times in the mean-field linear approximation 59

6 Accounting for thermal effects 61

6.1 Thermal fluctuations and renormalization of the mass term . . 61
6.2 Cooling quench 70

7 Results **75**
7.1 Technical details of the simulations 76
7.2 Ultra-fast quenches 79
7.2.1 Vortex formation at weak-anisotropy 79
7.2.2 Vortex formation at strong-anisotropy 86
7.2.3 Vortex network evolution 88
7.3 Finite quenches 88
7.3.1 Quenches varying the temperature of the Langevin term 88
7.3.2 Quenches varying the bare mass term of the theory . . 94

III Code scripts for numeric simulations **99**

8 Boundary conditions **104**

9 Step functions **110**

10 Initial conditions **119**

11 Observables **126**
11.1 Counting vortices 126
11.2 Correlation length. Power spectrum 140
11.3 Mean-field relaxation time and correlation length 141

12 Main function **143**

Comments and conclusions **151**

Bibliography **157**

Introduction

Topological defects are solutions of a field theory which cannot decay into a less energetic –more fundamental– solution due to topological restrictions. Some examples of topological defects are domain walls, vortices and monopoles. The importance of topological defects in physics lies on the fact that they are the relics of a phase transition. Thus, from the study of the network of topological defects left behind a phase transition, we are able to gain some insight about the underlying theory.

The emergence of topological defects as a consequence of phase transitions is described by the Kibble-Zurek mechanism. It was first introduced by Kibble [1] in the seventies in the context of high energies physics. Kibble argues that phase transitions must have occurred in the early universe. This is a natural consequence from the fact that the universe has been cooling since the Big Bang and the assumption that the unification theories of the standard model are correct. As a result of these early phase transitions, topological defects associated to them must have formed.

Later in the nineties, Zurek proposed to study topological defects in condensed-matter systems as an analogy for cosmic defects created in the primordial universe [2]. The advantages of topological defects in condensed-matter systems –such as vortices in liquid helium, ferromagnetic domains, disclination lines in liquid crystals...– over the defects created in cosmolog-

ical backgrounds is that the formers are accessible in the lab. Zurek also completed the argument of Kibble to take into account out-of-equilibrium phenomena during phase transitions of the second kind, which play a crucial role on the formation of topological defects. The complete Kibble-Zurek mechanism predicts a relationship between the spatial density of topological defects and the critical exponents of the theory. These critical exponents are universal, in the sense that they only depend on the symmetries of the theory. This is a consequence of the critical behaviour of the system at the transition point. However, there is yet one more reason to justify that the properties of a phase transition are universal for theories with the same symmetries. The underlying mechanism which allows the formation of topological defects is the spontaneous symmetry breaking which occurs during the phase transition [3]. Therefore, the nature of topological defects depend on the symmetries of the original theory and how they are broken.

All in all, we can relate theories from different contexts if they belong to the same universality class. Since the seminal Zurek's article, many experiments have been carried out in condensed-matter systems. The aim of these experiments has been twofold. First, experiments are performed to test the Kibble-Zurek mechanism. Secondly, they are used to investigate the physics of inaccessible high-energy systems through condensed-matter analogues. Hexagonal manganites are one of such systems on which experiments have been performed. They are multiferroic materials with very rich phenomenology. Their most remarkable feature is that the symmetry of the theory is broken in a discrete way when they undergo a structural phase transition.

In this thesis, we build an effective model for a two-components scalar field which reproduces the physics of the hexagonal manganites and perform

numerical simulations in different regimes. The main objectives of this work are the following:

- To discuss the usual prescription to model thermal fluctuations through a stochastic term in the equations of motion. This customary approach presents some problems –namely, the possible double-counting of thermal effects. Indeed, the temperature appears explicitly in two different terms in the Lagrangian of the theory: in the amplitude of the thermal stochastic force and also as a linear parameter in the mass term coefficient. We present an alternative approach to include thermal fluctuations in order to overcome this problem. In this new approach, the temperature only appears explicitly in the amplitude of the thermal noise term, but not in the coefficient of the mass term. Thus, we let the mass term be effectively renormalized by the fluctuations of the field due to thermal effects rather than force it to change following an external imposition.

- To analyse in detail the process of vortex formation after a thermic second-order phase transition with global symmetry. We identify some relevant observables and distinguish three different dynamical regimes, each with a characteristic time scale. We find that the formation of vortices is a continuous process whose time limits are difficult to define. In essence, this analysis is valid for the different quench implementations that we consider.

- To provide a universal criterium to determine the number of primordial defects. The Kibble-Zurek mechanism yields a prediction of the density of topological defects as a function of the quench rate at which the system is cooled down during the phase transition. However the

number of total defects decreases in time after their formation due to an annihilation process. Thus, it is important to determine the correct measurement time to test the prediction of the Kibble-Zurek mechanism. We identify this measurement time as the time at which the phase of the complex field has relaxed and, as a result, patches of homogeneous complex phase are formed.

- To test the Kibble-Zurek mechanism in different quench regimes. We are not only interested in the prediction of the density of topological defects for a given quench rate, but also in comparing the dynamical process described by the theoretical mechanism with the results of our model simulations. We find that our model does not reproduce the expected behaviour –specifically, criticality effects are not detected.

This thesis is organised as follows. In part I, we provide a detailed review of all the concepts presented in this introduction. We start by explaining the Landau theory of phase transitions, which entails the expansion of a thermodynamic potential in terms of powers of the order parameter of the system –chapeter 1. Next, we define what topological defects are and show how they arise as a consequence of the spontaneous symmetry breaking of a system –chapter 2. In chapter 3 we explain in detail the Kibble-Zurek mechanism. We demonstrate how the connection between the spatial density of vortices and the quench rate at which the system is cooled during the phase transition is obtained from it. Lastly, we introduce the hexagonal manganites in chapter 4. We describe their main features and use them to motivate our model.

In part II we present the results of our work. First, we describe our model in chapter 5. It consists of a Lagrangian whose potential is expanded

according to the Landau theory of phase transitions. Some terms are included in this theory in order to represent the features of the hexagonal manganites. We pay special attention to how thermal effects are taken into account. Our model simulates the thermal fluctuations of the system through a stochastic noise term in the equations of motion. This was first done by Langevin to simulate the dynamics of the Brownian motion, and since then it has been widely used. We discussed the issues that may arise from using the usual formulation of this approach, and propose alternatives to overcome them. We also discuss how quenches are modelled in these contexts and explain the prescription adopted in our model. This is done in chapter 6. Lastly, in chapter 7 we present the results of numeric simulations performed with our model.

In part III, the code scripts that have been used to simulate the dynamics of the system are collected. We explain in detail the boundary conditions, the algorithms to discretize the equations of motion and the setting of initial conditions in chapters 8, 9 and 10, respectively. In chapter 11 we introduce the functions which have been used to measure some relevant observables of the system. Of special importance is the function to count the number of topological defects. Lastly, we present the main function of the program, where all the previous ones are gathered 12.

Finally, in the conclusions we summarised our results and compare them with the ones from the literature. We discuss the limits and strengths of our model in view of what has been accomplished.

Introducción

Un defecto topológico es una solución de una teoría de campos que no puede decaer a otra menos energética (más fundamental) debido a restricciones topológicas. Muros de dominio, vórtices y monopolos son algunos ejemplos de defectos topológicos. La importancia de estos objetos en física reside en el hecho de que son los subproductos de una transición de fase. Por consiguiente, el estudio del patrón de defectos topológicos creados tras una transición de fase nos permite obtener información sobre la teoría física subyacente.

El mecanismo de Kibble-Zurek explica cómo los defectos topológicos aparecen como consecuencia de una transición de fase. Fue propuesto por primera vez por Kibble [1] en los años setenta en el contexto de física de altas energías. Kibble argumenta que, dado que el universo ha estado enfriándose desde el Big Bang y consideramos válidas las teorías de unificación del modelo estándar de partículas, es natural concluir que en el universo temprano debió haber transiciones de fase. Como resultado de dichas transiciones de fase, se debieron formar defectos topológicos.

Posteriormente, en la década de los noventa Zurek propone estudiar defectos topológicos en sistemas de materia condensada como analogías a los defectos cósmicos que emergieron en el universo primigenio [2]. La ventaja fundamentadal de los defectos topológicos en sistemas de materia condensada (tales como vórtices en helio líquido, dominos ferromagnéticos, líneas

de discinación en cristales líquidos ...) frente a los creados en escalas cósmicas es que los primeros son accesibles en el laboratorio. Zurek también completó la explicación de Kibble para transiciones de fase de segundo orden, en la que la dinámica fuera del equilibrio juega un papel crucial. El mecanismo de Kibble con la contribución de Zurek predice una relación entre la densidad espacial de defectos topológicos y los exponentes críticos de la teoría. Estos exponentes críticos son universales, en el sentido de que sólo dependen de las simetrías de la teoría. Esto se debe al comportamiento crítico del sistema en el punto de transición de una fase a otra. Sin embargo, hay otro argumento más que justifica que las propiedade de una transición de fase son universales para teorías con las mismas simetrías. El mecanismo físico subyacente que permite la formación de defectos topológicos es la ruptura expontánea de simetría que tiene lugar durante la transición de fase [3]. Por tanto, la naturaleza de los defectos topológicos depende de las simetrías de la teoría original y de qué forma se rompen.

En definitiva, podemos relacionar teorías de distintos contextos físicos si pertenecen a la misma clase de universalidad. Desde el artículo seminal de Zurek se han hecho muchos experimentos en sistemas de materia condensada con el objetivo, por un lado, de poner a prueba el mecanismo de Kibble-Zurek y, por otro, de investigar la física de sistemas de altas energías inaccesibles a través de sistemas análogos en materia condensada. Las manganitas hexagonales son uno de estos sistemas. Son materiales multiferroicos con una rica fenomenología, cuya característica más distintiva es que la simetría se rompe de forma discreta como resultado de una transición de fase estrucutral.

En esta tesis construimos un modelo teórico para un campo esclar de dos componentes que reproduce la física de las manganitas hexagonales y efectuamos simulaciones numéricas en varios regímenes. Los princpales objetivos

del trabajo son los siguientes:

- Analizar la prescripción usual para simular fluctuaciones térmicas a través de un término estocástico en las ecuaciones de movimiento. Esta forma de modelizarlas presenta algunos problemas (en particular, es posible que tenga en cuenta dos veces los efectos térmicos). En efecto, la temperatura aparece explícitamente en dos términos diferentes del Lagrangiano de la teoría: por un lado, en la amplitud de la fuerza estocástica térmica y, por otro, en el coeficiente del término de masa como un parámetro lineal. Proponemos una forma alternativa de incluir las fluctuaciones térmicas para tratar de solventar este problema. Desde esta nueva perspectiva, la temperatura sólo aparece explícitamente en la amplitud de la fuerza estocástica, pero no en el coeficiente del término de masa. Por tanto el valor que adquiere el término de masa es resultado de una renormalización efectiva debido a las fluctuaciones del campo inducidas por los efectos térmicos y no el resutlado de una imposición externa.

- Analizar en detalle el proceso de formación de vórtices tras una transición de orden térmica de segundo orden con una simetría global. Identificamos los observables relevantes para su descripción y distinguimos tres diferentes regímenes dinámicos, cada uno con un tiempo característico asociado. Constatamos que la formación de vórtices es un proceso contínuo difícil de delimitar en el tiempo. En esencia, este análisis es válido para las diferentes implementaciones de enfriamientos que tenemos en consideración.

- Dar un criterio universal para determinar el número de defectos primordiales. El mecanismo de Kibble-Zurek predice una dependencia entre

la densidad del número de defectos topológicos creados tras una transición de fase y el ritmo de enfriamiento al cual se ha efectuado dicha transición. No obstante, el número total de defectos no permanece constante, sino que decrece en el tiempo después de su creación debido a un proceso de aniquiliación. Por tanto, es importante determinar el tiempo de medición correcto para poner a prueba la predicción del mecanismo de Kibble-Zurek. Identificamos este tiempo de medida con el tiempo en el cual la fase del campo complejo se ha relajado y, en consecuencia, se han formado dominios de fase homogénea.

- Poner a prueba el mecanismo de Kibble-Zurek en diferentes regímenes de enfriamiento. No estamos sólo interesados en la predicción de la densidad de defectos topológicos para un cierto ritmo de enfriamiento, sino que también comparamos la dinámica del proceso descrito por el mecanismo de Kibble-Zurek con los resultados obtenidos a partir de las simulaciones de nuestro modelo. Hallamos que nuestro modelo no reproduce el compartamiento explicado por el mecanismo (en particular, no se detecta el papel que juega la criticalidad).

Esta tesis está organizada de la siguiente manera. En la parte I se proporciona una explicación detallada de todos los conceptos mencionados en esta introducción. Empezamos explicando la teoría de Landau para transiciones de fase, que consiste en la expansión de un potencial termodinámico en potencias del parámetro de orden del sistema (capítulo 1). A continuación definimos matemáticamente los defectos topológicos y explicamos cómo emergen como consecuencia de la ruptura espontánea de la simetría del sistema (capítulo 2). En el capítulo 3 explicamos en detalle el mecanismo de Kibble-Zurek y demostramos cómo obtener a partir de él la relación entre la densidad

espacial de vórtices y el ratio al que el sistema es enfriado durante la transición de fase. Por último, en el capítulo 4 introducimos las manganitas hexagonales. Describiemos sus características fundamentales, que usaremos para contruir nuestro modelo.

En la parte II exponemos los resultados de nuestro trabajo. En primer lugar, describimos nuestro modelo en el capítulo 5. Consiste en un lagrangiano con un potencial expandido en potencias del parámetro de orden, de acuerdo con la teoría de Landau para las transiciones de fase, al que se le han añadido unos términos particulares para representar el comportamiento característico de las mananitas hexagonales. Prestamos una atención especial a la forma de incluir efectos térmicos. En nuestro modelo, las fluctuaciones térmicas se simulan a través de un término de ruido estocástico en las ecuaciones de movimiento. Esta forma de proceder fue empleada originalmente por Langevin para simular la dinámica del movimiento Browninano, y desde entonces se ha empleado de forma habitual. Comentamos los posibles problemas que pueden surgir al aplicar este formalismo y proponemos alternativas para solucionarlos. También analizamos cómo se modelizan los enfriamientos en estos contextos y describimos de qué forma lo hemos reflejado en nuestro modelo. Todo esto constituye el contenido del capítulo 6. Por último, el el capítulo 7 presentamos los resultados de simulaciones numéricas efectuadas según nuestro modelo.

En la parte III se recogen las secuencias de código empleadas para simular la dinámica del sistema. Explicamos en detalle cómo implementar las condiciones de frontera, los algoritmos para discretizar las ecuaciones del movimiento y las condiciones iniciales en los capítulos 8, 9 y 10 respectivamente. En el capítulo 11 analizamos las funciones que hemos empleado para medir algunos observables relevantes. La función implementada para contar

el número de defectos topológicos es de especial importancia. En último lugar, incluimos el código de la función principal del programa, que articula el resto de funciones, en el capítulo 12.

Finalmente, en las conclusiones resumimos nuestros resultados y los comparamos con los obtenidos en la bibliografía. Analizamos los límites y fortalezas de nuestro modelo en vista de los resultados obtenidos.

Part I

State of the art

Chapter 1

Phase transitions. Phase transitions of the second kind and criticality.

In thermodynamics, a physical phase is defined as an homogeneous portion of a system which is in the same state of matter. Such state is defined by some physical properties related with symmetries, which are uniform within the phase. A phase transition is a process in which these symmetry properties that characterised a phase undergo a change as a response to variations of the external conditions of the system.

Let us introduce some definitions to make a more rigorous description of this phenomenon. The state of the body is characterised by a quantity called *order parameter*. For instance, the vector of total magnetization $\mathbf{M}$ plays the role of the order parameter in a ferromagnetic phase transition. Another example of order parameter is the displacement vector of some atoms of a crystal lattice in a phase transition between two different crystal structures. In addition to the order parameter, it is also necessary to introduce

a *control parameter*. It accounts for the external conditions of the system, whose variation induce the phase transition. This takes place when the control parameter surpasses a certain critical value. The most common control parameter is the temperature, though may be others.

For a phase transition to be possible, it is necessary that the symmetry of one phase be higher than the other, *i.e.*, the symmetry of one phase must contain all the symmetry elements –rotations, translations, reflections, etc.– of the other plus additional ones. Mathematically, if the group of symmetries of higher symmetric phase is G, and the group of symmetries of lower symmetric phase is H, H must be a subgroup of G. Nevertheless, this is not a sufficient condition, since there are still more restrictions to be taken into account.

The change that occurs at a phase transition is a *spontaneous symmetry breaking*. When the system is in the phase of higher symmetry –from now on, *symmetric phase*–, the symmetry of the state (described by the control parameter) is the same as the symmetry of the theory (described by some energetic functional, such as the Lagrangian). At the critical point, the state of the body chooses spontaneously one of the possible points of the vacuum manifold. This happens inhomogeneously in the space –*i.e.*, the state takes different values at different spatial points. As a consequence, in the phase of lower symmetry –from no on, *broken phase*– the symmetry of the state is reduced, whereas the symmetry of the theory remains the same.

There exists two types of phase transitions, which differ in how this spontaneous symmetry breaking develops. The *phase transitions of the first kind* involve a discontinuous change in the value of the order parameter. Thus, the state of the body changes discontinuously at the transition point. So does the thermodynamic functions which depend on them, such as the free-energy,

the entropy, the volume, etc. As a consequence, during the transition the system absorbs –or releases– a fixed amount of energy per volume without increasing the temperature. That is, first-order phase transitions carry a latent heat. A phase transition of the first kind occurs through a process called *nucleation*. Firstly, the new phase is reached at some small spatial regions randomly, with a certain probability. These small regions constitutes nuclei from which bubbles of new phase will grow –hence the name of the process. These bubbles of new phase grow within a medium which still remains in the old phase. While new nuclei are created and bubbles grow, the two phases coexist in equilibrium, and we can always tell at which phase belong every part of the system. Eventually, all the body will be in the new phase.

On the contrary, a *phase transition of the second kind* entails a continuous change in the order parameter. Both the physical properties and the thermodynamic functions of the state of the body varies continuously through the transition –although their derivatives are discontinuous at the transition point. In spite of this, the symmetry does still change discontinuously at the transition point. In a phase transition of the second kind, all spatial points reach the broken phase at the same time, so there is no coexistence of the two different phases.

In order to provide a quantitative explanation of the phenomenological features noted above, let us introduce the Landau theory for phase transitions of the second kind (pages 446-478 of reference [4]). This formalism can then be extended to describe first-order phase transitions as well. In a second-order phase transition, let us assume that the order parameter is zero in the symmetric phase and takes non-zero values in the broken phase. For instance, this is how the vector of total magnetization behaves in a ferromagnetic phase transition. It is zero in the paramagnetic phase, above the critical

point –which is also known as *Curie point*–, and different from zero in the ferromagnetic phase, below the critical temperature.

Let $\Phi(\eta, T)$ be the thermodynamic potential of the theory. It accounts on the free-energy of the system as a function of the order parameter, η, and the control parameter, the temperature T. It may also depend on other variables, but we will neglect them in this summary for the sake of simplicity. It is important to remark that the dependence of Φ on η is not of the same nature as the dependence on the temperature. Whilst the latter can be chosen arbitrary, the former takes its value from the equilibrium state. That is, the value which η actually takes is computed by imposing the condition that Φ is a minimum (for given temperature) –*i.e.*, $\partial\phi/\partial\eta = 0$.

The fact that the state of the body changes continuously in a second-order phase transition implies that the order parameter takes values arbitrary small near the transition point –recall that it vanishes in one of the phases, namely the symmetric one. Therefore, we can make an expansion of the thermodynamic potential Φ in powers of η in a neighbourhood of the critical point,

$$\Phi(T;\eta) = \Phi_0 + \alpha_1\eta + \alpha_2\eta^2 + \alpha_3\eta^3 + \alpha_4\eta^4 + \ldots, \tag{1.1}$$

where the coefficients α_i are functions of T. In order to reproduce the phenomenological behaviour described above, some restrictions on these coefficients must be imposed.

First of all, we must set that α_1 is identically zero. Otherwise, the order parameter –computed at equilibrium– is different from zero at any temperature, which is in contradiction with our assumption that $\eta = 0$ in the symmetric phase, where $T > T_c$.

The requirement that Φ must have a minimum at $\eta = 0$ for temperatures above the critical also implies that $\alpha_2 > 0$ in the symmetric phase. However,

the assumption in the broken phase is that the stable state –*i.e.* the minimum of Φ– corresponds to non-zero values of η. This can only be achieved if $\alpha_2 < 0$ below the critical temperature. Thus, by continuity, the coefficient α_2 must be zero at the transition point. Assuming that this coefficient is a function of T which has not singularity at the transition point T_c, it can be expanded by a series in temperatures up to first order, $\alpha_2 = a_0(T - T_c)$, where $a0$ is a positive constant. Notice that this expansion reproduced the desired dependence on the temperature of α_2 stated above.

Let us assume that the transition point itself is also a stable state. That is, it must be a minimum of Φ at $\eta = 0$. The quadratic coefficient α_2 is zero at this point. Therefore, for this requirement to be possible we must impose that $\alpha_3(T = T_c) = 0$ and $\alpha_4(T = T_c) > 0$. The coefficient of the cubic term α_3 can be chosen to be identically zero at all temperatures, not only at the critical. If the coefficient of the quartic term α_4 is positive at the transition point, by continuity is also positive in a neighbourhood of that point. Thus, we replace it by a positive constant, $\alpha_4 = b > 0$.

Taking into account all these considerations, we can rewrite the expansion (1.1), which now reads

$$\Phi(T;\eta) = \Phi_0 + a_0(T - T_c)\eta^2 + b\eta^4, \tag{1.2}$$

where a_0 and b are positive constants. From this expression, we can deduce the behaviour of the order parameter in a neighbourhood of the critical temperature. Indeed, it is obtained by imposing $\partial\Phi/\partial\eta$ to be zero, that is $\eta(a_0(T - T_c) + 2b\eta^2) = 0$. In the symmetric phase, there is only one solution, $\eta = 0$, which is a minimum. As the transition point is approached, the minimum of the potential as a function of the order parameter becomes flatter. This implies that the restoring force to return the system to equilibrium becomes steadily weaker, which entails the increase of the relaxation time

without limit. After the critical point is surpassed, the system enters the broken phase. There, $\eta = 0$ becomes a maximum; the minimum is smoothly displaced to

$$\eta = \pm\sqrt{-\frac{a_0(T - T_c)}{2b}}. \tag{1.3}$$

Notice that the order parameter changes continuously with the temperature along the transition, as we had assumed (figure 1.1)

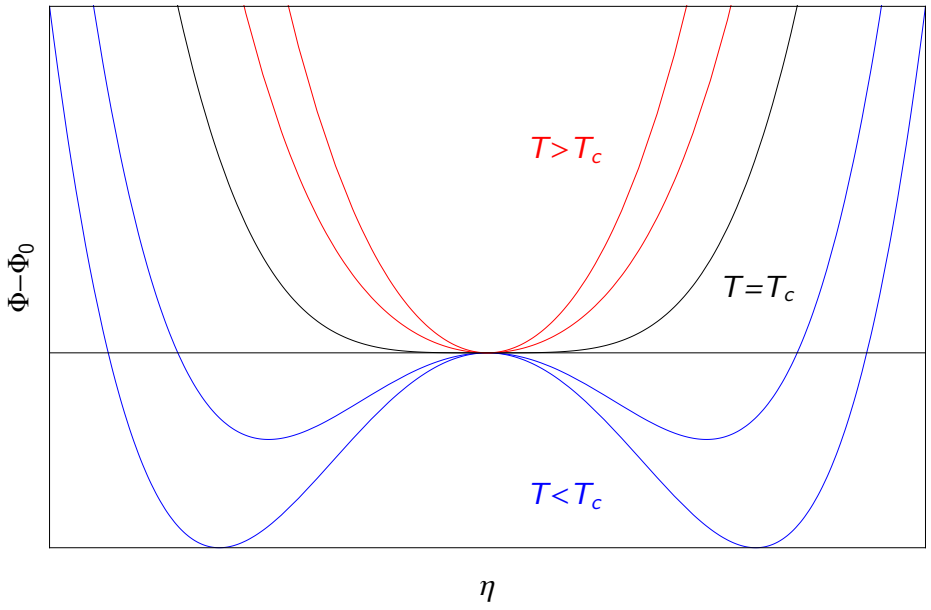

Figure 1.1: Thermodynamic potential Φ as a function of the order parameter η for several temperatures. Each line represents a higher temperature than the one below. Above the critical temperature (red lines), the minimum is located at the origin. At the transition temperature (black line), the potential flatters and the force that restores the field to the origin dissapears. Below the critical temperature (blue lines), two minima different from zero appears. As the temperature cools, they move away and the wells become deeper.

This expansion describe the energy of an homogeneous body. To account for the inhomogeneities, we must introduce spatial derivatives. For long-wave

fluctuations, only the derivatives of lowest order (and their lowest powers) need to be accounted for. Linear terms in first and second order derivatives can be neglected, since they only are responsible for surface terms once integrated in the volume. Thus, the first relevant contribution are the quadratic terms of first order derivatives. Adding this terms to the former expansion, we get

$$\Phi(T;\eta) = \Phi_0 + a_0(T - T_c)\eta^2 + b\eta^4 + g\left(\frac{\partial\eta}{\partial\mathbf{r}}\right)^2, \tag{1.4}$$

where we have defined g as the isotropic coupling factor for the gradients. This formula is only valid for long wavelengths, larger than the interatomic distances. We will make use of this expansion for the free-energy of a system which suffers a phase transition of the second kind as a basis to build our model in chapter 5.

From this expression, the correlation function –and also the correlation length, ξ– can be computed. An important remark is that this correlation length diverges when the critical temperature is approached [4],

$$\xi = \sqrt{\frac{g}{a_0(T - T_c)}}. \tag{1.5}$$

Actually, this is a manifestation of *criticality*. Criticality is an important feature of second-order phase transitions, which has not mentioned before in this chapter. In phase transitions of the second kind, the fluctuations of the order parameter grows anomalously when the transition point is approached. This have important implications. In the first place, it limits the range of application of the Landau theory. Indeed, the thermodynamic potential does have a singularity at the critical point. Hence, the expansion (1.4) is only valid in a regime where the fluctuations are sufficiently small. This expression is valid only if the following condition is fulfilled,

$$a_0\,|T - T_c| \gg \frac{T_c^2 b^2}{g^3}. \tag{1.6}$$

This criterion was derived by Levanyuk and Ginzburg [5] from the condition that the mean square fluctuation of the parameter of order averaged over a volume given by the correlation length is small compared with the characteristic value $\bar{\eta}^2 \sim a_0(T - T_c)/b$, obtained in (1.3). In a narrow interval close to the critical temperature, the left hand side of (1.6) is small and the criterion is not satisfied. This interval, called the *fluctuation range*, defines the region where the Landau theory is not applicable.

The second consequence of the large fluctuations of the order parameter near the transition point is that they cause the divergence of other quantities. We have already seen the divergence of the correlation length ξ –equation (1.5). As a consequence, the system at the transition point is fully correlated, and a perturbation on one point can affect the whole system. The correlation length is not the only quantity which diverges. The relaxation time of the system also diverges, which leads to a *critical slowing down* of the system. Other quantities such as the susceptibility or the specific heat also diverges. This divergences have the functional form of a law-scales. The exponents of these functions are called *critical indices*. These systems are universal, in the sense that they only depend on the symmetries of the theory beneath the phase transition.

The Landau theory can be extended to describe first-order phase transitions in a similar way. Nevertheless, the variation of the thermodynamic potential with respect the temperature is qualitatively different, since its expansion comprehends different terms. At high temperatures, the only minima of the potential is located at $\eta = 0$. As the temperature decreases, a second minima at some non-zero value of η appears. This minimum has a higher energy than the minima situated at the origin. However, if the temperature continues decreasing, this new minimum eventually becomes the global

minima of the theory. The phase transition occurs when the order parameter jumps from the minimum at the origin to the true minimum, which has less energy. To do so, it needs to get through a potential barrier –a local maximum between the two minima: the latent heat. This is accomplished thanks to the thermal fluctuations of the system. Unlike the second-order phase transitions, in this case the order parameter changes discontinuously from $\eta = 0$ to the value where the global minimum is.

Chapter 2

Topological defects

Topological defects are solutions of a field theory which cannot decay to a less energetic solution due to topological constraints. In the context of this work, their importance lies on the fact that they are the relics of a phase transition. From the pattern of topological defects, we can extract information about the underlying theory. This connection is made clear in the description of the Kibble-Zurek mechanism –cf. chapter 3. In this chapter, we will expose a brief summary of topological defects, paying special attention to vortices, because they are the defects which appears in our investigation. A more extensive description can be found in references [6, 7, 8] or in reviews such as [3], on which this summary is based.

A field theory is invariant under some transformation if it does no involve any changes in the Lagrangian. Mathematically, if the field ϕ transforms as $\phi \to g\phi$, with g being an element of a symmetry group G, then

$$\mathcal{L}[g\phi] = \mathcal{L}[\phi]. \tag{2.1}$$

This amounts to say that the Lagrangian is symmetric under the action of the group G. This symmetry is spontaneously broken whether the symmetry

of the state of the system is no longer the same as the symmetry of the Lagrangian.

Let us illustrate this with an example. Let $\mathcal{L}$ be a theory of a single complex scalar field $\phi = |\phi| \exp(i\theta)$,

$$\mathcal{L} = \partial_\mu \phi^* \partial^\mu \phi - V(|\phi|). \tag{2.2}$$

Global $U(1)$ transformations $\phi \to \exp(i\alpha)\phi$, with α constant in space and time, left the Lagrangian invariant. The vacuum state of that theory is the field solution which is constant in space and time and minimizes the potential V. Let us consider a potential of the form

$$V(|\phi|) = m^2|\phi|^2 + \lambda|\phi|^4. \tag{2.3}$$

In this instance, if $m^2 < 0$, all the points which satisfy $|\phi| = \sqrt{-m^2/2\lambda}$ belongs to the vacuum. Therefore, it is degenerated. Let $\mathcal{M}$ be the vacuum manifold, which amounts to the set of all possible vacua. Any two points of $\mathcal{M}$ can be related through symmetry transformations. However, the state of the system does not have this symmetry anymore –that is, small perturbations around the vacua does not remain invariant under a $U(1)$ transformation. Thus, the symmetry is broken.

In this case, the symmetry $U(1)$ is fully broken. However, in other cases where the symmetry group G is more complex, the symmetry can be partially broken. This amounts to say that the vacuum remains invariant under transformations of a subgroup H of G.

Let us consider the possible solutions of a theory whose symmetry has broken. For a classical solution to be admissible, the field configuration must approach the vacuum asymptotically at infinity. But there are multiple possible vacua to approach, as the vacuum is degenerated. Thus, there exist field configurations which approaches different points of $\mathcal{M}$ in different directions.

Let $\mathcal{S}^{D-1}$, with D being the spatial dimensionality, represent the spatial infinity. Then, the values of these field configurations at the spatial infinity constitute a map from the spatial infinity to the vacuum manifold,

$$\phi : \mathcal{S}^{D-1} \to \mathcal{M}. \tag{2.4}$$

A homotopy class of this map is formed by the set of field configurations which can transform into one another continuously. These homotopy classes are elements of the $(D-1)$-th homotopy group of $\mathcal{M}$, $\pi_{D-1}(\mathcal{M})$. We can also define lower homotopy groups, $\pi_n(\mathcal{M})$, $n < (D-1)$, by restricting the domain of the map to subsets $\mathcal{S}^n$ of $\mathcal{S}^{D-1}$.

We are now in condition to provide a rigorous definition of what a topological defect is. The vacuum solution –*i.e.*, the constant map– represents the identity element of any homotopy group. Besides, it is the less energetic solution of the theory. A topological defect is a solution which belongs to any $\pi_n(\mathcal{M})$ homotopy group, with $n \leq D-1$, provided $\pi_n(\mathcal{M})$ is nontrivial. Indeed, the field configuration which represents such solution cannot be continuously transformed into the vacuum solution because they belong to different homotopy classes.

In three dimensional space theories, field configuration belonging to nontrivial $\pi_0(\mathcal{M})$, $\pi_1(\mathcal{M})$ and $\pi_2(\mathcal{M})$ groups correspond to domain walls, vortices and monopoles, respectively. Let us consider the example of vortices in the theory (2.2) with potential (2.3) and $m^2 < 0$ to show that topological defects are solutions more energetic than the vacuum state. In this case the theory is $U(1)$ symmetric, and the vacuum manifold is $\mathcal{M} = S^1$.

Let us introduce a concrete case. Let ϕ to be a static field configuration $\phi(\rho, \varphi, z) = |\phi(\rho)| \exp(i\varphi)$ in cylindrical coordinates. It is clear that this solution belongs to a nontrivial homotopy class of $\pi_1(\mathcal{M})$, since the map $\phi : \mathcal{S}^1 \to U(1)$ –that is, the map from the angle in the physical space, φ, to

the angle of the complex phase of the field, θ– is not the constant map. Thus, this solution represents a topological defect, a vortex. If we assume that ϕ is a smooth configuration, it is necessary by continuity that it vanishes at $\rho = 0$, which requires some energy (V has a local maximum at the origin). Thus, it is more energetic than the vacuum solution, $\phi = |\phi(\rho)|$. Yet, the vortex cannot decay because it belongs to a different homotopy class. This is why topological defects are metastable solutions although they are not the less energetic.

Let us finish this chapter by introducing the concept of topological charge. It allows us to classify the topological defects within the same homotopy group. In the case of vortices, it is represented by the winding number, N_w. It is defined as the circulation of the complex phase of the field θ around a closed curve which enclosed the defect –which can be chosen to be $\mathcal{S}^1$ at infinity, $\rho = \infty$–, that is

$$N_w = \frac{1}{2\pi} \oint_C d\varphi \nabla\theta. \tag{2.5}$$

As the field must be periodic after a 2π shift in the polar angle φ –i.e., $\phi(\rho, \varphi, z) = \phi(\rho, \varphi + 2\pi, z)$–, it is clear that circulation of the complex phase of the field must be an integer number of times 2π, so N_w is an integer. Hence, each homotopy class is characterized by a topological charge which cannot change continuously, since it is essentially discrete. This is another manifestation of the impossibility to transform continuously one field configuration of one homotopy class to another configuration of a different class.

Chapter 3

Kibble-Zurek mechanism

The Kibble-Zurek (KZ) mechanism offers an explanation of how the topological defects arise after a phase transition. The mechanism was first proposed by Kibble [1, 9] in the seventies in the context of cosmology. Kibble argues that cosmological structures such as domain walls, cosmological strings or magnetic monopoles may be the relic of phase transitions which occurred in the early universe, as it cooled down from an initial hot state where all symmetries were unbroken. Later, Zurek took advantage of the analogy between cosmological strings and vortex lines in superfluid helium to extend the mechanism to condensed matter systems [2, 10]. Zurek also completed the argument of Kibble to include finite-time cooling quenches in second order phase transitions.

Topological defects emerge after a phase transition only if two conditions are fulfilled: First, there must be a symmetry which spontaneously breaks. After a symmetry is broken, the field is able to reach different vacuum states at different spatial locations. The second requirement is that the field configuration belongs to a non-trivial homotopy group. Otherwise, the field solution will decay to a trivial vacuum solution. This two conditions are

fulfilled after a phase transition. The change of the shape in the thermodynamic potential as the temperature have dropped below the critical one leads to the creation of a degenerate vacuum. In the new broken phase, the field takes different values of this degenerate vacuum in different locations, thus allowing non-trivial field configurations.

The dynamics described by the KZ mechanism is as follows. For the sake of clarity, let us consider a global $U(1)$ theory with a complex scalar field, $\phi = |\phi| \exp i\theta$. In the symmetric phase –*i.e.*, above the critical temperature– the equilibrium state of the field is the origin, $|\phi| = 0$. After the temperature of the system falls below the critical temperature, the system moves to the broken phase. The phase of the field takes at random any of the values of the vacuum manifold, $\theta \in [0, 2\pi)$, all with equal probability. In addition, depending on what type of phase transition is taking place –first or second order–, this process will be accomplished in different ways.

In phase transitions of first order, there is an energetic barrier between the two phases. This barrier can be overcome by means of thermal fluctuations, which are random. Consequently, not all the points will reach the new phase at the same time. The points which first fall to the vacuum manifold constitute a nucleus from which the new phase will expand. As a result, all the domain which grows from a single nucleus will be homogeneous – *i.e.*, the field at every point will take the same value.

In contrast, phase transitions of second order happen continuously. There is no energetic barrier, so all the points reach the vacuum manifold at the same time. The size of domains of homogeneous phase in this kind of transitions is argued to be of the order of magnitude of the correlation length of the system, ξ. This quantity represents the length scale within which points are correlated –*i.e.*, they can influence each other. Hence, the choice of vacuum

at every point is not independent, since it is affected by its neighbourhood. This is a statement which needs further discussion. It will be addressed later on this chapter.

Regardless of what kind of phase transition is taking place, domains of homogeneous phase will form, and they will be disconnected and spatially uncorrelated with each other. This is a condition of possibility for the vortices to exist, but it is not enough. Vortices will only form from these domains if they meet under suitable circumstances. Let us elaborate this concept.

Let us consider two domains of homogeneous phase that meet. The complex phase of the field takes two different values at both sides of the border. Then, there is an interpolation of the complex field between these two domains. Such interpolation is governed by the *geodesic rule*, which can be formulated as follows [1]: the complex phase θ of the scalar field must interpolate between the two domains across the junction following the shortest path on the vacuum manifold, S^1. Eventually, these two domains will merge and become one.

Naturally, if all encounters were this way, no vortex could form, since all patches will merge together in a one single common domain. To create a vortex, we need several patches colliding together. The complex phase need to interpolate continuously across borders of domain pairs in such a way that the circulation of the phase over a closed trajectory C which passes through all the domains is $\oint_C \partial\theta = 2n\pi$, where n is an integer number which is called *winding number*. By continuity, this implies that at some point enclosed in the trajectory C, the field is zero. This is the core of the vortex. There, the field still remains in the old symmetric phase, unlike the surrounding points, which all are in the new broken phase.

To create a vortex of winding number one, we need at least three patches

colliding together (see figure 3.1). Besides, the following condition must be fulfilled,

$$\theta_1 + \pi < \theta_3 < \theta_2 + \pi, \qquad \theta_1 < \theta_2 < \theta_3, \tag{3.1}$$

where $\{\theta_j\}$ represents the complex phase of the field of the $j-th$ domain. This condition is met with a probability of 1/4 [11]. Any vortex with winding number larger than 1 is also possible. The probabilities to form them are fewer, though, since the process entails the collision of more (suitable) domains, which is less likely to happen.

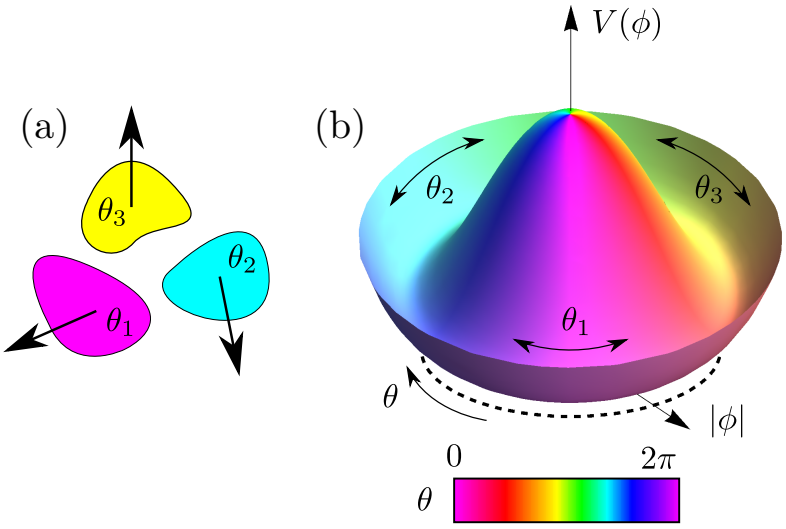

Figure 3.1: (a) Meeting of three domains. Within each domain, all the points have the same value of the complex phase of the field, $\{\theta_1, \theta_2, \theta_3\}$ (b) S^1 vacuum manifold, which amounts to the minima of the potential. The complex phase interpolates between pairs of domains following the shortest path on the vacuum manifold. As the phases fulfil the relation (3.1), a vortex of winding number 1 will emerge from the meeting.

Let us now return to the issue of the size of the primitive domains of homogeneous phase after a second order phase transition. It was argued that

the typical size of these domains is similar to the correlation length, ξ. Some remarks are worth mentioning. First, the correlation length is a quantity which can be derived from the computation of the correlation function –for instance, consult [4], pages 471-478. In this context, the correlation length ξ represents the length scale at which the correlation of the fluctuations of the field decreases significantly, i.e. $\langle \delta\phi(r)\delta\phi(r+\xi)\rangle \sim 0$. It is a well known fact that the long wave fluctuations heavily increase as the temperature of the system approaches the critical temperature in a second order phase transition. In fact, in a system of infinite size, they become infinite at the critical point. So does the correlation length. Consequently, as we approached the critical point, the size of the domains of homogeneous phase would become bigger and bigger. Eventually, at the critical point, the size of the domains would span the whole sample. The formation of topological defects would be impossible, since there would exist only one domain.

This apparent paradox was solved by Zurek. Zurek realizes that this scenario only would happen if the cooling was performed adiabatically – *i.e.*, the system was at equilibrium at every moment during the process. However, this is not possible, because the relaxation time of the system also diverges as the system approaches the critical point, a phenomenon called *critical slowing down*. That is, an adiabatic quench would last infinite time. Nevertheless, in real experiments, the time which the system spends cooling is finite. Therefore, the quench is performed out of equilibrium. This prevents the correlation length to become infinite and allows the formation of domains of homogeneous phase.

Let us expose the standard argument provided by Zurek to explain this out-of-equilibrium dynamics. There are two relevant time scales in the problem. The first one is the quench time, τ_q. It represents the time the system

spends cooling through the phase transition. The second is the relaxation time, τ, accounts to the time the system needs to return to the equilibrium after a perturbation. More precisely, it can be obtained from the mean-field theory by linearising the equation of motion and neglecting the inertial terms. Therefore, τ is inversely proportional to the mass term. Using causality arguments, this time can be related with the size of the domains of homogeneous phase. As the speed at which information propagates in the medium is finite, the relaxation time defines a region within which all the points can communicate their choice of vacuum with each other. Far from the critical temperature, the relaxation time remains approximately constant. So does the size of homogeneous domains. As the system approaches the transition point, both the critical point and the size of the domains start increasing due to the criticality. At some moment, the time that some information needs to propagate through the whole domain is equal to the time that the system is going to spend cooling through the critical point. Beyond this time, the system cannot transmit information fast enough, as the cooling will end before this transmission completes. Thus, this moment defines a freezing time, t_{fr}, at which the size of the domains stops growing (see figure 3.2).

The freezing temperature depends on the quench rate. The slower the cooling, the closer the freezing temperature will be to the critical temperature, which means that the domains will be larger. The larger the domains, the fewer will be created. Finally, the fewer domains, the lower the number of collisions between them, so the number of topological defects decreases. In conclusion, there exits a relationship between the density of topological defects created after a phase transition and the quench rate at which the cooling is performed.

A mathematical derivation of such relationship can be provided. Both

the relaxation time and correlation length are quantities which diverges at the critical temperature. They are known to diverge as power laws, namely

$$\tau(T) = \tau_0 \left| \frac{T - T_c}{T_c} \right|^{-\mu}, \qquad \xi(T) = \xi_0 \left| \frac{T - T_c}{T_c} \right|^{-\nu}. \tag{3.2}$$

Here, τ_0 and ξ_0 are the relaxation time and correlation length at zero temperature, respectively. This is a quantity which depends on the material

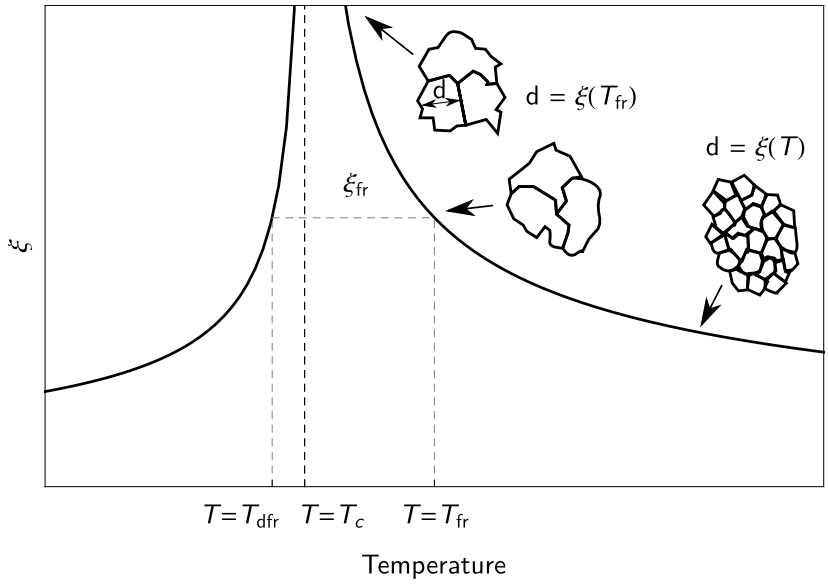

Figure 3.2: Domain formation according to the KZ mechanism. The correlation length defines the length scale of the size of the domains of homogeneous phase, d. We start our quench at temperatures above T_c and move towards the left as the system cools over time. When the freezing temperature T_{fr} is reached, the size of the domains freezes and no longer grows following the adiabatic curve pictured in the figure. This is due to the fact that perturbations have no time to propagate beyond this distance before the phase transition is completed (recall that the relaxation time also diverges). Below T_c, size of domains will follow again the adiabatic curve after the defreezing temperature T_{dfr}.

properties of the system we are dealing with. On the contrary, μ and ν, does not depend on the specific system. They are the critical exponents, which depends on the universality class of the theory, i.e., the symmetry properties of the phase transition.

From now on, we will use the reduced temperature, $\epsilon = (T - T_c)/T_c$, rather than the actual one, T, since it has the advantage of being dimensionless. Let us assume a linear quench, i.e. the temperature decreases linearly with the time. If we set $T = T_c$ at time $t = 0$,

$$\epsilon \;=\; -r_q\, t \;=\; -\frac{t}{\tau_q}, \tag{3.3}$$

where we have introduced the quench time as the inverse of the quench rate, $\tau_q \equiv r_q^{-1}$. From this equation we can tell that the freezing temperature ϵ_{fr} is achieved at a freezing time $t_{fr} = \tau_q \epsilon_{fr}$. Equating this time with the relaxation time computed at the freezing temperature from equation (3.2), that is, $t_{fr} = \tau(\epsilon_{fr})$, we obtain an expression for the reduced freezing temperature,

$$|\epsilon_{fr}| = \left(\frac{\tau_0}{\tau_q}\right)^{\frac{1}{\mu+1}}. \tag{3.4}$$

Substituting this value on equation (3.2) for the correlation length, we get

$$\xi_{fr} \equiv \xi(\epsilon_{fr}) = \xi_0 \left(\frac{\tau_q}{\tau_0}\right)^{\frac{\nu}{\mu+1}}. \tag{3.5}$$

This freezing length represents the scale length that the domains will get during the phase transition. On a plane, the size of these domains is of the order of ξ_{fr}^2. Since vortices will form in the intersections of domains, we can approximate the density of vortices per unit area as $n \sim \epsilon_{fr}^{-2}$. Thus, we obtain the following important scaling law between the density of defects and the quench rate,

$$n \sim \frac{1}{\xi_0^2} \left(\frac{\tau_0}{\tau_q}\right)^{\frac{2\nu}{\mu+1}}. \tag{3.6}$$

Note that terms of a very different nature appear in this relationship. The critical exponents depends on the symmetry properties of the phase transition, whilst the density of vortices is a measurable quantity. Therefore, the study of the pattern of topological defects left behind a phase transitions can give us information about its universality class.

This is the general scheme of the KZ mechanism. While its verification at cosmological scales is difficult, it has been successfully tested experimentally on many condensed matter systems [2, 3, 11, 12, 13, 14, 15, 16, 17, 18, 19, 20, 21, 22, 23, 24, 25, 26, 27, 28, 29, 30, 31, 32, 33, 34, 35, 36, 37, 38, 39, 40]. However, there are also some experimental results that departures from the postulated KZ scaling in the regime of fast quenches [37, 38, 39, 40]. In order to try and explain these discrepancies, work is still being done to extend and improve the mechanism. In particular, there have been efforts to consider more realistic quenches. The standard formulation of the model establish an homogeneous quench, that is, a quench where the critical temperature is reached at every point at the same moment. This is certainly an idealization. It will work well in some cases, whereas in many others it is not possible neglect that the phase transition does not occur uniformly. The most common approach to overcome this problem is to let the quench rate depend on the space coordinates too. Hence, a temperature front propagates through the sample with certain velocity [41, 42, 43]. The space of parameters of the model enlarges, and new regimes are found where the creation of vortices is suppressed. Some other works have also try other solutions, as consider a critical temperature inhomogeneous in space [44]. A more extensive explanation of the mechanism, its applications, as well as its limitations and further developments is provided in reference [45].

Chapter 4

Hexagonal manganites

Formation of topological defects after a phase transition is a ubiquitous phenomenon. It is present in many different physical systems, from cosmic to atomic length scales. The KZ mechanism is used to describe this process. Its verification is challenging in cosmic systems, but there are many condensed-matter systems in which experiments can be carried out in order to test this mechanism.

There is a second important reason to study condensed-matter systems in the context of topological defect formation. The scaling law which relates the density of defects with the cooling rate is claimed to be the same for all systems which belongs to the same universality class. This remarkable feature can be exploited to study systems which otherwise would be inaccessible. Hence, many cosmological systems can be studied not directly, but through an analogue condensed-matter system of the same universality class. This was the original idea of Zurek in reference [2]. Since then, there has been an increasing interest in condensed-matter systems in which topological defects can emerge.

Hexagonal manganites $RMnO_3$ are one of such systems, where R stands

for Y, Sc, or one rare earth ion (Dy, Ho, Er, Tm, Yb, Lu). They present a rich phenomenology, where several phase transitions occurs at different temperatures, thus creating different kinds of topological defects, such as ferroelectric vortices or neutral and charged domain walls. Hexagonal manganites are multiferroic material, in the sense that they exhibit several ferroic properties. Namely, they are improper ferroelectric, since electric polarization is a by-product of a previous structural phase transition. At low temperatures, an antiferromagnetic phase appears.

In this chapter, we will focus on the phase transition which occurs at higher temperature –the change in the structure of the crystal. This phase transition can be modelled using the Landau theory described in chapter 1. In references [35, 37, 38, 46, 47] a expansion of the free energy of the system as powers of the order parameter is presented, where the order parameter represents a displacement of atoms in the crystal lattice. Reference [47] introduce a more complete expansion, since it also includes couplings of the order parameter with the polarization vector. The interest of this material is that the potential includes anisotropic sextic terms. As a result, the vacuum manifold is discretized. Instead of the usual $U(1)$, the vacuum manifold becomes a $\mathbb{Z}_6$. Expansions of even higher terms are also proposed [48], but there are not considered here. This is the potential that we have used to build our model in chapter 5.

The defects which arise after this structural phase transition are domain walls and vortices. Reference [46] provides a detailed description of the structure of them. Other interesting feature about the hexagonal manganites is that recently some experiments have shown regimes where their behaviour deviates from the scaling predicted by the KZ mechanism. Those experiments are explained in references [37, 38].

Let us describe the crystal structure of the hexagonal manganites and define their order parameter. The structure of this material consist of planes of trigonal bi-pyramids (one atom of manganese in the center, five atoms of oxygen in the vortices) separated by planes of R ions, which are arranged in a hexagonal mesh (figure 4.1).

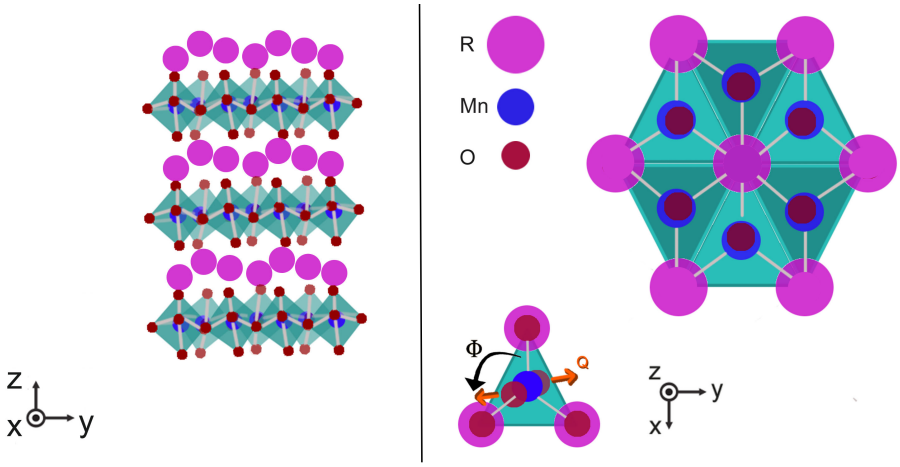

Figure 4.1: Left: side view of the planes of trigonal bi-pyramids and the R ions. Right: Top view of the unit cell. At the critical temperature, R ions move upwards (or downwards) and the axis of the bi-pyramids tilt towards (or away) from a common center. This causes the *trimerization* of the unit cell. The order parameter of the trimerization is $(Q\cos\phi, Q\sin\phi)$, with Q and ϕ being the magnitude and orientation of the tilt of the vertical axis of the bi-pyramid receptively.

At the transition point, a spontaneous symmetry breaking happens, and two phonon modes condensates. The first phonon mode involves a trimerization of the unit cell, that is, the formation of trimers –sets of three equal molecules. This trimerization consist of the tilt of the long axis of the bi-pyramids. This tilt amounts to the parameter of order. It is a two-component field, $(Q\cos\phi, Q\sin\phi)$, where Q represents the magnitude of the tilt and ϕ

the direction of such tilt. This phonon can condensate around three different centres, and the tilt can be *towards* or *away* –cf. figure 4.2. As a result, six different trimerization domains are formed. The tilts of the bi-pyramids induces the appearance of another phonon. This new phonon consists in the displacement of the R ions which lay between two layers of bi-pyramids. They move upwards if the tilt of the bi-pyramids converge to its position and downwards otherwise. This second phonon causes the spontaneous ferroelectric polarization $P \sim Q^3 \cos 3\phi$. However, it does not create new domains.

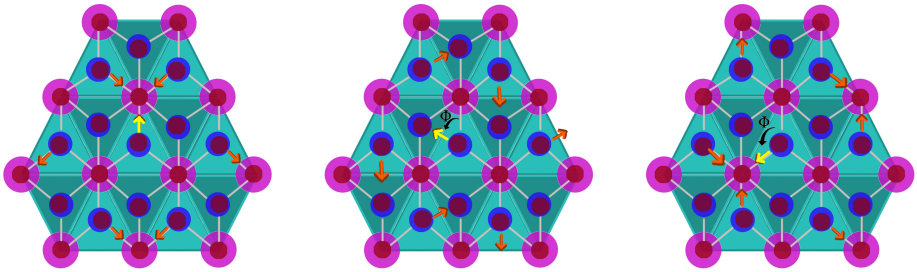

Figure 4.2: Three (of six) different forms to trimerize a cell unit, seen from above. Arrows correspond to the projections in the horizontal plane of the movement of the oxygen atoms at the top vertices of the bi-pyramids. One ion (yellow arrow) is chosen to define the trimerization phase. In the figure are shown the cases with $\phi = 0, \pi/3$ and $2\pi/3$, from left to right.

The model which we consider in part II is inspired in the phenomenology of this first phase transition. The order parameter is a two-component scalar field, and the potential is expanded up to six order to include the anisotropy terms which leads to the formation of six different domains.

Part II

Thermal vortices in Hexagonal Manganites

The aim of our work is to provide a detailed explanation of the process of vortex formation after a second-order phase transition has taken place. We also investigate different forms of taking into account the thermal effects. To do so, we build an effective model which reproduces the physics of certain condensed-matter systems and perform numerical simulations in various regimes.

Although the KZ mechanism gives general arguments to account for how vortices are created, there are some nuances which are not fully explained and require further clarification. One of the aspects which is worth considering more carefully is the fact that there is no clear separation between the regime of vortex formation and the subsequent regime of vortex interaction. Indeed, once the vortices are formed, they interact with each other, as well as with the borders of the sample. The result of such interactions leads to their annihilation. Hence, the total number of defects is a decreasing function of time.

If defining the end of the formation regime is difficult, it is no less problematic to unambiguously determine its beginning. The KZ mechanism argues that vortices form at the transition point, since it is at this moment where the patches of homogeneous phase –which have been created in the symmetric phase with a length scale determined at the freezing temperature– choose one of the degenerate values of the vacuum. However, this behaviour is not reproduced in our model. We see no evidence that patches are formed in the symmetric phase in our simulations. The complex phase of neighbour locations –which is at first chosen randomly and independently at the transition point– eventually take the same value, thus creating spatial domains of homogeneous phase already in the broken phase. In this scenario, to tell at which moment patches are already formed and start interacting is not

evident. A criterion must be specified.

From the above remarks, it is clear that the formation of vortices is a process which develops continuously on time rather than an event which happens at a single moment. This may be a problem to test the KZ prediction of scaling-laws –equation (3.6). As the number of vortices that enter in the formula is not constant over time, it is necessary to specify when to perform the measurement. This problem have been solved in the literature in different ways. For instance, in [49] the total number of vortices is chosen extrapolating backwards the time series of the number of vortices. In [10, 50], a more straightforward method is used: defects are counted at a fixed value of t/τ_q, where t stands for the time passed from the critical point and τ_q for the inverse of the quench rate.

As far as our model is concerned, we identify three different regimes in the process of vortex creation, each of one with a characteristic time scale –see chapter 7 for a detailed description. The prediction of the KZ mechanism can be tested with the number of vortices computed at these different times. In chapter 7 a more detailed explanation is provided.

Besides the ambiguity to characterised the times of the process of vortex formation, there is another important issue to take into consideration: the way thermal effects are taken into account. One of the most common manner to consider thermal fluctuations is to use Montecarlo simulations. However, we have employed a different approach. Thermal fluctuations are included in our model as random contributions to the equations of motion through a stochastic term which introduce random noise. This is a standard way to introduce the thermal noise since it was first proposed by Langevin [51]. For instance, this is how temperature is included in many time-dependent Ginzburg-Landau models of superconductors [52, 53, 54, 55, 56]. This noisy

term is necessary because it is the only contribution which forces the field to move from the origin when it becomes a maximum in the broken phase.

The thermal effects also alter the value of the mass term. It has been stated in chapter 3 that a topological defect can only occur if a symmetry is broken. This break happens if the sign of the mass term changes sign when the temperature crosses the transition point –chapter 1. Therefore, we need to explain this change in the sign of the mass term as a thermal effect. This can be achieved in different manners. The most straightforward way is to make the mass term a explicit function of the temperature. This is how simulations are performed in reference [57], for example. In this cases, the temperature appears explicitly in two different terms: as a linear parameter in the mass coefficient and also in the amplitude of the thermal noise term. An alternative approach is to consider that the mass term is effectively renormalized by the fluctuations of the field due to thermal effects [3]. Under this assumption, the temperature only appears explicitly in the amplitude of the thermal noise term, but not in the coefficient of the mass term. The change in sign of this coefficient is a consequence of its renormalization. We have performed simulations according to both formalisms. In chapter 6 a more extensive explanation is elaborated.

This second part is organised as follows: In chapter 5 we introduce the basic notions of our model and its motivation. We discuss general aspects and derive the equations of motion without defining yet the prescription to take into account the thermal effects. In section 5.1 we outline the computations of the correlation length ant the relaxation time in the mean field theory and linear approach. In chapter 6, we distinguish two different ways to perform a quench and take into account the thermal effects. The generic model described before will be adapted to fit each of this prescriptions. Lastly, the

numeric set-ups and results for this three cooling methods will be discussed in chapter 7.

Some part of this work has been already published in the following reference: Tello-Fraile, Marcos, Andrés Cano, and Manuel Donaire. *Topological thermalization via vortex formation in ultrafast quenches.* Physical Review E 101.5 (2020): 052113 [58].

Chapter 5

The model

Let us consider an effective Lagrangian model of a scalar field order parameter, $\mathcal{Q}$, in which temperature fluctuations are incorporated through a Langevin term in the equation of motion. Specifically, we consider a two-component scalar order parameter, $\mathcal{Q} = (Q_1, Q_2) = (Q\cos\phi, Q\sin\phi)$, with equations of motion

$$\frac{\partial \mathcal{L}}{\partial Q_i} - \nabla \frac{\partial \mathcal{L}}{\partial \nabla Q_i} = -\frac{\partial \mathcal{R}}{\partial \dot{Q}_i} + f_i. \tag{5.1}$$

Here $\mathcal{L}$ is the effective Lagrangian, $\mathcal{R}$ is the dissipative function, and f_i are the components of a stochastic Langevin force such that $\langle f_i(\mathbf{r},t) f_j(\mathbf{r}',t')\rangle = 2\gamma T \delta_{ij}\delta(\mathbf{r}-\mathbf{r}')\delta(t-t')$, with T being the temperature and γ the damping coefficient [4]. In this way, we effectively consider Gaussian fluctuations of $\mathcal{Q}$ satisfying the fluctuation-dissipation theorem at temperature T [59]. The physical idea of this theorem is that the interactions of the field with the thermal bath which causes its *microscopic* fluctuations are precisely the ones which lead its *macroscopic* evolution [51]. Let us elaborate on each of the objects which appears in equation (5.1).

In the following, we consider an effective Lagrangian of the form

$$\mathcal{L} = V_T(\mathcal{Q}) + \frac{g}{2}[(\nabla Q)^2 + Q^2(\nabla\phi)^2], \tag{5.2}$$

where the total potential V_T contains a $U(1)$-symmetric term, $V(Q)$, and a six-fold anisotropy term, $V_6(\mathcal{Q})$, $V_T(\mathcal{Q}) = V(Q) + V_6(\mathcal{Q})$,

$$V(Q) = \frac{a}{2}Q^2 + \frac{b}{4}Q^4 + \frac{c}{6}Q^6, \tag{5.3}$$

$$V_6(\mathcal{Q}) = \frac{c'}{6}[(Q_1^2 - 3Q_2^2)Q_1]^2 = \frac{c'}{6}Q^6\cos^2(3\phi). \tag{5.4}$$

This is nothing but the power expansion of the thermodynamic potential in powers of the order parameter $\mathcal{Q}$ prescribed by the Landau theory for phase transitions of the second kind –cf. chapter 1.

The coefficients $b, c, g > 0$ are all constant. The coefficient of the quadratic term, a, takes different forms depending on which way the thermal effects are taken into account. This will be discussed in full detail in chapter 6. The total effective potential according to these definitions is depicted in figure 5.1.

The critical behaviour of this model belongs to the XY universality class. However, the six-fold anisotropy term, $V_6(\mathcal{Q})$, can be tuned to describe either $U(1)$-symmetric systems like superfluids or $\mathbb{Z}_6$-symmetric ones like hexagonal multiferroic manganites [46, 47, 48]. In the latter case, although the symmetry that is initially broken below T_c is that of the $U(1)$ group, the subsequent evolution as well as the final structure of the vortices is generally affected by the $\mathbb{Z}_6$ anisotropy term for sufficiently large values of c'. In the instance of using this potential to describe hexagonal manganites, $\mathcal{Q}$ physically represents a structural order parameter describing the trimerization of the unit cell –cf. chapter 4.

In static equilibrium, the uniform order parameter for which the free

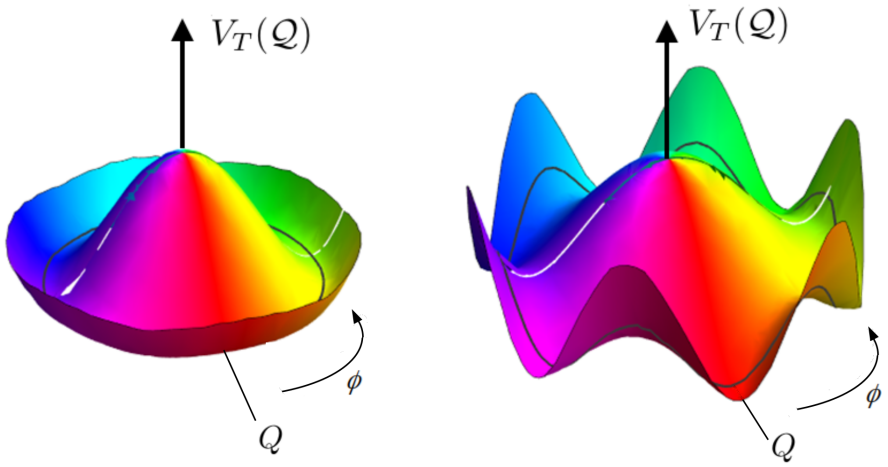

Figure 5.1: Sketch of the total effective potential of the order parameter in configuration space, $V_T(\mathcal{Q}) = V(Q) + V_6(\mathcal{Q})$, below the critical temperature. The field values at the minimum of $V_T(\mathcal{Q})$ form the vacuum manifold. Left, potential in the weak-anisotropy regime; right, potential in the strong-anisotropy regime.

energy presents a minimum value satisfies

$$\left[a + bQ^2 + \left(c + c' \cos^2(3\phi)\right)Q^4\right]Q = 0, \tag{5.5}$$

$$Q^6 \sin(6\phi) = 0. \tag{5.6}$$

The only solution above T_c ($a > 0$) is $Q_1 = Q_2 = 0$. Below T_c ($a < 0$), the above equation presents twelve possible solutions with $Q = Q_0 \simeq \sqrt{|a|/b}$, $\phi_n = n\pi/12$ ($n = 0, \ldots, 11$). However, the actual minima of the energy correspond to either $\phi_n = n\pi/3$ if $c' < 0$, or $\phi_n = (2n+1)\pi/6$ if $c' > 0$, where $n = 0, \ldots, 5$, unless higher-order terms are included [48]. Thus, the minimum energy state of the order parameter is six-fold degenerate. Therefore, the choice of any of those values by the order parameter breaks spontaneously the symmetry of the system whose phase is then said non-symmetric.

Regarding the dynamics, we neglect inertial terms and restrict ourselves to the over-damped dynamics of $\mathcal{Q}$ introducing the dissipative function $\mathcal{R}$, [4]

$$\mathcal{R} = \frac{\gamma}{2}(\dot{Q}_1^2 + \dot{Q}_2^2) = \frac{\gamma}{2}(\dot{Q}^2 + Q^2\dot{\phi}^2), \tag{5.7}$$

in accord with the Langevin force [59]. The inclusion of a dissipative term yields a dynamics of relaxation towards the equilibrium. This process introduce a characteristic time scale in the system. Neglecting the inertial terms is a valid approximation whether the typical time scales of the fluctuations of the field –which are induced by the thermal noise fluctuations– are much smaller than the relaxation time. In this regime, the thermal degrees of freedom can be regarded as white noise –that is, as an uncorrelated function in time. This is the case in many condensed-matter experiments.

All in all, the time evolution of the system is described by the stochastic diffusion equation (5.1) which contains a radial force f_Q acting upon the amplitude of the order parameter, and a tangential force f_ϕ upon its phase. For future purposes, it is convenient to distinguish three contributions to these forces as follows,

$$\begin{aligned} -\gamma\partial_t Q \equiv f_Q = & \underbrace{aQ + bQ^3 + \left[c + c'\cos^2(3\phi)\right]Q^5}_{\text{radial restoring force}} \underbrace{-g\left[\nabla^2 Q - Q(\nabla\phi)^2\right]}_{\text{radial tension force}} \\ & \underbrace{-f_1\cos\phi - f_2\sin\phi}_{\text{radial stochastic force}}, \end{aligned} \tag{5.8}$$

$$\begin{aligned} -\gamma\partial_t\phi \equiv f_\phi = & \underbrace{-c'\sin(6\phi)Q^4/6}_{\text{tangential restoring force}} \underbrace{-g\,Q^{-2}\nabla(Q^2\nabla\phi)}_{\text{tangential tension force}} \\ & \underbrace{+Q^{-1}(f_1\sin\phi - f_2\cos\phi)}_{\text{tangential stochastic force}}. \end{aligned} \tag{5.9}$$

Thus, we identify a *restoring force* associated to the effective potential; a *tension force* associated to gradient terms; and a *stochastic force* originated

from the Langevin term.

Finally, let us make some remarks about the boundary conditions of the problem. When the sample is isolated, the most suitable boundary conditions are the Neumann boundary conditions –*i.e.*, the annihilation of the derivative normal to the surface, $\mathbf{n} \cdot \nabla Q_{1,2}|_{\partial\Omega} = 0$. Physically, it means that the polarisation vector remains fixed at the boundary $\partial\Omega$, $\mathbf{n} \perp \partial\Omega$. This is what we have used in most of our simulations. We have also used periodic boundary conditions sometimes to simulate a larger sample. Although not considered in this work, there are experimental set-ups which requires different boundary conditions. For instance, in the experiments where the sample is in contact with some substrate [60], Dirichlet-like boundary conditions are more suitable, since the value of the field is fixed in the border.

5.1 Correlation lengths and relaxation times in the mean-field linear approximation

In this section we outline the definition of the correlation lengths and relaxation times in the mean field approximation, since equations can be obtained for the amplitude and phase zero modes, i.e., for uniform values of Q and ϕ, respectively.

In the symmetric phase, above T_c, the perturbations of the order parameter around its stable point $(0, 0)$ can be written such that $(Q_1, Q_2) = (0, 0) + (q_1, q_2)$. Thus, the effective Lagrangian associated to the Gaussian fluctuations is

$$\delta\mathcal{L} = \frac{g}{2}\left[\bar{\xi}^{-2}(q_1^2 + q_2^2) + (\nabla q_1)^2 + (\nabla q_2)^2\right], \tag{5.10}$$

where $\bar{\xi} = (g/a)^{1/2}$ is the correlation length, common to the q_1 and q_2 com-

ponents. Likewise, linearization of the equations of motion in the symmetric phase around $\mathcal{Q} = 0$, neglecting the Langevin force and the tensions, yields

$$-\partial_t q_{1,2} = (|a|/\gamma) q_{1,2}, \tag{5.11}$$

from which we identify $\bar{\tau} = \gamma/|a|$ with a relaxation time common to q_1 and q_2.

Below T_c, once in the non-symmetric phase, it is more convenient to write $\mathcal{Q}$ in terms of Q and ϕ instead. Hence, the value of the order parameter around any of the six minima of the effective potential can be written now as $(Q, \phi) = (Q_0, \phi_n) + (q, \varphi)$. In this case, the effective Lagrangian for the Gaussian fluctuations reads

$$\delta\mathcal{L} = \frac{g}{2}\Big\{\big[4\bar{\xi}^{-2} q^2 + (\nabla q)^2\big] + Q_0^2\big[\bar{\xi}_6^{-2}\varphi^2 + (\nabla\varphi)^2\big]\Big\}. \tag{5.12}$$

It is plain that, in addition to the correlation length of the amplitude zero mode, $\bar{\xi}$, there appears a second correlation length $\bar{\xi}_6 = [g/(3|c'|Q_0^4)]^{1/2}$ associated to the fluctuations of the phase zero mode, φ. Again, linearization around (Q_0, ϕ_n) as for equation (5.12) yields the following equations for the fluctuations of the amplitude and the phase modes, respectively,

$$-\partial_t q = \bar{\tau}^{-1} q, \tag{5.13}$$

$$-\partial_t \varphi = (3|c'|Q_0^4/\gamma)\varphi, \tag{5.14}$$

where both the Langevin force and the tension forces have been neglected. Again, φ presents a second relaxation time, $\bar{\tau}_6 = \gamma/(3|c'|Q_0^4)$.

As we see, the two components of the order parameter behave as equivalent degrees of freedom above T_c and there exist a unique correlation length and a unique relaxation time for both of them. In contrast, below T_c, there appears a second correlation length associated to the phase of the order parameter due to the $V_6(\mathcal{Q})$ potential.

Chapter 6

Accounting for thermal effects

In this chapter, we first introduce how the thermal effects are incorporated in models which use the Langevin prescription. Then, we discuss their limitations and propose an alternative method to take the thermal effects into account. Finally, we define the two methods to mimic a cooling quench that we have studied in detail.

6.1 Thermal fluctuations and renormalization of the mass term

Two are the contributions of the temperature which are relevant for the sort of systems we are interested in. First, the temperature plays the role of the control parameter which induces the transition point. As it is explained in chapter 1, the shape of the thermodynamic potential varies with the temperature. There is a critical value which defines the transition point. Above this point, only one minimum exits, and it is located at the origin. Below the critical point, the vacuum manifold degenerates and the symmetry of the state breaks spontaneously. The first scenario corresponds to a potential

whose mass term is positive; the second one, to a potential with a negative mass term. This is not the only thermal effect in the dynamics of the system. The fluctuations of the thermal degrees of freedom makes the field fluctuate. This is indeed a crucial contribution, since they force the field to move away from the equilibrium. Namely, they are responsible for the spontaneous symmetry breaking. Any model which describes a thermal phase transition need to reproduce this two features.

In the literature about models which employs the Langevin prescription, it is customary to take into account these two effects in two different ways. The Langevin term, $f_i(\mathbf{r}, t)$, is used to model the field fluctuations due to thermal effects. The variance of such term depends on the temperature T and the damping coefficient γ,

$$\langle f_i(\mathbf{r}, t) f_j(\mathbf{r}', t') \rangle = 2\gamma T \delta_{ij} \delta(\mathbf{r} - \mathbf{r}') \delta(t - t'). \tag{6.1}$$

It is uncorrelated in time since it accounts for thermal fluctuations which occurs much faster than the typical relaxation time of the field, as it was discussed in a previous chapter. However, this stochastic contribution is not used to explain the change in the shape of the potential. This feature is modelled by making the coefficient of the quadratic term of (5.2) to depend explicitly on the temperature as a linear function,

$$a = a_0 \frac{T - T_c}{T_c} = a_0 \epsilon, \tag{6.2}$$

where a_0 is a positive constant which represents the absolute value of the mass term at zero temperature and ϵ is the reduced temperature. It is clear from this assumption that the mass term has the correct sign for both regimes: above T_c and below T_c. Notice that in this case, the critical temperature is a free parameter which is fixed a priori. Some examples of this way to proceed can be found in references [49, 57, 61, 62, 63].

There are some aspects of this method which are worth remarking. First, in many cases, the temperature in the variance of the Langevin term (6.1) is not the same that the one which appears in the coefficient of the mass term $a(T)$ (6.2), although both are caused by the interaction of the system with the same thermal bath. Furthermore, when a quench is performed, the only temperature which changes in time is the temperature of the mass term, whilst the other remains constant. In fact, it is usual to considered the latter as a free parameter of the theory, which is chosen small with respect the mean value of a fluctuation of the field and constant in time. However, the most important issue is that, following this procedure, the effects of the interaction with the thermal bath might be counted twice. Indeed, the coefficient of the mass term is renormalized by the thermal noise. But this renormalization is omitted in this prescription, since the value of a is forced to vary with the temperature following an external imposition. There is no clear explanation on how the explicit variation of a with the temperature amounts to the renormalization due to thermal noise.

Bearing in mind this problems, we have opted for an alternative method to account for the thermal effects. We do not assume any dependence of the coefficient of the mass term on the temperature. It is fixed to a constant negative value, which amounts to the value of such coefficient at zero temperature. For convenience, let us write

$$a = -a_0, \qquad a_0 \geq 0, \tag{6.3}$$

It is important to distinguish between this nominal bare value, which is a free parameter to which we have access, and the effective value after the renormalization, which cannot be modified directly. The nominal bare value can be identified as the value of the coefficient at zero temperature. Indeed, at zero temperature there are no thermal fluctuations, so the value is not

renormalized and its effective value is the same as the nominal value.

The temperature only appears in the amplitude of the stochastic noise term. Let us define θ as the noise temperature. Then, the amplitude of the Langevin term A_L is

$$A_L = \sqrt{\frac{2\theta dt}{\gamma dx^3}}. \tag{6.4}$$

Here, dx and dt correspond to the discretized space-step and time-step in our simulations respectively [1].

At zero temperature, $\theta = 0$, there are no thermal fluctuations, since their amplitude is null. Therefore, no thermal renormalization occurs and the coefficient of the mass term is simply $a = -a_0$. At this temperature, a is clearly negative, so the system is in the broken phase. Once the temperature starts rising, thermal fluctuations appears and a is renormalized. As a result, its effective value is increased [3]. If the temperature is high enough, its effective value becomes positive, and the symmetric phase is restored. In this case, the critical temperature at which the transition happens is not a free parameter of the theory, as it is in the previous scheme, but a quantity which must be found. In figure 6.1, we present some numeric results which support this way to account for thermal effects. We have performed simulations at different temperatures θ without quench in order to study the value of some observables at thermal equilibrium.

We initialized the system at $\mathcal{Q} = (Q_0, 0)$, with $Q_0 \simeq \sqrt{a_0/b}$ being the value of the modulus of the field at zero temperature. We let the system evolve and reach an equilibrium. At this moment, we measure some observables, namely the mean of the modulus, $\langle Q \rangle$ and the mean value of each of the field components, $\langle Q_1 \rangle, \langle Q_2 \rangle$ (top figure) and its mean quadratic fluctuations

[1] An explanation of why the time-step and space-step must be included in the amplitude of the stochastic term can be found in the reference [59].

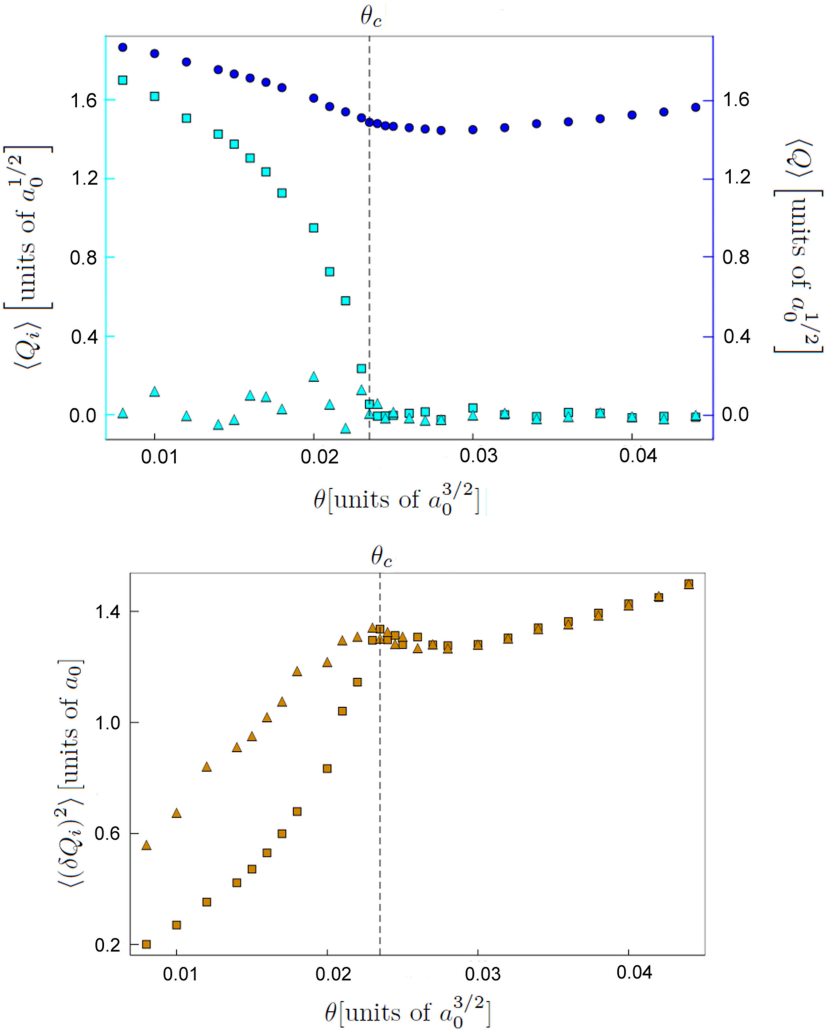

Figure 6.1: Top: mean value of the field components (Q_1 light blue squares, Q_2 light blue triangles) and mean value of the modulus Q (dark blue circles) versus temperature. Bottom: mean quadratic fluctuations of the field components ($(\delta Q_1)^2$ squares, $(\delta Q_2)^2$ triangles) versus temperature. Results for simulations with $a = -1$. The critical temperature is found to be $\theta_c = 0.0235$. a_0 is the fundamental unit of the system, to which all the others are referred.

$\langle (\delta Q_1)^2 \rangle$, $\langle (\delta Q_2)^2 \rangle$, where $\delta Q_i = Q_i - \langle Q_i \rangle$ (bottom figure).

In the top figure, we see that at low temperatures the mean equilibrium

value of the first component of the field (light blue squares) is different from zero, while the mean equilibrium value of the second (light blue triangles) remains zero. At higher temperatures, the mean value of the first component reduces its magnitude until it becomes zero at a certain critical temperature, θ_c. At this point, the symmetric phase is restored. Indeed, at temperatures above this one, the equilibrium value of the field is $\mathcal{Q} = (0, 0)$. Below θ_c, the mean equilibrium value of the modulus (dark blue circles) decreases as the critical temperature is approached. This is due to the decrease of the mean value of the first component of the field. However, for temperatures above the critical, it becomes larger and larger for higher temperatures. This is an effect of the thermal fluctuations, whose amplitude grows with the temperature. Thus, although the equilibrium value of the field in this regime is $\mathcal{Q} = (0, 0)$, its variance increases with the temperature.

In the bottom figure are depicted the mean quadratic fluctuations of both field components (orange squares for the variance of the first component and orange triangles for the variance of the second). Below the critical temperature, they increase with growing temperatures. Notice that the variance of the second component –which is initialized at zero– is larger than the variance of the first component –which is initialized at some non-zero value. Hence, in the initial set-up the first component represents the radial component whereas the second component represents the angular component. Since the potential only affects the radial component[2], it is natural that its variance is smaller. For temperatures above the critical, there is no difference between components. The behaviour of the mean quadratic fluctuations is the same as the mean modulus: they increase as the amplitude of the thermal

[2]We have set $c = c' = 0$ to perform these simulations, so the vacuum manifold is continuous and the angular mode is massless.

fluctuations does.

The above results correspond to simulations with a fixed bare value of the coefficient mass term, $a = -1$, and different temperatures of the Langevin term. We can also investigate the instance of fixed temperature and different values of a. Initial set-up of the field and the observables considered are the same as in the previous case. Results are shown in figure 6.2 for a fixed temperature of $\theta = 0.0235$. This corresponds to the critical temperature of the former set of simulations. Thus, we expect to find critical behaviour at $a = -1$.

Indeed, we see in the top figure that the mean value of the first component (light blue squares) is non-zero if the coefficient of the mass term is low enough –specifically, lower than $a = -1$. Lower values of a correspond to renormalized potential wells whose minima lays further from the origin. So the mean value of the first component of the field –which represents the radial component in the initial set-up– gets closer to zero as a increases. At $a = -1$, the mean value of this component becomes zero and the symmetric phase is restored. This is in agreement with the previous set of simulations. It still remains zero for higher values of a. On the other hand, the mean value of the second component (light blue triangles) remains zero –it initial value– for all values of a.

In the bottom figure of 6.2, mean square fluctuations of both components of the field grows as $a = -1$ is approached. This is a consequence of criticality. Values are finite rather than diverge because the size of the system is finite. Notice that the mean square fluctuations of the two components take the same value above $a = -1$ –*i.e.*, when the symmetric phase is restored– and differs below $a = -1$, with the fluctuations of the second component (orange triangles) –which corresponds to the angular mode– being larger than

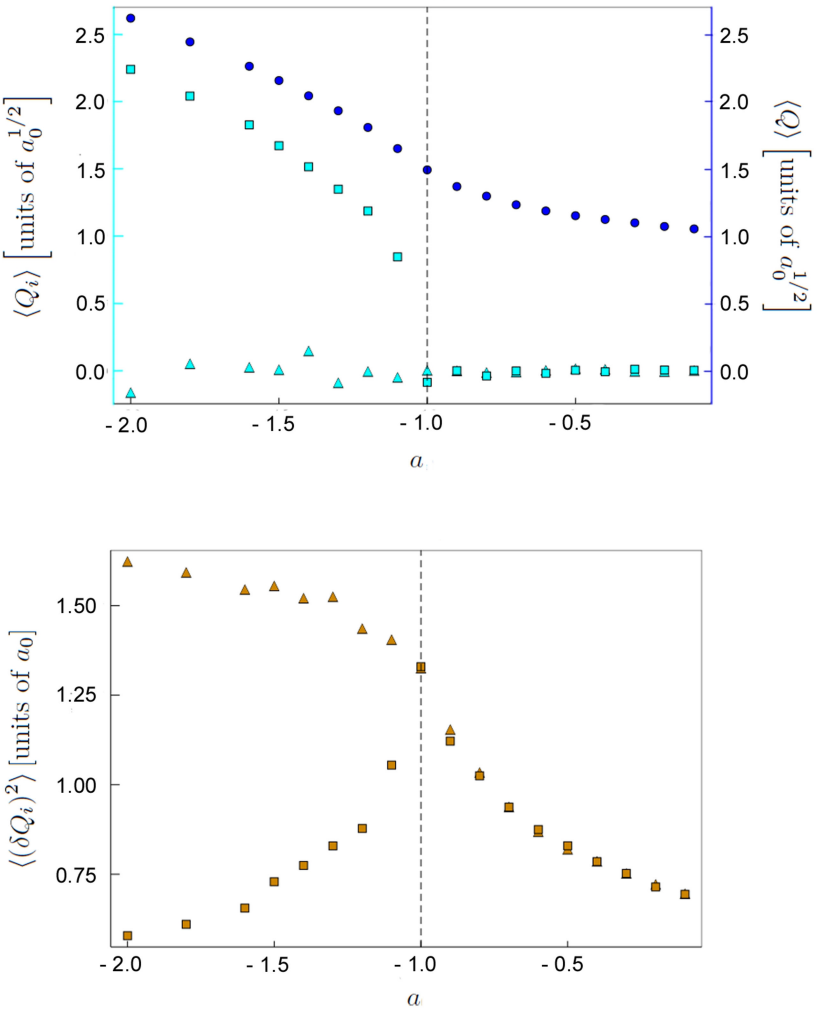

Figure 6.2: Top: mean value of the field components (Q_1 light blue squares, Q_2 light blue triangles) and mean value of the modulus Q (dark blue circles) versus a. Bottom: mean quadratic fluctuations of the field components ($(\delta Q_1)^2$ squares, $(\delta Q_2)^2$ triangles) versus a. Results for simulations with $\theta = 0.0235$. Dashed black line corresponds to $a = -1$. Simulations with this value of a and different temperatures are depicted in figure 6.1.

the fluctuations of the first component of the field (orange squares) –which represents the radial component. This can be explained with the same arguments as in the previous case: the synamics of the radial component is subjected to restoring forces which confine it in a potential well. Hence, its values is less disperse. On the contrary, the angular mode is not affected by the potential and its dispersion is larger.

Notice that in this case, the value of the mean modulus (dark blue circles, top figure) decreases monotonically. So do the mean square fluctuations of the field for values above $a = -1$. This is in contrast with the previous set of simulations, where they become larger and larger as the symmetric phase is consolidated. In the former case, this is a consequence of considering thermal fluctuations of increasing size. In the latter case, the size of the thermal fluctuations is always of the same size, since the temperature is constant. When the potential is flat enough –*i.e.*, $|a|$ is low enough–, the energetic barrier which separates the vacuum and the maximum at the origin can be easily surpassed by the thermal fluctuations. From this moment, the components of the field are not confined by the quadratic term of the potential, but by the quartic. Increasing values of a make the shape of this quartic well narrower. Since the size of the fluctuations remains constant, the narrower the quartic well walls are, the smaller the dispersion of the field is.

In both sets of simulations, we use a_0 as the fundamental unit of the problem, to which all other quantities refer to. This is also true for the rest of simulations in this chapter. In cases where the value of the coefficient of the mass term varies –as in this second set of simulations– we take as reference the case with $a = -1$. To avoid misunderstanding, in such cases we rather use $a = a'_0$ to note different values of a. Hence, the varying a'_0 is

noted differently than the a_0 used as reference.

6.2 Cooling quench

Let us focus our attention to the way of cooling a system. As a first approximation, the temperature can be made to decrease linearly with the time. As commented at the former section, in the literature it is customary to make the coefficient a a explicit function of the temperature, $a = a_0(T - T_c)/T_c = a_0\epsilon$. Let us define τ_q as the typical time scale of the quench, and the quench rate r'_q as the inverse of this time. Then,

$$\epsilon = \epsilon_{init} - r_q t = \epsilon_{init} - \frac{t}{\tau_q}. \tag{6.5}$$

This quench only modifies the temperature which appears in this term, whilst the temperature in the amplitude of the noise term remains constant and small enough so as to hardly affect the dynamics of the phase transition. Since the mass term does not depend explicitly with the temperature in our alternative approach to account for thermal effects, this way to simulate a quench is not useful.

Let us introduce two different ways to perform a quench in our model, where the temperature only appears in the amplitude of the Langevin term. This two methods can be related, as we will explain later. The first method consist of forcing this temperature to decrease linearly in time,

$$\theta = \theta_{init} - R_q t. \tag{6.6}$$

In our simulations of quenches, we will start at a temperature θ_{init} above the critical θ_c. The critical temperature which has been already found numerically through simulations at thermal equilibrium such as the ones discussed above. We let the system evolve at that temperature in the symmetric phase

for some time, so it is thermalised before the quench starts. When the quench begins, the temperature decreases. At some point, the critical temperature θ_c is crossed and the system enters in the broken phase. There it evolves for some time, until some final temperature θ_f is reached and the quench ends. Then, we let the system evolve at this final temperature without varying the temperature anymore.

The second method to quench a system consist of forcing the mass-term coefficient to increase linearly in time,

$$a = a_{init} - \rho_q t. \tag{6.7}$$

In this case, the temperature of the Langevin term remains constant, whereas the potential changes. To vary a amounts to effectively change the critical temperature. Indeed, flatter potentials need smaller thermal fluctuations for the symmetric phase to be recovered. That is, the critical temperature decreases as a increases. In this case the phase transition process is as follows. We start at a given temperature, θ, which will be the same during all the process, and a given value of a which guarantees that the critical temperature is below θ. We let the system evolve for some time to ensure that the system is thermalised and then the quench starts. As the parameter a is decreased with time, the effective critical temperature increases. At the transition point, the critical temperature reaches the value of the temperature of the noise term. As time evolves further, the critical temperature becomes bigger than θ, that is, the system is in the broken phase. When the quench stops, we let the system evolve at that final a for some time without no further changes in the shape of the potential.

This second method may seem the same as the one which is usually employed in the literature: the noise term is kept constant whereas the mass term is decreased. Nevertheless, there are important differences between

them. In our approach, the nominal value of a is always negative. The required change in sign for a phase transition to be possible is due to the thermal fluctuations which renormalizes the coefficient. This is in contrast with the usual method, where the change in sign of this coefficient is an external imposition. In the second place, in the usual approach, the critical temperature is a free parameter of the theory. Once fixed, it remains constant during the quench. Conversely, in our approach the critical temperature effectively changes with the mass term coefficient.

The two methods to perform quenches according to our formalism can be related. The quench rate for the first method, introduced in (6.6), can be defined as $R_q = -\partial\theta/\partial t$. In a similar way, we define the quench rate of the second method (6.7) as $\rho_q = -\partial a/\partial t$. In order to compare them, the quench rate ρ_q need to be expressed in the same units as R_q. Let us define R'_q as the rate at which the effective critical temperature changes in the second scenario, *i.e.*, $R'_q = \partial\theta_c/\partial t$. Making use of the chain rule, we can write

$$\rho_q = -\frac{\partial a}{\partial t} = -\frac{\partial a}{\partial \theta_c}\frac{\partial \theta_c}{\partial t} = -\frac{\partial a}{\partial \theta_c}R'_q. \tag{6.8}$$

Rearranging, we obtain an expression of R'_q in terms of ρ_q,

$$R'_q = -\left[\frac{\partial a}{\partial \theta_c}\right]^{-1}\rho_q. \tag{6.9}$$

Once quench rates are expressed in the same units, comparisons between them are possible.R_q and R'_q can be redefined so as to be conveniently expressed in units of inverse time. This is achieved by dividing both rates by some common temperature θ.

The dependence of a on the effective critical temperature θ_c is shown in figure 6.3. In the range of relevant values of a, this dependence is approximate linear. Each point has been computed numerically in the same

manner as it was done previously in this chapter –cf. figure 6.1. Namely, for a set of simulations with the same fixed value of a, we identify the critical temperature as the one at which the first component of the field vanishes. It coincides with the temperature at which the mean square fluctuations of both components become the same.

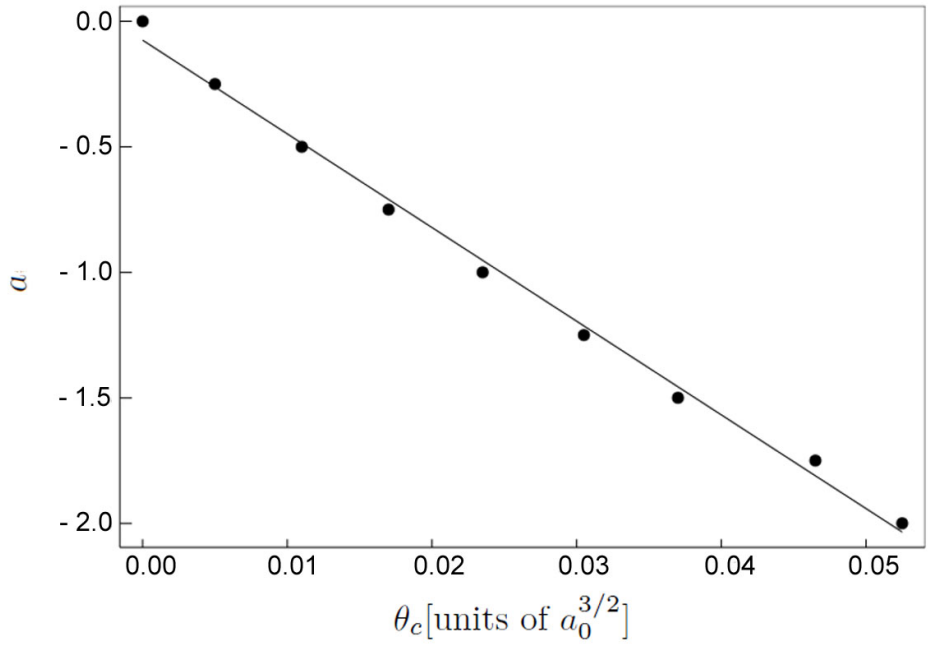

Figure 6.3: Functional dependence of a on the effective critical temperature θ_c. A linear fit yields $a = -37.32\,\theta_c - 0.08$.

To conclude this section, let us include a specific regime of quenches, which can be regarded as a limit case of the above methods. In reference [58], we investigate the formation of vortices under extremely-fast-quenching conditions. An ultra-fast quench refers to a quench which is fully accomplished in times much shorter than any other relevant time scale of the problem. This implies that the vortices emerge in a process that is entirely driven by the dynamics of the system after the quench. In particular, the order-parameter correlations evolve according to its diffusive fluctuating dynamics at the fi-

nal temperature of the quench, rather than being imprinted by its critical behaviour just before the freezing. This is simulated by initializing the field in the origin –*i.e.*, the equilibrium state in the symmetric phase, before the quench starts– and letting it evolve according to the potential at the final temperature –*i.e.* the final form of the potential after the quench ends. To investigate this scenario, we have not used the formalism developed in this chapter, but the one usually employed in the literature, with the exception that we have evaluated at the same temperature both the noise term and the mass term. Since there are no finite quench rates in this limit case, the reinterpretation in terms of the new formalism is straightforward. It can be thought as a limit case of any of the two quench methods introduced in this chapter, where R_q or R'_q tends to infinity.

Chapter 7

Results

In this chapter, we present the results of numerical simulations considering three different situations. First, we consider the limit case of quenches in the ultra-fast regime, where the relevant quantity to describe the phenomenology is not the quench rate, but the final temperature [58]. In the second place, we perform some quenches at different rates varying the temperature of the thermal noise term θ for a fixed value of the mass term coefficient a –equation (6.6). Lastly, we investigate how the system behaves when the quench modifies the mass term a whilst maintaining the amplitude of the thermal fluctuations θ –equation (6.7).

In all these cases, a phase transition occurs during the quench of the system. This induces the formation of topological defects –vortices. We provide a detailed description of the different regimes in which the process can be split and discuss the underlying physical mechanisms. We also pay attention to the evolution of the network of defects once they are formed.

We base our study on data obtained from a set of relevant observables. These observables are the mean modulus of the field through the time, $\langle Q \rangle$; the mean absolute value of the forces which acts on the angular component of

the field, $\langle |f_\phi| \rangle$ –this force is defined in (5.9)–; and the density of total defects measured in the equatorial plane of the sample n. The two first observables are straightforward to measure. Conversely, the total number of defects is challenging to determine. Two are the reasons for such difficulty. First, the data are inherently noisy, since equations of motion include an stochastic term which acts at every time-step. Secondly, the process of formation domains of homogeneous phase is not clearly bounded in time. A discussion about how to overcome these difficulties can be found in chapter 11.1, where the algorithm used to perform this measurements is presented and analysed.

From the data provided by the two first observables, we are able to identify some remarkable features in the dynamics of the system along the quench. We will use them to bound different regimes and define relevant times. The number of total defects at these times are used to test the KZ predictions. Furthermore, we will use the time-evolution of the number of defects to get some insight into the annihilation process of vortices which follows after their formation.

This chapter is organised as follows. In section 7.1, we collect all the technical details of the simulations. In sections 7.2, 7.3.1 and 7.3.2, we present the results of the numeric simulations performed according to the three different scenarios stipulated above.

7.1 Technical details of the simulations

Simulations in the ultra-fast regime

In this limit case, we consider two different situations. In the first place, we consider that the system is effectively $U(1)$-symmetric, and refer to this situation as *weak-anisotropy regime*. That is, we choose the parameters in the

potential V_T such that the anisotropic term becomes irrelevant, i.e., $V_T(\mathcal{Q}) \approx V(Q)$. In particular, for the simulations in subsection 7.2.1, we take for the side lengths, $L_x = L_y \approx 400\, l$, $L_z \approx 120\, l$ –recall that l is the lattice spacing. The discretized version of the algorithm to integrate the equations of motion is explained in chapter 9. The numerical values of the parameters in those equations are $a_0 = 1$, $b = 2$, $c = 0$, $c' = 2/3$, $g = 1$, $T_c = 0.0025$, which are chosen such that $a_0^{-1/2}$ becomes the unit of length scale and, at temperature $T_c/2$, $\epsilon = -0.5$, $\bar{\xi}(T_c/2) = 1/\sqrt{2}$, and $\bar{\tau}(T_c/2) = 0.2$ for $\gamma = 0.1 a_0^{1/2}$. In terms of the correlation lengths and relaxation times of the mean field approximation, this implies also that $\bar{\xi} \ll \bar{\xi}_6$, $\bar{\tau} \ll \bar{\tau}_6$ in the weak-anisotropy regime –cf. table 7.1 below.

As for the situation in which $V_6(\mathcal{Q})$ becomes relevant, that we refer to as *strong-anisotropy regime*, the coefficient c' is enlarged so that the phase zero mode gets massive and the relationship between the mean field correlation lengths and relaxation times turns into $\bar{\xi} > \bar{\xi}_6$, $\bar{\tau} > \bar{\tau}_6$. In particular, for the simulations in subsection 7.2.2, we take for the side lengths $L_x = L_y = 1314 l$, $L_z = 43\, l$. The numerical values of the rest of parameters are as in the weak-anisotropy regime, except for the value of c' that is taken $c' = 128/3$. Simulations in the strong-anisotropy regime are performed for a single final temperature, $\epsilon_f = -0.3$, for which $\bar{\xi} = 0.71$, $\bar{\xi}_6 = 0.59$.

Since the vortex radius scales approximately with the minimum correlation length of the mean field approximation, the lattice spacing l is adapted in either case to each temperature according to the formula $l = \min(\sqrt{2}\bar{\xi}, \bar{\xi}_6)/4$.

It is worth mentioning that, with the numerical values chosen for the parameters, the Ginzburg region reduces to $\epsilon \in [-3.96 \cdot 10^{-10}, 3.96 \cdot 10^{-10}]$, which is negligible in all our simulations. Therefore, effects related to the strongly nonperturbative dynamics of the order parameter within this region

can be fairly discarded. Lastly, the boundary conditions imposed upon $\mathcal{Q}$ are of the kind of no-flux boundary conditions.

In all the simulations we consider ultra-fast quenches from the initial temperature $T_i > T_c$ in the symmetric phase, to the final temperature $T_f < T_c$, assuming a uniform rate $(T_f - T_i)/\tau_{cool}$ with τ_{cool} being the cooling time. Ultra-fast quenches are defined by the inequality

$$\tau_{cool}(T_c - T_f)/(T_i - T_f) \ll \tau_0, \tag{7.1}$$

where the term on the left hand side of this inequality is the time lapse corresponding to the temperature interval $[T_c, T_f]$, and τ_0 is the vortex formation time measured from the time the quenching passes through T_c. This means that the time spent by the system during the quench below T_c is negligible in comparison to the vortex formation time τ_0. Also, it implies that its dynamics is independent of the initial temperature. Important is to note that in our simulations the stochastic forces act on the system all the way through from the start. Finally, since the dynamics of $\mathcal{Q}$ from equations (5.8) and (5.9) is determined by the ratio T/γ, we fix the value of the diffusion coefficient at $\gamma = 0.1 a_0^{1/2}$ in all the simulations without loss of generality.

Simulations for finite quench rates

This are the data for simulations in sections 7.3.1 and 7.3.2.

We perform numerical simulations on a cubic sample. In this two cases, we consider that the system is $U(1)$-symmetric. That is, we choose the parameters in the potential V_T such that the anisotropic term is absent –*i.e.*, $V_T(\mathcal{Q}) = V(Q)$. For the simulations in sections 7.3.1 and 7.3.2, we take side lengths $L_x = L_y = 800\, l$, $L_z = 3\, l$, where l is the lattice spacing, which takes the constant value $l = 0.2$ in all the simulations. We impose periodic

boundary conditions in the $z-$direction and Neumann boundary conditions in the others. Thus, we are effectively dealing with two-dimensional samples. The dynamics of the order parameter is governed by a discretised version of the equations (5.8) and (5.9). The numerical implementation of the boundary conditions and the algorithm to integrate these equations is explained in chapters 8 and 9 respectively.

The numerical values of the parameters in those equations are $a = -a_0$ $b = 0.25$, $c = c' = 0$, $g = 0.06$. In all simulations $a_0^{-1/2}$ is the unit of length scale. We fix the value of the diffusion coefficient at $\gamma = 0.5 a_0^{1/2}$ in all the simulations without loss of generality.

For simulations in section 7.3.1, the coefficient a is set to $a = -1$ for all simulations. The initial and final temperatures for all quenches are, respectively, $\theta_{init} = 0.042$ and $\theta_f = 0$. In section 6.1, it is shown that the critical temperature for this set-up is $\theta_c = 0.0235$. Thus, the initial and final reduced temperatures are $\epsilon_{init} = 0.8$ and $\epsilon_f = -1$.

For simulations in section 7.3.2, the temperature is $\theta = 0.0235$ for all simulations. In this case, the quench modifies the values of the mass parameter. Its starting value is $a_{init} = -0.267$ and its final value is $a_f = -1.83$ for all cases. Quenches rates of both simulations are chosen to be the same in both scenarios. They can be related through (6.9).

7.2 Ultra-fast quenches

7.2.1 Vortex formation at weak-anisotropy

First, we analyse the effective $U(1)$-symmetric case in which the six-fold anisotropy of our model is extremely weak. That is, the case in which the phase zero mode is effectively massless and the tangential restoring force in

equation (5.9) is negligible.

In our analysis, we first define the time τ_0 at which primordial vortices form as the time at which a pattern of domains of well-defined uniform and stable phase ϕ shows up for the first time. This is the relaxation time of the phase ϕ, and can be determined from the tangential force f_ϕ acting on ϕ –see equation (5.9). The behavior of the sample-averaged strength of this force $\langle |f_\phi| \rangle$ as a function of time is illustrated in figure 7.1(a) for $\epsilon_f = -0.3$.

As we can see, this force drops to a small asymptotic value signaling the formation of metastable domains. In such a quasi-stationary state, only the stochastic component of equation (5.9) survives. Therefore, since the anisotropic tangential restoring force term in equation ()refeqd is negligible, we infer that it is the tangential tension force that causes the relaxation of ϕ until domains of quasi-uniform phase get formed. This is nothing but the realization of the geodesic rule in a second order phase transition, formulated for the first time by Kibble in first order phase transitions [1, 11].

Thus, τ_0 can be identified with the time at which the slope of the tangential force at its saddle point intercepts its long-time asymptote –see figure 7.1(a). We use this time to define the density of primordial vortices, $n_0 \equiv n(\tau_0)$, which further evolves in time as illustrated in figure 7.1(b).

To further clarify the evolution of the vortex distribution we track the related changes in the amplitude of order parameter. These changes reveal three dynamical regimes –see figure 7.1(a). In a first stage, the linear dynamics of Q is dominated by its diffusion in configuration space as a result of the stochastic force. Diffusion dominates completely the dynamics up to certain *diffusion time*, τ_d, at which $\mathcal{Q}$ starts rolling down the effective potential and non-linear effects become apparent. Diffusion causes an effective delay of the phase transition, whereas the steep descent is caused by the radial restoring

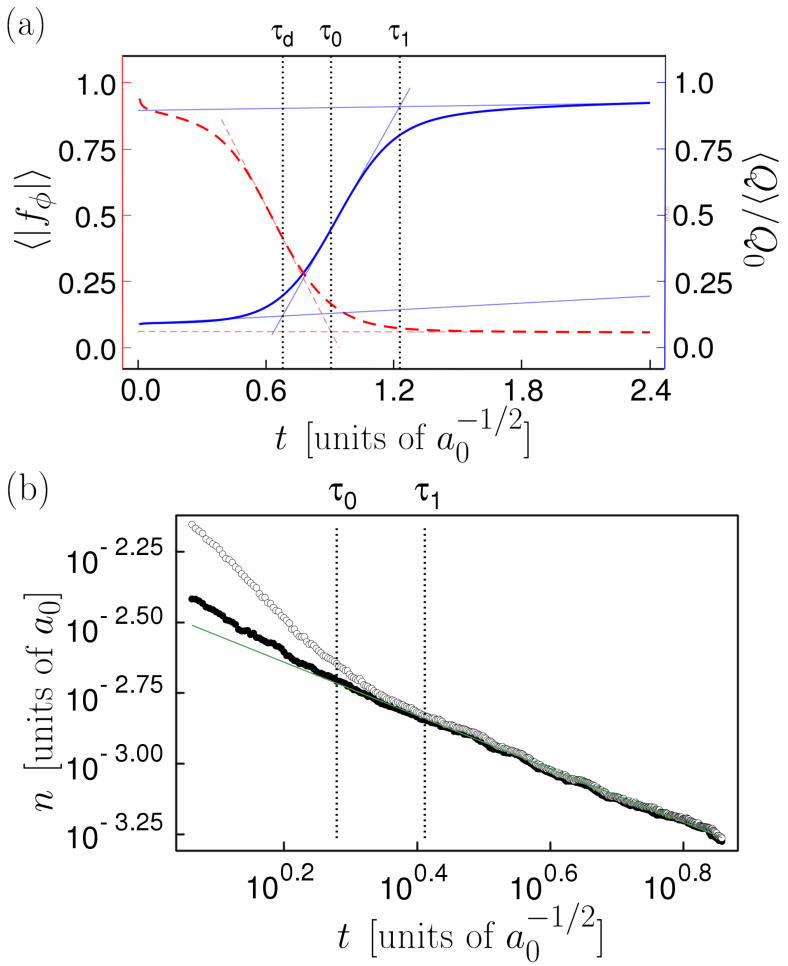

Figure 7.1: (a) Sample-averaged tangential force strength (dashed red, in arbitrary units) and normalized amplitude of the order parameter (solid blue) as a function of time, in the weak-anisotropy case, for $\epsilon_f = -0.3$. The vertical dotted lines indicate the diffusion time, τ_d, the phase relaxation time, τ_0, and the vortex consolidation time, τ_1, as defined in the main text. (b) Graphical determination of the corresponding vortex density as a function of time (log-log scale). The same power-law behavior is obtained according to two different methods (solid and open circles, respectively, cf. section 11.1) beyond τ_1.

force which derives from the effective potential. The phenomenon of *delayed bifurcation* was firstly noticed by Lythe in the dynamics of the phase transition of a field theory [57]. However, in contrast with Lythe's approach and other works [49, 61], our treatment of the Langevin term –the temperature in the amplitude of the Langevin term is the same as the temperature in the mass term– causes the control parameter ϵ (analogous to the bifurcation parameter in reference [57]) to take its final value much earlier than τ_d. In fact, once the system is below the transition point, the stochastic Langevin force is the dominant force all the way until the diffusion time τ_d is reached. This prevents the formation of actual vortices during the quench towards the final temperature, and thus any scaling with the quench rate. This condition is in fact an alternative definition for the ultra-fast character of the quench. Accordingly, the order parameter starts deviating from zero much later than the moment at which the reduced temperature has reached its final value ϵ_f.

Subsequently, the amplitude Q eventually reaches its equilibrium value, Q_0, at any of the six minima of the effective potential, except at those points where the transition is frustrated by the presence of the topological defects. We identify this event with the *vortex consolidation time*, τ_1, which is slightly longer than τ_0. τ_1 is the relaxation time of the amplitude Q, and thus signals the accomplishment of the phase transition. In fact, during the intermediate regime between τ_d and τ_1, Q is mainly driven by the radial restoring force –see equation (5.8), while in the final stage the stochastic force takes over so that the total radial force f_Q tends to an asymptotic stationary value. The consolidation time τ_1 is thus associated to the crossover between these two regimes –see figure 7.1(a).

The evolution of the vortex pattern obtained in this case is illustrated in figure 7.2.

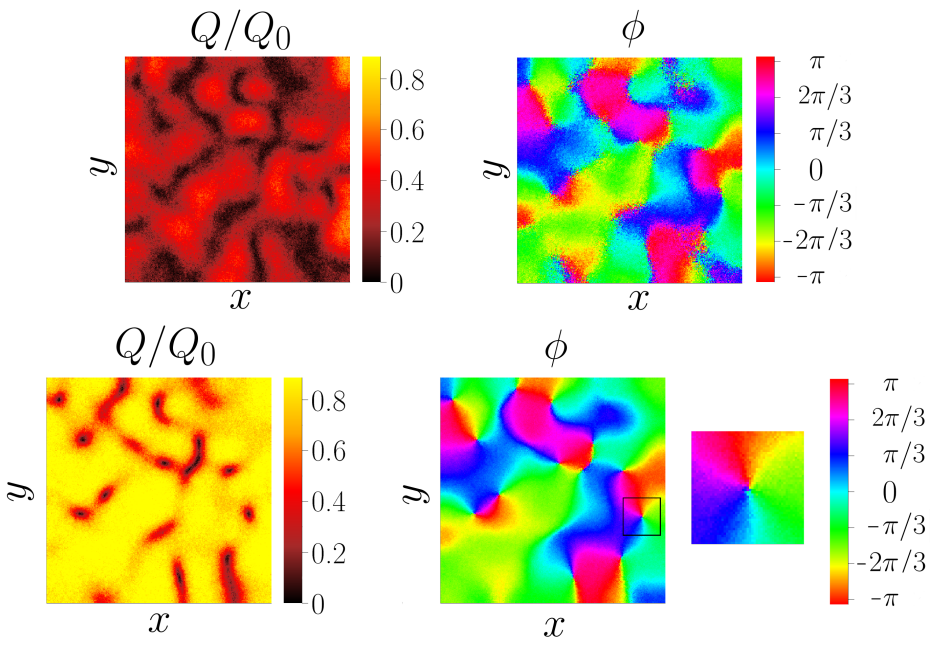

Figure 7.2: Snapshots of the amplitude Q (left) and the phase ϕ (right) of the order parameter in the weak-anisotropy case for $\epsilon_f = -0.7$. They illustrate the distribution of vortices at the formation time τ_0 (primordial vortices, top) and at the vortex consolidation time τ_1 (bottom). The zoomed area emphasizes the $U(1)$ character of the vortices in this case.

The density of primordial vortices n_0 as a function of the final reduced temperature ϵ_f is summarized in table 7.1, together with the average distance between those vortices, $\xi_0 \simeq n_0^{-1/2}$, relaxation times and mean field values –cf. section 5.1.

We note that the density of primordial vortices increases monotonically with the decrease of ϵ_f (so that the average distance between vortices decreases). The three characteristic times, in their turn, decrease as the final temperature of the quench does. We interpret that these tendencies have their root in the diffusive dynamics of the order parameter in configuration space, which is enhanced by the temperature. That is, the higher the tem-

ϵ_f	-0.3	-0.4	-0.5	-0.6	-0.7	-0.8
$n_0[a_0]$	0.0021	0.0027	0.0036	0.0041	0.0042	0.0054
$\xi_0[a_0^{-1/2}]$	21.77	19.21	16.61	15.56	15.35	13.64
$\bar{\xi}$	0.91	0.79	0.71	0.65	0.60	0.56
$\bar{\xi}_6$	4.71	3.54	2.83	2.36	2.02	1.77
$\tau_d[a_0^{-1/2}]$	1.4	1.1	0.88	0.77	0.68	0.62
τ_0	1.9	1.4	1.1	0.97	0.82	0.71
τ_1	2.61	1.98	1.59	1.37	1.19	1.05
$\bar{\tau}$	0.33	0.25	0.20	0.17	0.14	0.13
$\bar{\tau}_6$	2.2	1.3	0.80	0.56	0.41	0.31

Table 7.1: Compilation of the results of the numerical simulations for different final temperatures, ϵ_f, in the weak-anisotropy regime. Lengths and times are given in units of $a_0^{-1/2}$, whereas the values for n_0 are in units of a_0.

perature, the longer the period in which the stochastic force causes $\mathcal{Q}$ to fluctuate randomly around $\mathcal{Q} = 0$. Hence, τ_d increases with the final temperature. In turn, diffusion slows down the rolling of $\mathcal{Q}$ towards any of the minima at $Q = Q_0$, delaying this way the start of the non-linear dynamics and thus the relaxation processes. The latter implies that τ_0 and τ_1 do also increase with the final temperature. In addition, the persistent thermal fluctuations after the diffusion period do also enhance the periods of relaxation of the phase and the amplitude of the order parameter, causing an increase of the time intervals, $\tau_0 - \tau_d$ and $\tau_1 - \tau_0$, with the final temperature. Altogether, it results in an effective increase of the vortex separation with the final temperature of the quench.

It is also remarkable that the computed vortex correlation lengths, ξ_0, and

relaxation times, τ_0 and τ_1, differ in an order of magnitude with respect to the values computed in the mean-field linear approximation. Yet, the relative variations of ξ_0, τ_0 and τ_1 with the temperature are approximately proportional to the variations of the mean-field correlation lengths and relaxation times, respectively, as illustrated in figure 7.3 for the lengths.

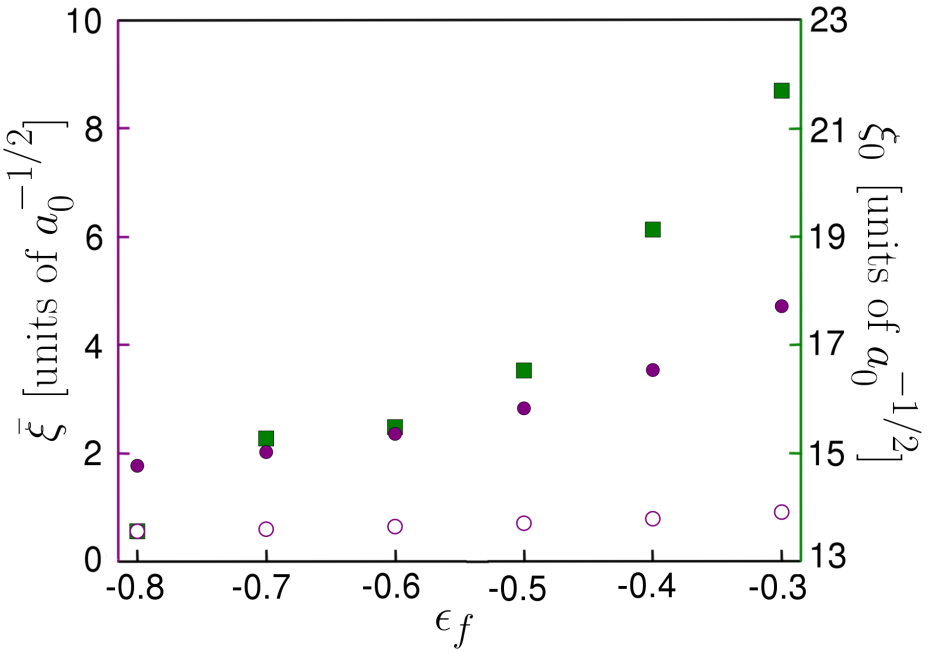

Figure 7.3: Average distance between vortices, ξ_0, as a function of the final temperature of the quench ϵ_f in the weak-anisotropy regime (squares), compared to the mean-field correlation lengths, $\bar{\xi}$ (open circles) and $\bar{\xi}_6$ (solid circles).

The extrapolation of this result to the standard KZ picture implies that the non-universal prefactor of the KZ scaling can play a role for the quantitative analysis of the vortex formation. Finally, it is worth noting that, in comparison to previous works in which the amplitude of the noise term is considered small [49, 57, 61], the vortex density here is not affected by

the relationship between that amplitude and the quench rate, but by the relationship of the final temperature and the damping rate.

7.2.2 Vortex formation at strong-anisotropy

Next, we investigate the impact of the six-fold anisotropy on the formation of vortices. Thus, we consider the extended $\mathbb{Z}_6$ case described by equation (5.2) in which the phase zero mode becomes massive as described in section 5.1. As previously mentioned, this is the situation found in hexagonal multiferroic manganites [46, 47, 48].

Compared with the previous $U(1)$ situation, the diffusion regime is shortened –see figure 7.4(a). This is mainly due to the additional contribution to radial restoring force generated by the anisotropy. However, the phase relaxation interval extends longer due to the anisotropy contribution to the tangential restoring force that opposes to the balance of the tangential tension (that is, $\tau_0 - \tau_d$ increases).

As a result, the phase relaxation time τ_0 is approximately equivalent in both cases –see figure 7.4(a), which further yields a similar density of primordial vortices –see figure 7.4(b). Lastly, once the phase gets relaxed, it takes shorter for the vortices to consolidate under the action of the additional anisotropic radial restoring force. We note that, due to the increased size of the vortex cores, the sample-averaged amplitude $\langle Q \rangle$ is noticeably smaller than its equilibrium value Q_0 at all times –see figure 7.4(a). This was previously pointed out in [46] from an experimental analysis of the static distribution of an order parameter described by the same $\mathbb{Z}_6$ model.

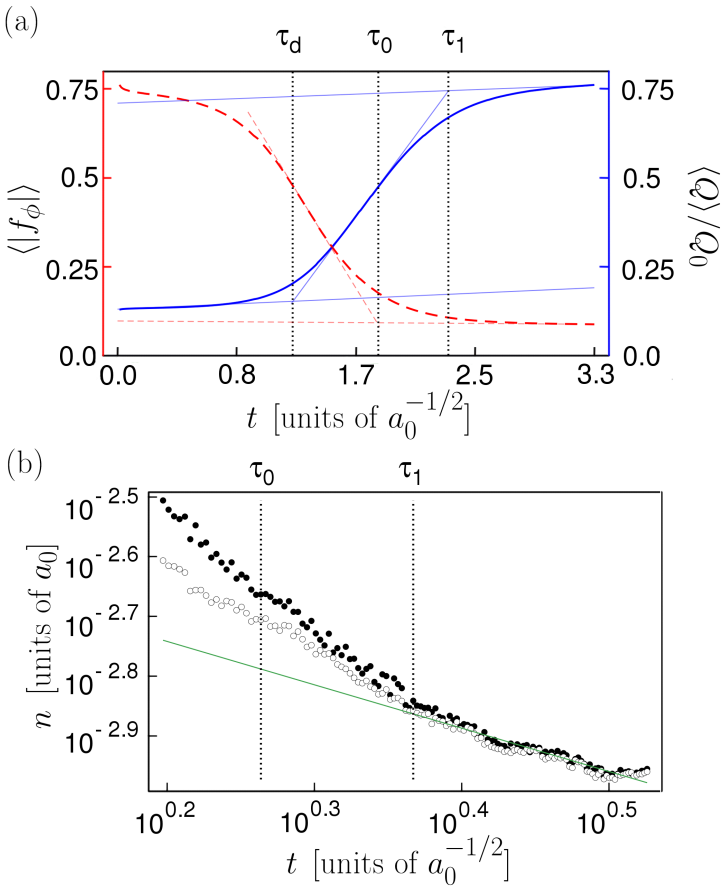

Figure 7.4: (a) Sample-averaged tangential force strength (dashed red, in arbitrary units) and normalized amplitude of the order parameter (solid blue) as a function of time in the strong-anisotropy case for $\epsilon_f = -0.3$. The vertical dotted lines indicate the diffusion time, τ_d, the phase relaxation time, τ_0, and the vortex consolidation time, τ_1, as defined in the main text.
(b) Graphical determination of the corresponding vortex density as a function of time (log-log scale). The same power-law behavior is obtained according to two different methods (solid and open circles, respectively –cf. section 11.1) beyond τ_1.

7.2.3 Vortex network evolution

Finally, we analyse the subsequent evolution of the vortex network and, in particular, the vortex-antivortex annihilation process that eventually results in a homogeneous non-symmetric phase[1]

For this purpose, we fit the time evolution of the vortex density for each of the temperatures of the quench to a power-law function $n(t) \simeq n(\tau_1)/t^{\alpha}$ for $t \geq \tau_1$, as shown in figures 7.1(b) and 7.4(b). We find $\alpha \approx 1$ in the $U(1)$ weak-anisotropy case and $\alpha \approx 3/4$ in the $\mathbb{Z}_6$ strong-anisotropy one. This means that, despite the fact that the overlap between vortices is larger in the strong-anisotropy case for the vortex core is larger, the annihilation rate is slower. This signals the impact of the $\mathbb{Z}_6$-anisotropy in the short-range vortex-antivortex interaction.

7.3 Finite quenches

7.3.1 Quenches varying the temperature of the Langevin term

In this section, we perform simulations varying the temperature of the Langevin term, while maintaining the bare coefficient of the mass term fixed. As in the previous case, let us first focus our attention on the sample-averaged absolute value of the force on the phase mode and the normalized sample-averaged modulus. Their time evolution is shown in figure 7.5.

In this case, the time evolution also involves a change in temperature, so the comparison with the results of the previous section is not straightforward.

[1] See the supplemental material of reference [58] for a movie illustrating the evolution of the complete thermalization process.

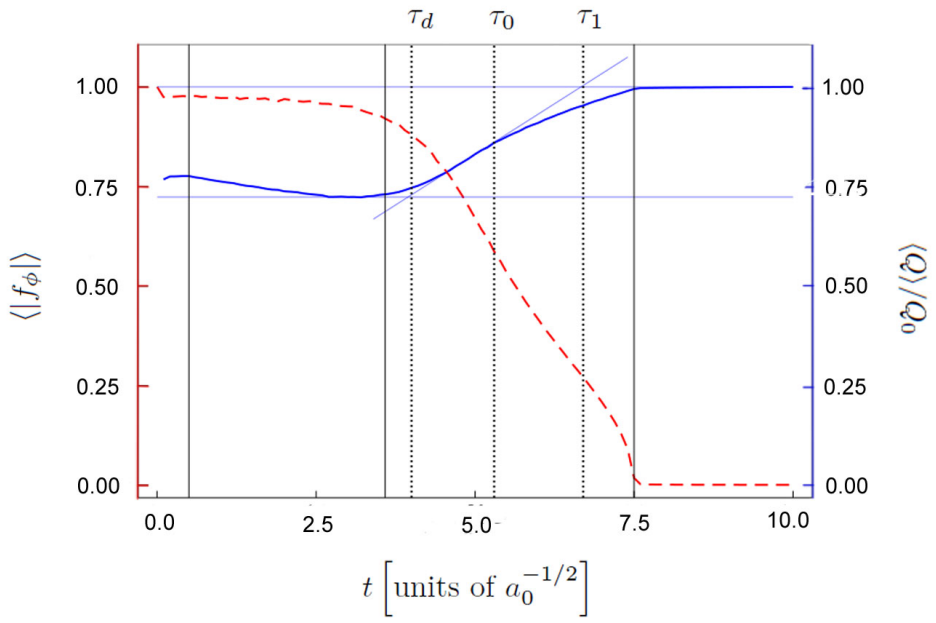

Figure 7.5: Sample-averaged tangential force strength (dashed red, in arbitrary units) and normalized amplitude of the order parameter (solid blue) as a function of time, for $R_q = 0.255$. The vertical solid lines represent, form left to right, the time at which the quench starts, the time at which the critical temperature is reached, and the time at which the quench ends. The vertical dotted lines indicate the diffusion time, τ_d, the phase relaxation time, τ_0, and the vortex consolidation time, τ_1, as defined in the main text.

However, we see that the qualitative behaviour of the curves is similar. Thus, we can exploit this fact to interpret the physics of this quench in the same terms as in the former case, highlighting and explaining the main differences.

As in the previous case, let start our analysis with the forces on the angular phase. The system starts at a temperature above the critical and evolves without quenching for some time, up to the first solid vertical line – see figure 7.5. At that moment, the temperature starts to decrease. However, we see that it remains more or less constant up to the second solid vertical

line, which represents the time at which the critical temperature is reached. From that moment, the curve drops until the quench ends (third solid vertical line) and the force almost vanishes. In this case, we have chosen the final temperature to be zero. Thus, the only surviving contribution in (5.9) is the tangential force[2]. The reason for this asymptotic value to be so small is that the relative weight of the Langevin contribution is in this case much larger than in the previous case.

The curve behaves smoothly everywhere except in the last interval of the quench, where a small bump is appears. This is due to the fact that the amplitude of the stochastic term decreases as $\sim \theta^{1/2}$ –see equation (6.4)–, so near $\theta = 0$ its derivative diverges. This implies that the langevin force changes sharply in the limit $\theta \to 0$. We can still use this force to define the time τ_0 of formation of primordial vortices. However, the criterion employed in the previous section it is no longer valid. Indeed, the intersection of the tangent at the saddle-point and the asymptotic value of $\langle |f_\phi| \rangle$ does not only depend on the quench rate, but also on the final temperature –the higher the final temperature, the higher the asymptote at late times, so the intersection point is not always to same. To avoid this problem, we choose a different criterion. We define τ_0 as the moment at which the curve of the forces on the angular mode reaches its saddle point –without taking into consideration the final bump, which can be explained by other reasons. This criterion has the advantage to depend only on the quench rate. However, it is not valid if the quench is too fast and the saddle point happens after the quench has ended. At τ_0, domains of homogeneous phase are formed –see top figure 7.6.

[2]This simulations are performed in the fully $U(1)$-symmetric case, that is, we do not take into account the anisotropic terms of the potential. As a consequence, the phase zero mode is massless and the tangential restoring force in equation (5.9) does not contribute.

An important remark is that τ_0 is always later than the time at which the critical temperature is crossed (second vertical solid line).

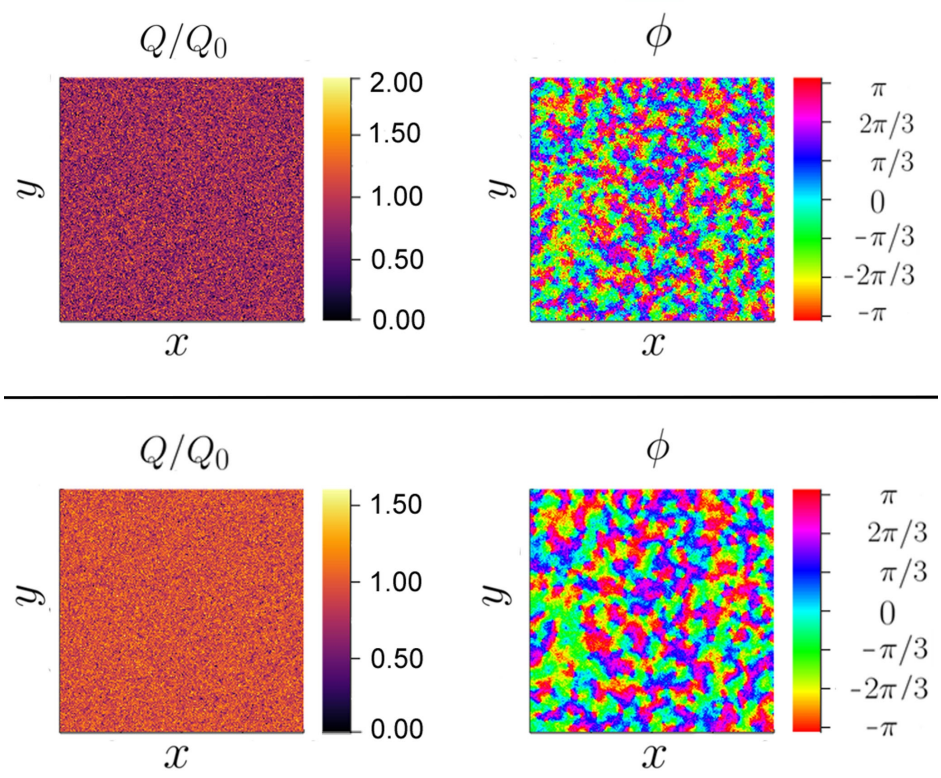

Figure 7.6: Snapshots of the amplitude Q (left) and the phase ϕ (right) of the order parameter for $R'_q = 0.255$. They illustrate the distribution of vortices at the formation time τ_0 (primordial vortices, top) and at the vortex consolidation time τ_1 (bottom).

Let us now describe the time evolution of the mean value of the field. As a remarkable fact, we perceive that it decreases during the time that the system spends cooling in the symmetric phase –that is, between the first and the second solid vertical lines. Then, it increases again and consolidate at the asymptotic value given by $Q_0 = \sqrt{a_0/b}$ –*i.e.*, the value of the bulk at zero temperature. This behaviour is the same as the one appreciated in figure

6.1, and can be explained by the same arguments.

The consolidation of the modulus at the consolidation time τ_1 signals that the phase transition has been accomplished. Its computation and its meaning is the same as in the case of ultra-fast quenches, so we do not elaborate further on that. A snapshot of the field at this time can be seen in the bottom figure 7.6. However, the definition of the diffusion time τ_d requires some explanation.

In the case of ultra-fast quenches, the value of τ_d accounts for the time that the system evolves in a small neighbourhood of the origin in the configuration space, describing a random walk due to the stochastic noise, before it starts its rolling-down towards the minima of the potential. This picture is not valid in this scenario, since the size of the thermal fluctuations are much larger, and the diffussion of the order parameter is not restringed to a small region around the maxima –this explains why the initial value of $\langle Q \rangle$ is so high in comparison with the former case. However, the definition of τ_d in this simulation also accounts for the moment at which nonlinear effects start to be noticed by the field. It is only in this sense that the diffusion time can be compared with the former case.

We have computed the value of the density of vortices measured at times τ_0 and τ_1 as a function of the quench rate –see figure 7.7. In the range of slow quenches, a scaling behaviour is obtained –$n \sim R_q^{0.37}$ and $n \sim R_q^{0.36}$ for τ_0 and τ_1, respectively.

The value of these exponents is lower than the expected in the mean field theory

For this purpose, we fit the time evolution of the vortex density for each of the temperatures of the quench to a power-law function $n(t) \simeq n(\tau_1)/t^{\alpha}$ for $t \geq \tau_1$, as shown in figures 7.1(b) and 7.4(b). We find $\alpha \approx 1$ in the $U(1)$

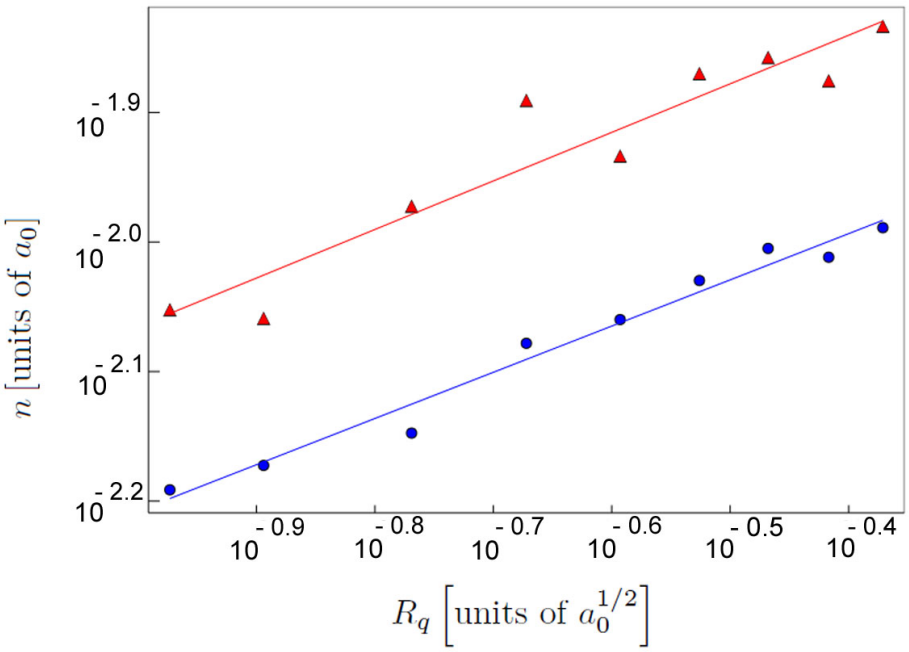

Figure 7.7: Density of vortices n as a function of the quench rate R_q (log-log scale). Red triangles correspond to measurements at τ_0 and blue circles represents measurements performed at τ_1. Power-law fit of the data is displayed.

weak-anisotropy case and $\alpha \approx 3/4$ in the $\mathbb{Z}_6$ strong-anisotropy one. This means that, despite the fact that the overlap between vortices is larger in the strong-anisotropy case for the vortex core is larger, the annihilation rate is slower. This signals the impact of the $\mathbb{Z}_6$-anisotropy in the short-range vortex-antivortex interaction.

To conclude this section, we analyse the evolution of the vortex network after the formation of vortices has finished. As in the previous case, we investigate the rate of the annihilation process between pairs of vortex and antivortex. We fit the time evolution of the vortex density to a power-law function $n(t) \simeq n(\tau_1)/t^{\alpha}$ for $t \geq \tau_1$ –see figure 7.8. In this case, the exponent of the fit is $\alpha = 0.57$. That is, the decay in this case is slower than in the

two scenarios considered in the ultra-fast limit.

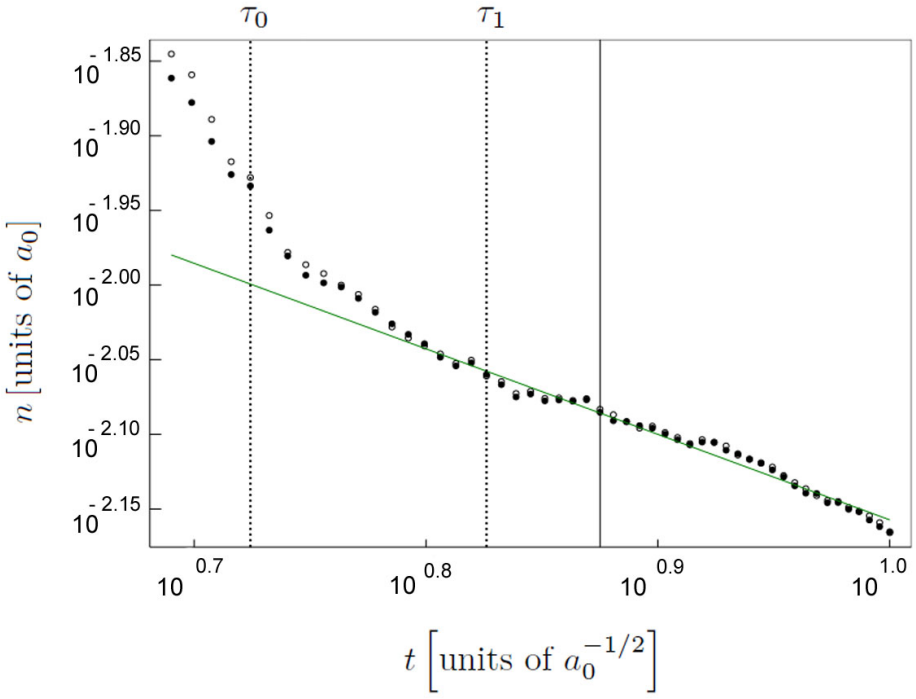

Figure 7.8: Graphical determination of the corresponding vortex density as a function of time (log-log scale). The same power-law behavior is obtained according to two different methods (solid and open circles, respectively –cf. section 11.1) beyond τ_1. Solid vertical line represents the time at which the quench ends.

7.3.2 Quenches varying the bare mass term of the theory

Finally, let us analyse the results of quenches performed with the temperature of the Langevin term evaluated at a constant value and varying the value of the bare mass term coefficient, which entails to effectively vary the critical temperature of the system. As in the previous section, we make use of the

same observables to describe the dynamics of the quench. We only elaborate to signal relevant differences with the cases already commented.

Let us start by analysing the time evolution of the observables $\langle |f_\phi| \rangle$ and $\langle Q \rangle / Q_0$, which corresponds respectively to the sample-averaged force on the angular mode, given by equation (5.9) and the sample-averaged modulus of the order parameter. In this case, the constant of normalization Q_0 corresponds to the value of the bulk field at $a = -1.83$, that is, the final value of a after the quench. Its behaviour is displayed in figure 7.9. Notice that the quench rate chosen to illustrate this kind of quench, $R'_q = 0.255$, is the same as the one in the previous section. Recall that both quench rates can be related by equation (6.9) –cf. section 6.2.

Let us start describing the behaviour of the force on the angular mode. In the first interval, before the quench stats, it takes a stationary value, meaning that the system is thermalised. When the quench starts cooling (first solid vertical line), it starts dropping. This is in contrast with the case of quench varying the Langevin temperature, where the force only starts to drop after the transition point. Nevertheless, this drop does not become relevant until the transition point is crossed (second solid vertical line). This is the moment at which the effective critical temperature has become larger than the constant temperature θ of the Langevin fluctuations. The drop continues until the quench finishes (third solid vertical line) and it stabilises in a stationary value. Notice that in this case, this asymptotic value is much larger than in the two scenarios considered before. The issues to determine a valid criterion to compute τ_0 are the same as in the previous case. We again opt to define the vortex formation time as the time at which the sample-averaged force reaches its saddle-point. As in the former cases, this time represents the moment at which domains of homogeneous phase are unambiguously formed,

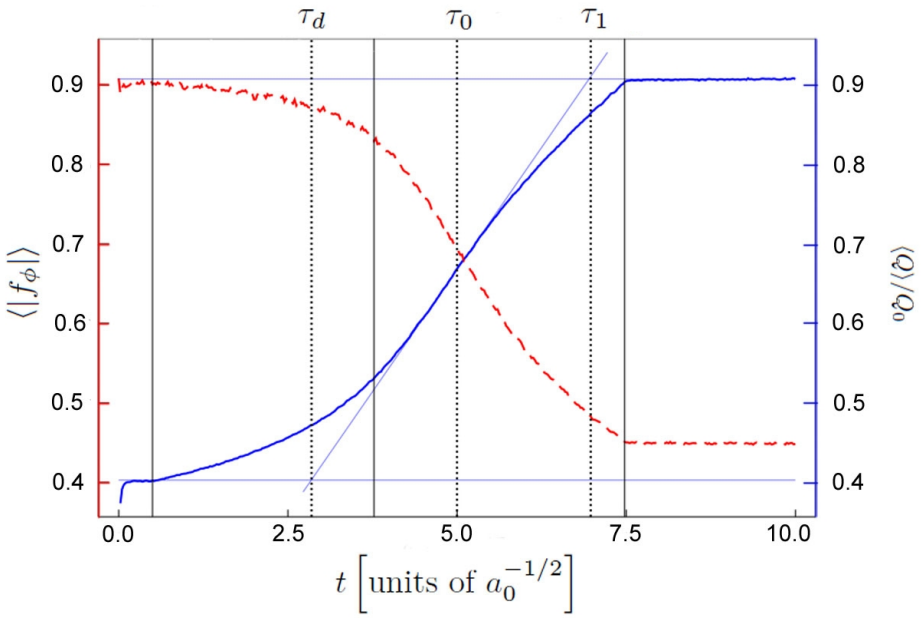

Figure 7.9: Sample-averaged tangential force strength (dashed red, in arbitrary units) and normalized amplitude of the order parameter (solid blue) as a function of time, for $R'_q = 0.255$. The vertical solid lines represent, form left to right, the time at which the quench starts, the time at which the critical temperature is reached, and the time at which the quench ends. The vertical dotted lines indicate the diffusion time, τ_d, the phase relaxation time, τ_0, and the vortex consolidation time, τ_1, as defined in the main text.

and is associated with a relaxation of the tangent forces on the angular mode of the order parameter.

Next, let us examine the time evolution of the mean modulus of the field. Conversely with the quenches with varying Langevin temperature, in this instance the modulus grows monotonically. This is in accordance with the behaviour analysed in section 6.1 –see figure 6.2. Diffusion time τ_d and consolidation time τ_1 have the same physical meaning as in the previous case. Namely, the diffusion time signals when the field starts noticing the

potential force contributions, whereas the consolidation time indicates that the modulus has almost reached its asymptotic value. Notice that in this case this value does not exactly corresponds to the value of equilibrium predicted by $Q_0 = \sqrt{a_0/b}$. This is expected, since the the minimum of the effective potential is not in the same point as the nominal value Q_0. The evolution of the vortex pattern obtained in this case is illustrated in figure 7.10.

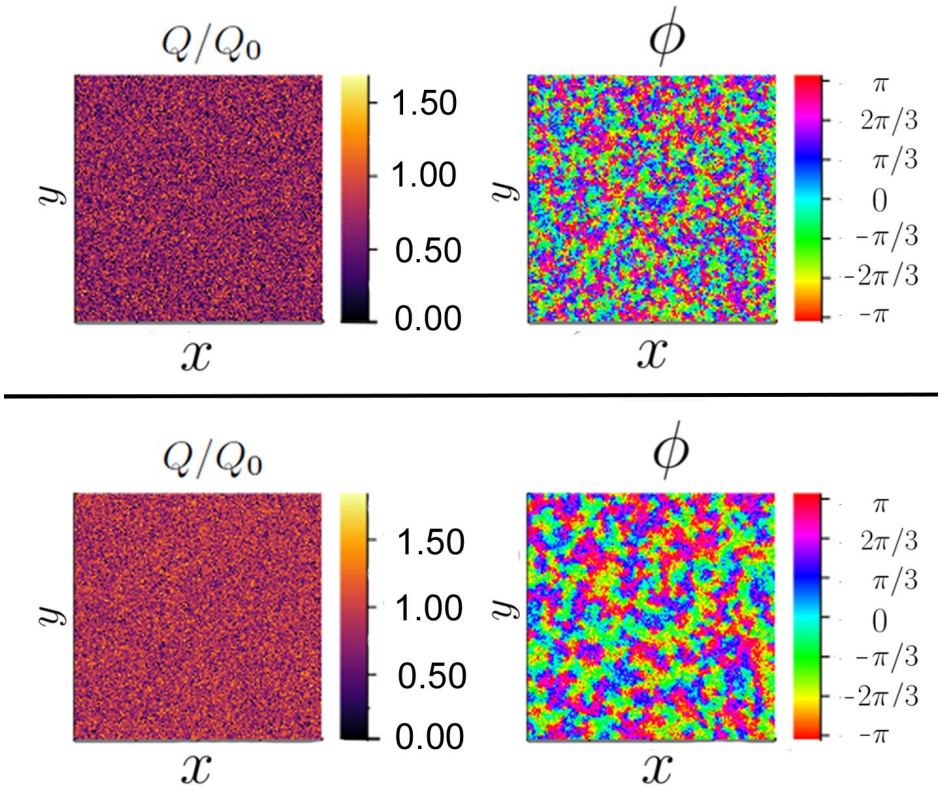

Figure 7.10: Snapshots of the amplitude Q (left) and the phase ϕ (right) of the order parameter for $R'_q = 0.255$. They illustrate the distribution of vortices at the formation time τ_0 (primordial vortices, top) and at the vortex consolidation time τ_1 (bottom).

Lastly, let us study the scaling behaviour of the density of the topological defects n with respect the quench rates R'_q –see figure 7.11. Notice that the

values of the quench rates considered here are the same of the ones discussed in figure 7.7, so a direct comparison is allowed. The fits performed shows that $n \sim {R'_q}^{0.13}$ for τ_0 and $n \sim {R'_q}^{0.43}$ for τ_1. In this instance, the scaling behaviour yields two different exponents. Whilst the latter exponent is similar to the exponents considered in the previous case, the former significantly deviates.

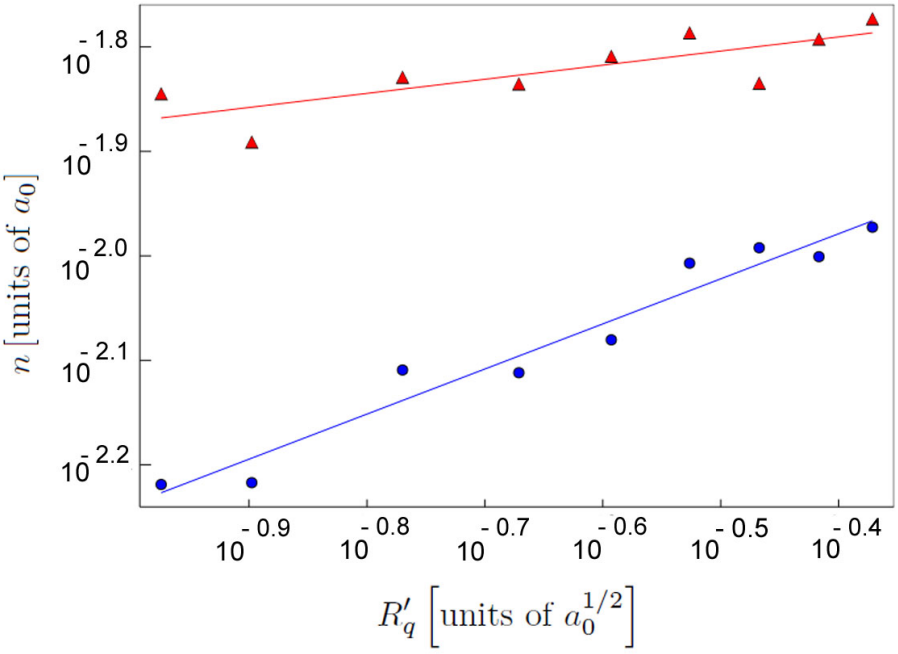

Figure 7.11: Density of vortices n as a function of the quench rate R'_q (log-log scale). Red triangles correspond to measurements at τ_0 and blue circles represents measurements performed at τ_1. Power-law fit of the data is displayed.

Part III

Code scripts for numeric simulations

In this part, the code used to perform all the numeric simulations of this work is presented. Let us define the main objects with which we operate. The sample on which the field is defined is discretized as a three-dimensional rectangular grid of size `(Nx,Ny,Nz)`. Let `dx` be the space-step which defines the distance between two adjacent points in the x-direction. Space-steps in the y and z-direction are `dy` and `dz` respectively. They may take different values, although we have set `dx=dy=dz` in all our simulations.

The size of the grid and the magnitude of the space step are adapted in each simulation, The space step is set to be at least four times smaller than the correlation length computed within the mean-field formalism –it depends on the bath temperature as well as on the parameters of the theory. The total length of the sample, `Nx*dx`, is set to be several times bigger than the mean-field correlation length. In most of the simulations, this size is at least ten times bigger. Let `dt` be the time-step, which has also been adapted to each simulation.

The complex scalar field $\mathcal{Q}(\mathbf{r}, t)$ is defined on this grid. It is a three-dimensional complex array, `q = q1 + q2*im`, whose elements corresponds to the value of the field on the discretized sample. For convenience, most functions works with the rectangular components of the field rather than the polar.

The most important function of the program is the one which integrates the equations of motion. It will be described in chapter 9. There are several versions of this function in order to account for the different manners to include the thermal effects, as well as the different methods to cool down the system, as discussed in the previous chapter.

In order to integrate the equation, it is necessary to specify first the boundary conditions. In chapter 8, we introduce a set of functions which

model a variety of such conditions. We also pay attention to the initial conditions. We have developed a great amount of initial configurations of the field, a part of which can be found in chapter 10. Some of them have not been employed in this work ; nevertheless, we think it is worth to include them in this chapter , for the sake of completeness, and also because they implement interesting starting configurations to do further research.

In chapter 11, we introduce a set of important functions. These are some of the observables that we have used to comprehend the dynamics of the system and describe it. We do not present here some observables that are straightforward to calculate –*e.g.*, the mean of the modulus of the field– but the ones which require some elaborate computation. Namely, the number of vortices and the correlation length. We also include in this chapter the functions to compute the mean-field values of the correlation length and relaxation time, computed in section 5.1.

All these functions meet in the main function of the program, described in the last chapter 12. This function implement the whole quench process. The field is set in an initial condition. Then, the equations of motion are integrated a given number of times. At some time intervals, observables are computed and saved.

Many of the functions described in this chapter are written in two different ways. The reason is that the definition of the parameters of the theory depends on what cooling method we are considering –cf. chapter 6. Apart from that, the algorithms beneath are essentially the same. Whenever this happens, we will only write one of the versions for the sake of avoiding repetition. We have also removed some lines of code where we feel there is no chance of confusion; those suppressions are signalled by a comment in the code.

The code has been written in the programming language *julia*, version 1.1.1. It is an open source project which is made available under the MIT License. The election of this language was motivated for the need of high performance – *julia* is a compiled language. Indeed, the numeric simulations carried out were extremely time-consuming, so the language program which must be used was required to be highly efficient. More information can be found in the web page of the project [3]. To perform the simulations, we have made use of the strong performance computing resources of the Castilla y León Supercomputing Center (SCAYLE [4]).

Some specific packages are required to run these functions suitably. The most important ones are listed below.

```
using RandomNumbers.Xorshifts
import Random: rand!
using Statistics
using CurveFit
using Polynomials
using FFTW
using DelimitedFiles
using Plots
```

[3] https://julialang.org/

[4] https://www.scayle.es

Chapter 8

Boundary conditions

The first set of boundary conditions accounts to the most common boundary conditions. `ZeroFluxBC` imposes to Neumann boundary conditions –*i.e.*, the annihilation of the normal derivative of the field at the boundary, `ZeroFieldBC` implements Dirichlet boundary conditions –*i.e.*, the annihilation of the field at the boundary, and `PeriodicBC` corresponds to periodic boundary conditions.

```
function ZeroFluxBC(A,Nx,Ny,Nz)
    #Long
    A[1,:,:] = A[2,:,:]
    A[Nx,:,:] = A[Nx-1,:,:]
    #Wide
    A[:,1,:] = A[:,2,:]
    A[:,Ny,:] = A[:,Ny-1,:]
    #High
    A[:,:,1] = A[:,:,2]
    A[:,:,Nz] = A[:,:,Nz-1]
    return A
end

function ZeroField(A,Nx,Ny,Nz)
    #Long
    A[0,:,:] = 0.0 + 0.0*im
    A[Nx,:,:] = 0.0 + 0.0*im
    #Wide
    A[:,0,:] = 0.0 + 0.0*im
    A[:,Ny,:] = 0.0 + 0.0*im
```

```
    #High
    A[:,:,0] = 0.0 + 0.0*im
    A[:,:,Nz] = 0.0 + 0.0*im
    return A
end

function PeriodicBC(A,Nx,Ny,Nz)
    #Long
    A[1,:,:] = A[Nx-1,:,:]
    A[Nx,:,:] = A[2,:,:]
    #Wide
    A[:,1,:] = A[:,Ny-1,:]
    A[:,Ny,:] = A[:,2,:]
    #High
    A[:,:,1] = A[:,:,Nz-1]
    A[:,:,Nz] = A[:,:,2]
    return A
end
```

We may also impose periodic boundary conditions on some directions and zero-flux on others. This boundary conditions have been used to perform simulations in two-dimensional systems.

```
function XYPeriodicBC(A,Nx,Ny,Nz)
    #We impose periodic boundary conditions on the plane x,y
    and zero flux boundary conditions on the z direction
    A[1,:,:] = A[Nx-1,:,:]
    A[Nx,:,:] = A[2,:,:]
    A[:,1,:] = A[:,Ny-1,:]
    A[:,Ny,:] = A[:,2,:]
    A[:,:,1] = A[:,:,2]
    A[:,:,Nz] = A[:,:,Nz-1]
    return A
end

function ZPeriodicBC(A,Nx,Ny,Nz)
    #We impose zero flux boundary conditions on the plane x,y
    and periodic boundary conditions on the z direction
    A[1,:,:] = A[2,:,:]
    A[Nx,:,:] = A[Nx-1,:,:]
    A[:,1,:] = A[:,2,:]
    A[:,Ny,:] = A[:,Ny-1,:]
    A[:,:,1] = A[:,:,Nz-1]
    A[:,:,Nz] = A[:,:,2]
    return A
end
```

Furthermore, we may choose other non-trivial boundary conditions. We may let the field take some non-equilibrium value at certain relevant spatial points, and force it to remain constant in time. For instance, we may recreate a domain wall by choosing two different values on the opposite edges of the sample in one direction. Rather, we may choose to fix only the field at one of the edges. Notice that the perturbation is defined based on the definition of the mass term given in (6.3). The nature of the perturbation depends on whether the system is in the symmetric phase or the broken phase.

```
function XYDomainWallBC(A,Nx,Ny,Nz,a0)
    #There are several versions of this funcion:
    #In the x-direction, we impose either fixed boundary conditions on both edges, or fixed in one border and zero-flux in the other.
    #Comment or uncomment code lines to get the desired function.
    #In the y-direction, we impose zero flux  OR periodic boundary conditions.
    #In the z-direction, we always impose periodic boundary conditions.

    #x-direction
    a_aux = zeros(ComplexF64,Ny,Nz)
    ################################################
    #Perturbation for symmetric phase (0.95 of the mass term)
    #amplitude_perturbation = sqrt(a0)*0.95
    #Perturbation in both edges
    #A[1,:,:] = a_aux .+ amplitude_perturbation*im
    #A[Nx,:,:] = a_aux .- amplitude_perturbation*im
    #Perturbation in one edge
    #A[1,:,:] = a_aux .+ amplitude_perturbation*im
    #A[Nx,:,:] = A[Nx-1,:,:]
    ################################################
    #Perturbation for broken phase: modulus (put the system in the maximum)
    #amplitude_perturbation = 0.0
    #Perturbation in both edges
    #A[1,:,:] = a_aux
    #A[Nx,:,:] = a_aux
    #Perturbation in one edge
    #A[1,:,:] = a_aux
    #A[Nx,:,:] = A[Nx-1,:,:]
    ################################################
    #Perturbation for broken phase: angle
```

```
    amplitude_perturbation = sqrt(a0/2) #Q_0 in the bulk,
   provided b=2
    phi = pi/6
    #Perturbation in both edges
    A[1,:,:] = a_aux .+ amplitude_perturbation*(cos(phi+pi/3)
   +im*sin(phi+pi/3))
    A[Nx,:,:] = a_aux .+ amplitude_perturbation*(cos(phi)+im*
   sin(phi))
    #Perturbation in one edge
    #A[1,:,:] = a_aux .+ amplitude_perturbation*(cos(phi+pi
   /3)+im*sin(phi+pi/3))
    #A[Nx,:,:] = A[Nx-1,:,:]

    #y-direction
    A[:,1,:] = A[:,2,:] #A[:,Ny-1,:]
    A[:,Ny,:] = A[:,Ny-1,:] #A[:,2,:]

    #z-direction
    A[:,:,1] = A[:,:,Nz-1]
    A[:,:,Nz] = A[:,:,2]
    return A
end
```

Alternatively, we may set a perturbation at the central point of the sample.

```
function PerturbationCenterSample(A,Nx,Ny,Nz,a0)
    #We impose zero-flux or periodic boundary conditions.
   Besides, we make a perturbation at the center of the
   sample which is constant in time.

    #x-direction
    A[1,:,:] = A[2,:,:] #A[Nx-1,:,:]
    A[Nx,:,:] = A[Nx-1,:,:] #A[2,:,:]
    #y-direction
    A[:,1,:] = A[:,2,:] #A[:,Ny-1,:]
    A[:,Ny,:] = A[:,Ny-1,:] #A[:,2,:]
    #z-direction
    A[:,:,1] = A[:,:,2] #A[:,:,Nz-1]
    A[:,:,Nz] = A[:,:,Nz-1] #A[:,:,2]

    #Perturbation at the central point
    #Perturbation for symmetric phase (0.95 of the mass term)
    perturbation = sqrt(a0)*0.95*im
    #Perturbation for broken phase: modulus (set the field in
    the maximum)
    #perturbation = 0.0 + 0.0*im
```

```
    #Perturbation for broken phase: angle (set the field in the neighbour minimum)
    #amplitude_perturbation = sqrt(a0/2) #Q_0 in the bulk, provided b=2
    #phi = pi/6
    #perturbation = amplitude_perturbation*(cos(phi+pi/3)+im*sin(phi+pi/3))

    A[round(Int,Nx/2),round(Int,Ny/2),round(Int,Nz/2)] = perturbation
    return A
end
```

These last boundary conditions enable us to study how a perturbation –in phase or in modulus– propagates through space and thus determine the actual correlation length of the system. This is one of the various way in which we have calculated the correlation length.

Lastly, we may let the boundaries of the $xy-$plane to be in different minima so as to the global circulation of the phase around these edges is an integer multiple of 2π. This boundary condition is suitable to try and get a time-stable vortex.

```
function XYVortexBC(A,Nx,Ny,Nz)
    #The circulation of the phase around the edges of a plane is an integer.

    Q_min = 0.4 # This value is computed apart as Q_min=sqrt(a0/b)
    winding_number = 1
    phi = [i*pi/3 + pi/6 for i in 0:(winding_number*6-1)] #Provided c1>0
    epsilon_space = 0.00025 #This small displacement is set to prevent the vortex-core from being a site of the grid
    core_vortex_x, core_vortex_y = Nx/(2 + epsilon_space), Ny/(2 + epsilon_space)

    #Long
    ny = range(1-core_vortex_y, stop=Ny-core_vortex_y)
    theta_1 = atan.(ny,1-core_vortex_x) .+ pi #atan corresponds to a standard atan2 function
    theta_2 = atan.(ny,Ny-core_vortex_x) .+ pi
    l1 = ceil.(Int,winding_number * 6 .* theta_1./(2*pi)) #ceil rounds to the upper integer
```

```
    l2 = ceil.(Int,winding_number * 6 .* theta_2./(2*pi))
    A[1,:,:] = repeat(Q_min*cos.(phi[l1]) .+ Q_min*sin.(phi[
    l1]).*im,1,Nz)
    A[Ny,:,:] = repeat(Q_min*cos.(phi[l2]) .+ Q_min*sin.(phi[
    l2]).*im,1,Nz)

    #Wide
    nx = range(1-core_vortex_x, stop=Nx-core_vortex_x)
    theta_1 = atan.(1-core_vortex_y,nx) .+ pi
    theta_2 = atan.(Ny-core_vortex_y,nx) .+ pi
    l1 = ceil.(Int,winding_number * 6 .* theta_1./(2*pi))
    l2 = ceil.(Int,winding_number * 6 .* theta_2./(2*pi))
    A[:,1,:] = repeat(Q_min*cos.(phi[l1]) .+ Q_min*sin.(phi[
    l1]).*im,1,Nz)
    A[:,Ny,:] = repeat(Q_min*cos.(phi[l2]) .+ Q_min*sin.(phi[
    l2]).*im,1,Nz)

    #High
    A[:,:,1] = A[:,:,Nz-1]
    A[:,:,Nz] = A[:,:,2]

    return A
end
```

Chapter 9

Step functions

The functions included in this chapter constitute the core of the program. They are designed to perform a single integration step of the equations of motion (5.1). They will be called in the main function to integrate the equation recursively a given number of times –cf. chapter 12. We present here three different versions of the `step` function. Let us comment some common features shared by the three versions, and afterwards we will discuss their differences.

First of all, we need to introduce an auxiliary function to compute the laplacian which appears in the equations of motion. The prescription given here is a standard symmetrized discretization of the laplacian operator which can be found in the literature. Notice that we have include the coupling factors, g_i, in the definition of the operator.

```
function laplacian(A,Nx,Ny,Nz,dx,dy,dz,gx,gz)
    #Laplacian operator (symmetrized). Takes as an input a
    complex 3D-array (A) of dimensions (Nx,Ny,Nz) and returns
    the laplacian when the spatial steps are (dx,dy,dz) and
    the couplings are gx=gy and gz.

    #x-direction
    function Dx_forward(A,Nx,Ny,Nz)
        F = zeros(ComplexF64,Nx,Ny,Nz)
        F[1:Nx-1,:,:] = A[2:Nx,:,:]
        return (F-A)
    end
```

```
    function Dx_backward(A,Nx,Ny,Nz)
        B = zeros(ComplexF64,Nx,Ny,Nz)
        B[2:Nx,:,:] = A[1:Nx-1,:,:]
        return (A-B)
    end
    Dx(A,Nx,Ny,Nz,dx,gx) = (gx/(dx^2))*(Dx_forward(A,Nx,Ny,Nz)-Dx_backward(A,Nx,Ny,Nz))

    #y-direction
    function Dy_forward(A,Nx,Ny,Nz)
        F = zeros(ComplexF64,Nx,Ny,Nz)
        F[:,1:Ny-1,:] = A[:,2:Ny,:]
        return (F-A)
    end
    function Dy_backward(A,Nx,Ny,Nz)
        B = zeros(ComplexF64,Nx,Ny,Nz)
        B[:,2:Ny,:] = A[:,1:Ny-1,:]
        return (A-B)
    end
    Dy(A,Nx,Ny,Nz,dy,gx) = (gx/(dy^2))*(Dy_forward(A,Nx,Ny,Nz)-Dy_backward(A,Nx,Ny,Nz))

    #z-direction
    function Dz_forward(A,Nx,Ny,Nz)
        F = zeros(ComplexF64,Nx,Ny,Nz)
        F[:,:,1:Nz-1] = A[:,:,2:Nz]
        return (F-A)
    end
    function Dz_backward(A,Nx,Ny,Nz)
        B = zeros(ComplexF64,Nx,Ny,Nz)
        B[:,:,2:Nz] = A[:,:,1:Nz-1]
        return (A-B)
    end
    Dz(A,Nx,Ny,Nz,dz,gz) = (gz/(dz^2))*(Dz_forward(A,Nx,Ny,Nz)-Dz_backward(A,Nx,Ny,Nz))

    return Dx(A,Nx,Ny,Nz,dx,gx) + Dy(A,Nx,Ny,Nz,dy,gx) + Dz(A,Nx,Ny,Nz,dz,gz)
end
```

We will also need a function which deals with the possible leaf change when subtracting two phases.

```
function diff_phase(x0,xf)
    D_ph = angle.(xf) - angle.(x0)
    for i in 1:length(D_ph)
        if abs(D_ph[i]) > pi
            D_ph[i] = D_ph[i]<0 ? D_ph[i]+2*pi : D_ph[i]-2*pi
```

```
        end
    end
    return D_ph
end
```

In the three versions of the function, we first compute the stochastic contribution due to Langevin forces. Next, we compute the forces derived from potential and gradient terms. The combined action of these two latter forces are referred as *restoring forces*, since they push the field to the equilibrium state, whilst the random forces push it away. Notice that the notation is slightly different of the one used in (5.8) and (5.9). Then the field matrix is upgraded and some boundary condition operator acts on it to get the final new state. Then, we update the parameter which takes into account the cooling of the system, which is different in the three versions. Lastly, we may split the different contributions of the forces, as they may be useful observables in the subsequent analysis.

Let us focus our attention on the **first version** of the `step` function. It was used to perform the numeric simulations for the ultra-fast regime, whose results are discussed in detail in section 7.2.

```
#FIRST VERSION of the step function
function step(q, a0, b, c, c1, gx, gz, gamma, eps, Tc, r_q,
    dt, Nx, Ny, Nz, dx, dy, dz, S_rng)
    # Update the value of the filed matrix q for a single
    time step according to the discretized field equation and
    apply BC
    #PARAMETERS
    # q: Field matrix - complex 3d-array
    # a0: Absolute value of the mass-term coefficient at zero
     temperature. The mass-term depends on the temperature in
    the following way: a=a0*eps, where eps is the reduced
    temperature.
    # b,c,c1,gx,gz: parameters of the lagrangian
    # gamma: damping coefficient
    # eps: reduced temperature, adimensional (eps=(T-Tc)/Tc)
    # Tc: critical temperature
    # r_q: quench rate (units of inverse time)
```

```
    # dt,dx,dy,dz,Nx,Ny,Nz: time-step, space-step, grid dimensions
    # S_rng: Random number generator algorithm seeded, S_rng = Xoroshiro128Star(seed)

    #Langevin thermal perturbation
    theta =  Tc*(eps+1) #acual temperature
    amplitude_langevin = sqrt(2*theta*dt/(gamma*dx*dy*dz))
    langevin_source = amplitude_langevin*sqrt(2)*randn(S_rng, ComplexF64,(Nx,Ny,Nz)) #randn generate an array of normally-distributed random numbers with mean 0 and std 1

    #Dissipative force: contribution from the potential and gradient terms
    q1,q2 = real(q),imag(q)
    Sq1,Sq2 = q1.^2,q2.^2
    leading_order_terms = a0*eps*ones(Float64,Nx,Ny,Nz) + b*(Sq1+Sq2) + c*(Sq1+Sq2).^2
    restoring_force_1 = -(dt/gamma)*(q1.*(leading_order_terms
    + c1*(Sq1-3*Sq2).*(Sq1-Sq2)) - laplacian(q1,Nx,Ny,Nz,dx,dy,dz,gx,gz))
    restoring_force_2 = -(dt/gamma)*(q2.*(leading_order_terms
    - 2*c1*(Sq1-3*Sq2).*Sq1) - laplacian(q2,Nx,Ny,Nz,dx,dy,dz,gx,gz))
    restoring_force = restoring_force_1 + restoring_force_2*im

    #New value of the field
    dq = restoring_force + langevin_source
    q_new = q + dq

    #Boundary conditions
    #We may change the boundary conditions for different runs
    q_new = ZeroFluxBC(q_new,Nx,Ny,Nz)

    #New temperature - if there is a quench
    eps_new = eps-dt*r_q

    #Supplementary data (optional). We split the contributions to the force
    #Forces from potential terms
    pot_forces_a1, pot_forces_a2 = -(dt/gamma)*(q1.*(a0*eps*ones(Float64,Nx,Ny,Nz))), -(dt/gamma)*(q2.*(a0*eps*ones(Float64,Nx,Ny,Nz)))
    pot_forces_b1, pot_forces_b2 = -(dt/gamma)*(q1.*(b*(Sq1+Sq2))), -(dt/gamma)*(q2.*(b*(Sq1+Sq2)))
    pot_forces_c1, pot_forces_c2 = -(dt/gamma)*(q1.*(c*(Sq1+Sq2).^2 + c1*(Sq1-3*Sq2).*(Sq1-Sq2))), -(dt/gamma)*(q2.*(c*(Sq1+Sq2).^2 - 2*c1*(Sq1-3*Sq2).*Sq1))
```

```
    #Forces from grad terms
    grad_forces_1, grad_forces_2 = (dt/gamma)*(q1.*(laplacian(q1,Nx,Ny,Nz,dx,dy,dz,gx,gz))), (dt/gamma)*(q2.*(laplacian(q2,Nx,Ny,Nz,dx,dy,dz,gx,gz)))
    #Forces from stochastic terms
    langevin_forces_1, langevin_forces_2 = real(langevin_source), imag(langevin_source)
    #Forces on the modulus of the field, and on the phase of the field - with and without the langevin contribution
    mod_forces, phase_forces = abs.(q_new)-abs.(q), diff_phase(q,q_new)#diff_phase is a function to deal with the possible leaf change when substracting two phases
    mod_forces_withoutlang, phase_forces_withoutlang = abs.(ZeroFluxBC(q+restoring_force,Nx,Ny,Nz))-abs.(q), diff_phase(q,ZeroFluxBC(q+restoring_force,Nx,Ny,Nz))

    return q_new, eps_new, pot_forces_a1, pot_forces_a2, pot_forces_b1, pot_forces_b2, pot_forces_c1, pot_forces_c2, grad_forces_1, grad_forces_2, langevin_forces_1, langevin_forces_2, mod_forces, phase_forces, mod_forces_withoutlang, phase_forces_withoutlang
end
```

In this case, the temperature of the external reservoir is taken into account in two different terms. In the first place, it is present in the coefficient of the mass term, a, which is defined as $a = |a_0|\epsilon$, where a_0 is the value of the mass term at zero temperature and $\epsilon = (T - T_c)/T_c$ is the reduced temperature, dimensionless. In the second place, it also appears in the amplitude of the stochastic term, the Langevin force. A detailed discussion on why the amplitude of this term depends on the temperature in this particular way can be found in chapter 5. We have forced the temperature to be the same in both terms, since it is considered that there is only one temperature on the problem: the temperature of the external reservoir. This is why we claim that this procedure is *self consistent*. In this version, the cooling method modifies the reduced temperature `eps`, so the quench rate `r_q` has units of inverse time. Whenever the temperature is updated, both the mass term and the stochastic amplitude varies at the same time. However, this is in contrast

with many previous works in the literature [49, 57, 61, 62, 63], which work with two different unrelated temperatures, one of which remains constant over time –the one that appears in the noise term. If we want to reproduce such behaviour, we just need to remove the line of code number 15 and make `theta` a constant input of the function.

Now, let us consider the `step` functions employed in sections 7.3.1 and 7.3.2. The main difference with the previous one is that the temperature dependency of the mass term has been dropped. The temperature only appears in the noise term. The **second version** implements the cooling by reducing the temperature while maintaining the mass term fixed. We will suppress some redundant code lines with comment lines.

```
1  #SECOND VERSION of the step function
2  function step(q, a, b, c, c1, gx, gz, gamma, theta, R_q, dt,
       Nx, Ny, Nz, dx, dy, dz, S_rng)
3      # Update the value of the filed matrix q for a single
       time step according to the discretized field equation and
       apply BC
4      #PARAMETERS (Only mentioned those which differ from FIRST
       VERSION of the step function)
5      # a: Mass-term coefficient at zero temperature, a<0.
6      # theta: temperature of the system
7      # R_q: quench rate (units of temperature by inverse time)
8
9      #Langevin thermal perturbation
10     amplitude_langevin = sqrt(2*theta*dt/(gamma*dx*dy*dz))
11     langevin_source = amplitude_langevin*sqrt(2)*randn(S_rng,
       ComplexF64,(Nx,Ny,Nz)) #randn generate an array of
       normally-distributed random numbers with mean 0 and std 1
12
13     #Dissipative force
14     q1,q2 = real(q),imag(q)
15     Sq1,Sq2 = q1.^2,q2.^2
16     leading_order_terms = a*ones(Float64,Nx,Ny,Nz) + b*(Sq1+
       Sq2) + c*(Sq1+Sq2).^2
17     restoring_force_1 = -(dt/gamma)*(q1.*(leading_order_terms
       + c1*(Sq1-3*Sq2).*(Sq1-Sq2)) - laplacian(q1,Nx,Ny,Nz,dx,
       dy,dz,gx,gz))
18     restoring_force_2 = -(dt/gamma)*(q2.*(leading_order_terms
       - 2*c1*(Sq1-3*Sq2).*Sq1) - laplacian(q2,Nx,Ny,Nz,dx,dy,dz
       ,gx,gz))
```

```
19      restoring_force = restoring_force_1 + restoring_force_2*
        im
20
21      #New value of the field
22      dq = restoring_force + langevin_source
23      q_new = q + dq
24
25      #Boundary conditions
26      #We may change the boundary conditions for different runs
27      q_new = ZPeriodicBC(q_new,Nx,Ny,Nz)
28
29      #New temperature - if there is a quench
30      theta_new = theta - dt*R_q
31
32      #Supplementary data (optional). We split the
        contributions to the force
33      #(Same lines 40-50 of FIRST VERSION of the step function
        except for the chage a0*eps -> a)
34
35      return q_new, theta_new, pot_forces_a1, pot_forces_a2,
        pot_forces_b1, pot_forces_b2, pot_forces_c1, pot_forces_c2
        , grad_forces_1, grad_forces_2, langevin_forces_1,
        langevin_forces_2, mod_forces, phase_forces,
        mod_forces_withoutlang, phase_forces_withoutlang
36  end
```

The first thing to notice is that the critical temperature is no longer a free parameter, but a quantity we need to find out. As a consequence, we do not know a priori the reduced temperature of the system, ϵ, so the quench cannot refer to it. Instead, we can update the actual temperature of the system, `theta`. That implies that the quench rate `R_q` is not in the same units as the quench rate of the first version, `r_q`. However, once the critical temperature is obtained, both can be related ($r_q = R_q/\theta_c$).

Lastly, consider the **third version** of the step function.

```
1  #THIRD VERSION of the step function
2  function step(q, a, b, c, c1, gx, gz, gamma, theta, rho_q, dt
       , Nx, Ny, Nz, dx, dy, dz, S_rng)
3      # Update the value of the filed matrix q for a single
       time step according to the discretized field equation and
       apply BC
4      #PARAMETERS (Only mentioned those which differ differ
       from FIRST VERSION of the step function)
```

```
    # a: Mass-term coefficient at zero temperature, a<0.
    # theta: temperature of the system
    # rho_q: quench rate (units of a by inverse time)

    #Langevin thermal perturbation
    amplitude_langevin = sqrt(2*theta*dt/(gamma*dx*dy*dz))
    langevin_source = amplitude_langevin*sqrt(2)*randn(S_rng,
   ComplexF64,(Nx,Ny,Nz))#randn generate an array of normally
   -distributed random numbers with mean 0 and std 1

    #Dissipative force
    q1,q2 = real(q),imag(q)
    Sq1,Sq2 = q1.^2,q2.^2
    leading_order_terms = a*ones(Float64,Nx,Ny,Nz) + b*(Sq1+
   Sq2) + c*(Sq1+Sq2).^2
    restoring_force_1 = -(dt/gamma)*(q1.*(leading_order_terms
    + c1*(Sq1-3*Sq2).*(Sq1-Sq2)) - laplacian(q1,Nx,Ny,Nz,dx,
   dy,dz,gx,gz))
    restoring_force_2 = -(dt/gamma)*(q2.*(leading_order_terms
    - 2*c1*(Sq1-3*Sq2).*Sq1) - laplacian(q2,Nx,Ny,Nz,dx,dy,dz
   ,gx,gz))
    restoring_force = restoring_force_1 + restoring_force_2*
   im

    #New value of the field
    dq = restoring_force + langevin_source
    q_new = q + dq

    #Boundary conditions
    #We may change the boundary conditions for different runs
    q_new = ZPeriodicBC(q_new,Nx,Ny,Nz)

    #New mass term - if there is a quench
    a_new = a - dt*rho_q

    #We split the contributions to the force
    #(Same lines 40-50 of FIRST VERSION of the step function
   except for the change a0*eps -> a)

    return q_new, a_new, pot_forces_a1, pot_forces_a2,
   pot_forces_b1, pot_forces_b2, pot_forces_c1, pot_forces_c2
   , grad_forces_1, grad_forces_2, langevin_forces_1,
   langevin_forces_2, mod_forces, phase_forces,
   mod_forces_withoutlang, phase_forces_withoutlang
end
```

The only difference with the previous one is that, in this case, the quantity we modify to quench the system is the mass term, whereas the temperature

remains constant. This entails an effective change of the critical temperature, as it is explained in chapter 6.2. This version's quench rate, `rho_q`, is not in the same units as `r_q`, nor is `R_q`. To relate them, the functional dependence of a on T_c is required, as it is explained in section 6.2.

Chapter 10

Initial conditions

We can classify the initial conditions in two categories, depending on the phase at which the system starts. If the starting temperature is above the critical –in terms of reduced temperature, it amounts to $\epsilon > 0$–, the potential has one minimum at $q = (0, 0)$. Perturbations of different nature around this minimum define three different initial conditions: **no_perturbation**, **homogeneous_perturbation** and **noisy_perturbation**.

In the broken phase –**i.e.**, when the initial temperature is below the critical temperature, $\epsilon < 0$– there are more interesting configurations to start from. The potential six different minima, located at $\phi_n = (2n + 1)\pi/6$, provided $c' > 0$, whereas the point $q = (0, 0)$ is a maximum. Some initial conditions consists of perturbations around one or several minima (**homogeneous_pertrubation_one_well**, **noisy_perturbation_one_well**, **noisy_perturbation_six_wells**). Others perturb the maximum (**no_perturbation**, **noisy_perturbation_maximum**). Those are the initial conditions chosen to simulate a ultra-fast quench in section 7.2. We can also initialise the system with a configuration where a vortex is already formed (**vortex_xy**), or with a configuration which opposes

a vortex and an anti-vortex(**vortex_vs_antivortex**)[1]. The initial condition **domain_wall** reproduces a domain wall between two adjacent minima. Lastly, **modulus_perturbation_center** and **phase_perturbation_center** corresponds to initial conditions where the central point of the sample is perturbed –in the radial or angular direction, respectively– whilst the rest of the sample is set in one of the minima of the potential.

```
function init(a0,b,c,c1,gx,gz,gamma,eps,Tc,Nx,Ny,Nz,dx,dy,dz,
    initial_state,amplitude_perturbation,S_rng=
   Xoroshiro128Star())
    if eps > 0 # Symmetric phase
        #In the symmetric phase, we start from the equilibrim
    state an add a perturbation
        q_0 = zeros(ComplexF64,Nx,Ny,Nz) #Field matrix with
   every point at equilibrium
        if initial_state == "no_perturbation"
            #All the spatial points starts in the minimum of
   the potential q=(0,0)
            q_pert = copy(q_0)

        elseif initial_state == "homogeneous_perturbation"
            #Each point begins in the minimum of the
   potential q=(0,0) and then is displaced a certain amount,
   the same for every spatial point.
            q_pert = zeros(ComplexF64,Nx,Ny,Nz) .+ im*(
   amplitude_perturbation)

        elseif initial_state == "noisy_perturbation"
            #Each point starts in the minimum of the
   potential q=(0,0) and then is desplaced a certain amount,
   different for every spatial point.
            q_pert = copy(q_0)
            q_pert = amplitude_perturbation*((rand(S_rng,
   Float64,(Nx,Ny,Nz))*2 .-1)+im*(rand(S_rng,Float64,(Nx,Ny,
   Nz))*2 .-1))
        end
        return q_0 + q_pert
    end


    if eps < 0 #Broken phase
        Q_min = Q_0(a0,b,eps) #Minimum value of the modulus
```

[1]The profile of the radial component of the field in a vortex configuration is taken from [46].

```
of the field (provided c=0).
24          amplitude_perturbation = Q_min*0.05 #In the broken
    phase, the amplitude of the initial perturbation is a
    fraction (we chosse 0.05 as a default value, though a
    different value can be set) of the equilibrium value of
    the modulus of the field.
25
26          #Initial conditions which perturbates the field
    around a certain point of the potential.
27          if initial_state == "
    homogeneous_pertrubation_one_well"
28              #Each point begins in the same well (one of the
    six possible) and then is desplaced a certain amount, the
    same for every spatial point.
29              #Random choice of the well, the same for all
    points. If we want the well to lay on an axis (y-axis),
    set this value to pi/2
30              phi_min = rand(S_rng,0:5)*pi/3 + pi/6
31              q_0 = Q_min*cos(phi_min)*ones(Float64,(Nx,Ny,Nz))
     + Q_min*sin(phi_min)*ones(Float64,(Nx,Ny,Nz))*im
32              q_pert = amplitude_perturbation*((rand(S_rng,
    Float64,(Nx,Ny,Nz))*2 .-1)+im*(rand(S_rng,Float64,(Nx,Ny,
    Nz))*2 .-1))
33              q = q_0 + q_pert
34
35          elseif initial_state == "noisy_perturbation_one_well"
36              #Each point begins in the same well (one of the
    six possible) and then is desplaced a certain amount,
    different for each spatial point.
37              q = zeros(ComplexF64,(Nx,Ny,Nz))
38              #Random choice of the well, the same for all
    points. If we want the well to lay on an axis (y-axis),
    set this value to pi/2
39              phi_min = rand(S_rng,0:5)*pi/3 + pi/6
40              for i in 1:Nx, j in 1:Ny, k in 1:Nz
41                  q_x = Q_min*cos(phi_min) +
    amplitude_perturbation*(rand(S_rng)*2-1)
42                  q_y = Q_min*sin(phi_min) +
    amplitude_perturbation*(rand(S_rng)*2-1)
43                  q[i,j,k] =  q_x+ q_y*im
44              end
45
46          elseif initial_state == "noisy_perturbation_six_wells
    "
47              #Each point begins in different minima (one of
    the six possible) at random and then is desplaced a
    certain amount, different for every spatial point.
48              q = zeros(ComplexF64,(Nx,Ny,Nz))
49              for i in 1:Nx, j in 1:Ny, k in 1:Nz
```

```
50                  phi_min = rand(S_rng,0:5)*pi/3 + pi/6
51                  q_x = Q_min*cos(phi_min) +
    amplitude_perturbation*(rand(S_rng)*2-1)
52                  q_y = Q_min*sin(phi_min) +
    amplitude_perturbation*(rand(S_rng)*2-1)
53                  q[i,j,k] =  q_x+ q_y*im
54              end
55
56          elseif initial_state == "no_perturbation"
57              #Each point starts in the maxima q=(0,0) without
    any displacement.
58              q = zeros(ComplexF64,Nx,Ny,Nz)
59
60          elseif initial_state == "noisy_perturbation_maximum"
61              #Each point begins in the maximum q=(0,0) and
    then is desplaced a certain amount, different for every
    spatial point.
62              q = zeros(ComplexF64,(Nx,Ny,Nz))
63              for i in 1:Nx, j in 1:Ny, k in 1:Nz
64                  q[i,j,k] = amplitude_perturbation*((rand(
    S_rng,Float64,(Nx,Ny,Nz))*2 .-1)+im*(rand(S_rng,Float64,(
    Nx,Ny,Nz))*2 .-1))
65              end
66
67          #Initial conditions which reproduces different
    votices configurations
68          elseif initial_state == "vortex_xy"
69              #The initial configuration of the field in the
    space is that of a single vortex of fixed winding number
    in the plane xy, whose core is centered in the middle of
    the sample.
70              winding_number = 1 #A different winding number
    can be set.
71              q = zeros(ComplexF64,(Nx,Ny,Nz))
72              phi = [i*pi/3 + pi/6 for i in 0:(winding_number
    *6-1)] #Array of the six minima of the phase, provided c1
    >0.
73              epsilon_space = 1/(max(Nx,Ny)*10.0) #This small
    displacement is set to prevent the vortex-core from being
    a site of the grid
74              core_vortex_x, core_vortex_y = Nx/(2 +
    epsilon_space), Ny/(2 + epsilon_space) #Coordinates of the
     vortex core
75              xi = zeta(a0, b, c, c1, gx, gz, eps)[1][1] #Mean
    field value of the correlation length at the given
    temperare eps
76              for i in 1:Nx, j in 1:Ny, k in 1:Nz
77                  nx, ny = i-core_vortex_x, j-core_vortex_y #
    Coordinates with respect the core of the vortex
```

```
78                theta = atan(ny,nx) + pi #atan corresponds to
    a standard atan2 function
79                l = ceil(Int,winding_number * 6 * theta/(2*pi
   )) #ceil rounds to the upper integer
80                rr = sqrt((nx*dx)^2 + (ny*dy)^2)/xi #
   Normalized radial distance from the vortex core
81                q_x = Q_min*cos(phi[l])* (rr/sqrt(2+rr^2))
82                q_y = Q_min*sin(phi[l])* (rr/sqrt(2+rr^2))
83                q[i,j,k] = q_x + q_y*im
84            end
85
86        elseif initial_state == "vortex_vs_antivortex"
87            #We build a vortex in the xy-plane with a given
   winding number and far enough an antivortex whose winding
   number is equal as the vortex but with opposite sign.
88            q = zeros(ComplexF64,(Nx,Ny,Nz))
89            winding_number = 1 #A different winding number
   can be set.
90            distance_vortex_antivortex = Ny/2 #Distance
   between the cores of the vortex and the anti-vortex. Ca be
    set a different value.
91            eps_spatial = 1/(max(Nx,Ny)*10.0) #This small
   displacement is set to prevent the vortex-core from being
   a site of the grid
92            #Vortex
93            phi = [i*pi/3 + pi/6 for i in 0:(winding_number
   *6-1)] #Array of the six minima of the phase, provided c1
   >0.
94            #Coordinates of the vortex core
95            core_vortex_x = (Nx/(2 + eps_spatial))
96            core_vortex_y = Ny/(2 + eps_spatial) -
   distance_vortex_antivortex/2
97            #Mean field value of the correlation length at
   the given temperare eps
98            xi = zeta(a0, b, c, c1, gx, gz, eps)[1][1]
99            for i in 1:Nx, j in 1:floor(Int,Ny/2)
100               nx, ny = i-core_vortex_x, j-core_vortex_y #
   Coordinates with respect the core of the vortex
101               theta = atan(ny,nx) + pi #atan corresponds to
    a standard atan2 function
102               l = ceil(Int,winding_number*6 * theta/(2*pi))
    #ceil rounds to the upper integer
103               rr = sqrt((nx*dx)^2 + (ny*dy)^2)/xi #
   Normalized radial distance from the vortex core
104               q_x = Q_min*cos(phi[l])* (rr/sqrt(2+rr^2))
105               q_y = Q_min*sin(phi[l])* (rr/sqrt(2+rr^2))
106               q[i,j,k] = q_x + q_y*im
107           end
108           #Antivortex
```

```
109             phi = [i*pi/3 + pi/6 for i in (winding_number
    *6-1):-1:0] #Array of the six minima of the phase,
    provided c1>0. It is sorted in the opposite order as the
    phi array uset to generate the vortex
110             core_antivortex_x =  (Nx/(2 + eps_spatial))
111             core_antivortex_y = Ny/(2 + eps_spatial)  +
    distance_vortex_antivortex/2
112             for i in 1:Nx, j in ceil(Int,Ny/2):Ny
113                 nx, ny = i-core_antivortex_x, j-
    core_antivortex_y #Coordinates with respect the core of
    the anti-vortex
114                 theta = sc.arctan2(ny,nx) + sc.pi
115                 rr = sqrt((nx*dx)^2 + (ny*dy)^2)/xi #
    Normalized radial distance from the anti-vortex core
116                 q_x = Q_min*cos(phi[l])* (rr/sqrt(2+rr^2))
117                 q_y = Q_min*sin(phi[l])* (rr/sqrt(2+rr^2))
118                 q[i,j,k] = q_x + q_y*im
119             end
120
121         #Other initial conditions
122         elseif initial_state == "domain_wall"
123             #We split the xy-plane in two halfs. The field at
     each half takes the value of one of the minima of the
    potential. Those minima are adjacent, so a domain wall
    will form in the middle of the plane.
124             q = zeros(ComplexF64,(Nx,Ny,Nz))
125             for i in 1:Nx, j in 1:Ny, k in 1:Nz
126                 amplitude_perturbation = Q_min
127                 phi = (i<Nx/2) ? pi/2 : pi/6
128                 q[i,j,k] = amplitude_perturbation*(cos(phi)+
    im*sin(phi))
129             end
130
131         elseif initial_state == "modulus_perturbation_center"
132             #We se the field to be in one of the minima of
    the potential. Then, we perturbate only the modulus of the
     field at the central point
133             phi = pi/6
134             q = zeros(ComplexF64,(Nx,Ny,Nz)) .+ Q_min*(cos(
    phi)+im*sin(phi))
135             q[round(Int,Nx/2),round(Int,Ny/2),round(Int,Nz/2)
    ] = 0.0 #The central point is set at the maximum of the
    potential
136
137         elseif initial_state == "phase_perturbation_center"
138             #We se the field to be in one of the minima of
    the potential. Then, we perturbate only the phase of the
    field at the central point
139             phi = pi/6
```

```
            q = zeros(ComplexF64,(Nx,Ny,Nz)) .+ Q_min*(cos(
    phi)+im*sin(phi))
            q[round(Int,Nx/2),round(Int,Ny/2),round(Int,Nz/2)
    ] = Q_min*(cos(phi+pi/3)+im*sin(phi+pi/3)) #The central
    point is set in an adjacent minima
        end
        return q
    end
end
```

Notice that in this case, we have used the definition of the mass parameter most common in the literature –equation (6.2)– because it allows an easy way to tell at which phase the system is initialized.

Let us include a last initial condition which was used to compute the simulations in section 6.1, **restoring_symmetric_phase**. There, the first component starts in the minimum of the potential well, whilst the second starts at zero. With this election, the first component plays the role of the radial component, and the second one the role of the angular component. We are interested in seeing how the symmetric phase is recovered.

```
if initial_state == "restoring_symmetric_phase"
    # We start with the real part of the field in the bulk
    minimum and the imaginary part equal to zero
    q = zeros(ComplexF64,Nx,Ny,Nz)
    q_0 = (a0>0) ? sqrt(a0/b) : 0.0
    q = q .+ q_0_renormalized
    return q
end
```

Chapter 11

Observables

11.1 Counting vortices

Among all the observables, the number of topological defects is one of the most relevant. Indeed, it is necessary to test the predictions of the Kibble-Zurek mechanism. Also, it allows us to compare the outcome of different cooling mechanisms. As discussed in chapter 3, the study and characterization of the topological defects after a phase transition can be used to infer properties of the underlying theory.

To compute the number of defects is a hard task. Firstly, it is important to determine the time of measurement. In a second order phase transition, the displacement of the field to the vacuum of the potential is a smooth process. So it is the creation of topological defects. As a consequence, it is not easy to resolve the exact moment at which the vortex is already formed. In addition to this, the subsequent dynamics of the already formed vortices entails their annihilation by merging or escaping through the edges, and therefore the reduction of their number over time. A detailed discussion on how to deal with this issue can be found in chapter 7.

Let us focus in this section on the other main difficulty to perform a measurement of the number of vortices: the noisy data. By construction, our model introduces stochastic noise. It is necessary to model the thermal fluctuations and compel the system to leave the vacuum. The negative counterpart is that the output data from the simulations are noisy. In order to make a meaningful measurement, we must first handle this problem.

We present here two different methods to smooth the data and eliminate the noise. The first one is based in the standard binning method, which consist of replacing all data in an interval by its mean. In our case, we measure the number of vortices on a plane, namely the equatorial plane of the sample. Thus the intervals are two-dimensional patches. As input parameters, we must specify the radius of the patch and the number of times this method is going to be applied.

```
function smooth_binning(q,Nx,Ny,diameter_patch_mean=4,
    iterations=1,patch_indices=false)
     #We take a 2-dimensional matrix and smooth it by
    substituing the value of each point p for the mean value
    of a patch of radius R centered in p.
     R = round(Int,diameter_patch_mean/2)
     if patch_indices == false #This next lines are only
    computed the first iteration
         patch_indices = []
         for ii in -R:R, jj in -R:R
             (ii^2 + jj^2 <= R^2) && (push!(patch_indices,[ii,
    jj]))
         end
     end

     for it in 1:iterations
         q1,q2 = real(q),imag(q)
         #We create an empty array with the same dimensions as
     the field matrix
         q1_smooth = zeros(Nx,Ny)
         q2_smooth = copy(q1_smooth)
         #Bulk of the field matrix
         for i in R+1:Nx-R, j in R+1:Nx-R
             q1_smooth[i,j] = mean([q1[i+k[1],j+k[2]] for k in
     patch_indices])
             q2_smooth[i,j] = mean([q2[i+k[1],j+k[2]] for k in
```

```
    patch_indices])
        end
        #Next two "for"-loops runs over the edges of the field matrix
        for i in union(1:R,Nx-R+1:Nx), j in 1:Ny
            patch_indices_border = []
            for k in patch_indices
                i_aux,j_aux = i+k[1],j+k[2]
                ((1<=i_aux<=Nx) & (1<=j_aux<=Ny)) && push!(patch_indices_border,[i_aux,j_aux])
            end
            q1_smooth[i,j] = mean(q1[k[1],k[2]] for k in patch_indices_border)
            q2_smooth[i,j] = mean(q2[k[1],k[2]] for k in patch_indices_border)
        end
        for i in R+1:Nx-R, j in union(1:R,Ny-R+1:Ny)
            patch_indices_border = []
            for k in patch_indices
                i_aux,j_aux = i+k[1],j+k[2]
                ((1<=i_aux<=Nx) & (1<=j_aux<=Ny)) && push!(patch_indices_border,[i_aux,j_aux])
            end
            q1_smooth[i,j] = mean(q1[k[1],k[2]] for k in patch_indices_border)
            q2_smooth[i,j] = mean(q2[k[1],k[2]] for k in patch_indices_border)
        end
        #We substitute the original field matrix by the smoothed one
        q = q1_smooth + q2_smooth*im
    end
    return q,patch_indices
end
```

An alternative smoothing method consist of running some iterations of the program without considering noise terms nor cooling. In this case, it is the action of the restoring forces of the potential and gradient terms the ones which kill the noise. We must specify the number of runs without Langevin as an input parameter.

```
function smooth_no_langevin(q, a0, b, c, c1, gx, gz, gamma, eps, dt, Nx, Ny, Nz, dx, dy, dz, number_steps)
    #Smooths a 3-dimensional matrix by updating its state number_steps times without langevin terms. Then returns
```

```
    the equatorial plane

    for t in 1:number_steps
        q1,q2 = real(q),imag(q)

        #Dissipative force
        q1,q2 = real(q),imag(q)
        Sq1,Sq2 = q1.^2,q2.^2
        leading_order_terms = a0*eps*ones(Float64,Nx,Ny,Nz) + b*(Sq1+Sq2) + c*(Sq1+Sq2).^2
        restoring_force_1 = -(dt/gamma)*(q1.*(leading_order_terms + c1*(Sq1-3*Sq2).*(Sq1-Sq2)) - laplacian(q1,Nx,Ny,Nz,dx,dy,dz,gx,gz))
        restoring_force_2 = -(dt/gamma)*(q2.*(leading_order_terms - 2*c1*(Sq1-3*Sq2).*Sq1) - laplacian(q2,Nx,Ny,Nz,dx,dy,dz,gx,gz))
        restoring_force = restoring_force_1 + restoring_force_2*im

        #New value of the field
        dq = restoring_force
        q += dq

        #Boundary conditions
        #The boundary condition must be the same as the one employed in the main function
        q = ZeroFluxBC(q,Nx,Ny,Nz)
    end
    z0 = size(q)[3]/2 #Equatorial plane
    return q[:,:,trunc(Int,z0)]
end
```

Let us introduce the main function to count defects. It provides the number of defects on the equatorial plane of the sample at a given time. Also, it returns the total winding number. The algorithm is based on the integration of the phase of the field over a series of closed loops. It starts with a small closed loop centred at a random point of the sample, on which it measures the circulation of the phase. Then, the loop increases its size and the circulation is again computed. It proceeds recursively until the loop encloses the whole sample. Comparing the result of the circulation of phase of two consecutive loops, we are able to detect if a new vortex (or anitivortex)

has entered in the loop. Indeed, for every new vortex (antivortex) that gets into the loop, a 2π (-2π) factor is added to the circulation of the former (smaller) loop. Thus, we can estimate the total number of defects by counting the number of jumps of magnitude $|2\pi|$ in the series of phase circulations measured on the series of growing loops.

This method may underestimate the total number of defects if the new loop encloses at the same time a vortex and an antivortex, since then the leap in phase circulation may be $2\pi - 2\pi = 0$. However, if the grid is small enough, this possibility must be small. In any case, we compute several series of loops, starting from different points, and then take the statistical mean.

The function uses two alternative algorithms to grow the loops: the first algorithm, `"spiral"`, make the loops grow as spirals from a core, whilst the second algorithm, `"circle"`, make them grow as circles centred at an origin. This latter algorithm is simpler, but works worst than the former. The reason is that the chance of enclosing a vortex and an antivortex at the same time when computing a new loop is bigger, since the area between two subsequent loops is bigger.

```
function counting_defects(q, a0, b, c, c1, gx, gz, gamma, eps
    , dt, Nx, Ny, Nz, dx, dy, dz, boundary,
    diameter_patch_mean_binning=5, iterations_binning=1,
    patch_indices_binning=false, number_steps_no_Langevin=100,
     spiral_step=3, circle_step=3, version_algorithm="spiral",
     seed_cores0=false)
     #Counts the number of vortices by integrating the phase
    over a series of closed loops.
     #Includes two different algorithms: the first algorithm
    computes a serie of loops which grow from a core forming a
     spiral. The second algorithm make the loops grow as
    circles centered in an origin.
     #The function also returns the total winding number of
    the equatorial plane of the sample.

     #We prepare the two smooth 2d-matrices on which we will
    count defects
     q_binning_whole, patch_indices_binning =
    smooth_binning_2d(q[:,:,trunc(Int,size(q)[3]/2)],Nx,Ny,
```

```
diameter_patch_mean_binning,iterations_binning,
patch_indices_binning)
 q_no_langevin_whole = smooth_no_langevin(q, a0, b, c, c1,
 gx, gz, gamma, eps, dt, Nx, Ny, Nz, dx, dy, dz,
number_steps_no_Langevin)
 #We remove the border of the sample and focus on the
phase of the field
 border_remove = 1 #We remove the border since it only
accounts for boundary effects and has no real physical
meaning
 q_binning = angle.(q_binning_whole[1+border_remove:Nx-
border_remove,1+border_remove:Ny-border_remove])
 q_no_langevin = angle.(q_no_langevin_whole[1+
border_remove:Nx-border_remove,1+border_remove:Ny-
border_remove])
 Nx,Ny = Nx-2*border_remove, Ny-2*border_remove

 #Auxiliary function: Phase difference. It deals with the
change of leaf in the phase
 function Ph_diff(x0,xf)
     D_ph = xf-x0
     for i in range(1,stop=length(D_ph))
         if abs(D_ph[i])> pi
              D_ph[i] = (D_ph[i]<0) ?  D_ph[i]+2*pi : D_ph
[i]-2*pi
         end
     end
     return D_ph
 end

 #Cores of the loops
 #We use a random number generator with his own seed to
choose the random cores from which the loops grow
 seed_cores = (seed_cores0 == false) ?  rand(1:1000)  :
seed_cores0
 S_cores =  Xoroshiro128Star(seed_cores)
 #We select the initial points from which we are going to
grow our spirals
 core_spirals = [[1,1],[1,Ny],[Nx,1],[Nx,Ny],[trunc(Int,Nx
/2),trunc(Int,Ny/2)]] #The four corners plus the center
 #We add some random points
 number_random_cores = 1000
 for i in range(1,stop=number_random_cores)
    push!(core_spirals,[rand(S_cores,1:Nx),rand(S_cores,1:
Ny)])
 end

 #Algorithms
 if version_algorithm == "spiral"
```

```
40          #We set the arrays to count the number of defects for
     each smoothing method.
41          ndefects_binning, ndefects_no_langevin = [], []
42          #Also, we set an array to keep the value of the last
    circulation loop
43          wn_total_binning, wn_total_no_langevin = [], []
44          for cs in core_spirals
45              #Initial loop. Loops start in the southwest (SW)
    point and continue in counterclockwise order.
46              # (W,E), (S,N) are the x and y coordinates (
    respectively) of the most exterior points of the loop.
47              cs_x, cs_y = cs
48              if (cs_x != Nx) & (cs_y != Ny)
49                  W,S = cs_x, cs_y
50                  E,N = cs_x+1, cs_y+1
51              elseif (cs_x == Nx) & (cs_y != Ny)
52                  W,S = cs_x-1, cs_y
53                  E,N = cs_x, cs_y+1
54              elseif (cs_x != Nx) & (cs_y == Ny)
55                  W,S = cs_x, cs_y-1
56                  E,N = cs_x+1, cs_y
57              else
58                  W,S = cs_x-1, cs_y-1
59                  E,N = cs_x, cs_y
60              end
61              loop = [[W,S],[E,S],[E,N],[W,N],[W,S]]
62
63              #CIRCULATION OF THE PHASE ON THE FIRST LOOP
64              #Binning_2d
65              L = length(loop)
66              phi_0_binning = [q_binning[i[1],i[2]] for i in
    loop] #Array with the field phase at every site which
    belongs to the loop
67              phi_f_binning = copy(phi_0_binning)
68              phi_f_binning[1:L-1] = phi_0_binning[2:L] #Copy
    the phase at every point of the loop but displaced one
    index
69              phase_circulation_loop_binning = sum(Ph_diff(
    phi_0_binning,phi_f_binning))/(2*pi) #Sum of all the small
     phase differences around the loop
70              #We set an array to save the value of the
    integration of the phase for each loop in the series of
    closed loops
71              PH_CIRC_LOOPS_BINNING = [0.0]
72              push!(PH_CIRC_LOOPS_BINNING,
    phase_circulation_loop_binning)
73              #No_langevin
74              phi_0_no_langevin = [q_no_langevin[i[1],i[2]] for
     i in loop] #Array with the field phase at every site
```

```
which belongs to the loop
75          phi_f_no_langevin = copy(phi_0_no_langevin)
76          phi_f_no_langevin[1:L-1] = phi_0_no_langevin[2:L]
 #Copy the phase at every point of the loop but displaced
one index
77          phase_circulation_loop_no_langevin = sum(Ph_diff(
phi_0_no_langevin,phi_f_no_langevin))/(2*pi) #Sum of all
the small phase differences around the loop
78          #We set an array to save the value of the
integration of the phase for each loop in the series of
closed loops
79          PH_CIRC_LOOPS_NO_LANGEVIN = [0.0]
80          push!(PH_CIRC_LOOPS_NO_LANGEVIN,
phase_circulation_loop_no_langevin)
81
82          #SERIES OF LOOPS
83          spiral_branch = 0
84          spiral_spin = rand(S_cores,[1,-1]) #Some spirals
will grow counterclockwise (+1) and other clockwise(-1)
85          while (N-S) + (E-W) < (Nx+Ny)-2 #The maximum loop
 goes from [1,1] to [Nx,Ny]
86              spiral_direction = abs(spiral_branch%4)
87              if spiral_direction == 0 #The loop increases
including the next southern row
88                  spiral_branch += spiral_spin
89                  if S == 1 #If we have reached the bottom
edge of the sample, we skip this step
90                      continue
91                  elseif S <= spiral_step
92                      S = 1
93                  else
94                      S -= spiral_step
95                  end
96              elseif spiral_direction == 1 #The loop
increases including the next eastern column
97                  spiral_branch += spiral_spin
98                  if E == Nx #If we have reached the right
edge of the sample, we skip this step
99                      continue
100                 elseif E > Nx-spiral_step
101                     E = Nx
102                 else
103                     E += spiral_step
104                 end
105             elseif spiral_direction == 2 #The loop
increases including the next northern row
106                 spiral_branch += spiral_spin
107                 if N == Ny #If we have reached the top
edge of the sample, we skip this step
```

```
                        continue
                    elseif N > Ny-spiral_step
                        N = Ny
                    else
                        N +=spiral_step
                    end
                elseif spiral_direction == 3 #The loop
increases including the next western column
                    spiral_branch += spiral_spin
                    if W == 1 #If we have reached the left
edge of the sample, we skip this step
                        continue
                    elseif W <= spiral_step
                        W = 1
                    else
                        W -= spiral_step
                    end
                end

                #Loop
                loop = union([[i,S] for i in W:E], [[E,j] for
 j in S:N], [[k,N] for k in E:-1:W], [[W,l] for l in N:-1:
S], [[W,S]])
                L = length(loop)

                #Circulation loops
                #We proceed in the same way as with the
circulation of the first loop
                #Binning_2d
                phi_0_binning = [q_binning[i[1],i[2]] for i
in loop]
                phi_f_binning = copy(phi_0_binning)
                phi_f_binning[1:L-1] = phi_0_binning[2:L]
                phase_circulation_loop_binning = sum(Ph_diff(
phi_0_binning,phi_f_binning))/(2*pi)
                push!(PH_CIRC_LOOPS_BINNING,
phase_circulation_loop_binning)
                #No_langevin
                phi_0_no_langevin = [q_no_langevin[i[1],i[2]]
 for i in loop]
                phi_f_no_langevin = copy(phi_0_no_langevin)
                phi_f_no_langevin[1:L-1] = phi_0_no_langevin
[2:L]
                phase_circulation_loop_no_langevin = sum(
Ph_diff(phi_0_no_langevin,phi_f_no_langevin))/(2*pi)
                push!(PH_CIRC_LOOPS_NO_LANGEVIN,
phase_circulation_loop_no_langevin)
            end

```

```
145             #We consider now the arrays in capital letters.
    Each element of the array consist of the phase circulation
     around one loop. The first element accounts for the first
     loop. The subsequent elements accounts for the loops
    which have grown from this first loop. Eventually, the
    last element accounts for a loop which includes the whole
    sample.
146             #We compute the number of times the difference
    between the circulation along two consecutive loops in the
     series has changed sign
147             #Binning_2d
148             PH_CIRC_LOOPS_BINNING_0 = PH_CIRC_LOOPS_BINNING
149             PH_CIRC_LOOPS_BINNING_1 = copy(
    PH_CIRC_LOOPS_BINNING_0)
150             L_series_loops_binning = length(
    PH_CIRC_LOOPS_BINNING_0)
151             PH_CIRC_LOOPS_BINNING_1[1:L_series_loops_binning
    -1] = PH_CIRC_LOOPS_BINNING_0[2:L_series_loops_binning]
152             nbinning = sum(abs.(PH_CIRC_LOOPS_BINNING_1-
    PH_CIRC_LOOPS_BINNING_0))
153             push!(ndefects_binning,nbinning)
154             push!(wn_total_binning, pop!(
    PH_CIRC_LOOPS_BINNING))#This array records the circulation
     of the last loop
155             #No_langevin
156             PH_CIRC_LOOPS_NO_LANGEVIN_0 =
    PH_CIRC_LOOPS_NO_LANGEVIN
157             PH_CIRC_LOOPS_NO_LANGEVIN_1 = copy(
    PH_CIRC_LOOPS_NO_LANGEVIN_0)
158             L_series_loops_no_langevin = length(
    PH_CIRC_LOOPS_NO_LANGEVIN_0)
159             PH_CIRC_LOOPS_NO_LANGEVIN_1[1:
    L_series_loops_no_langevin-1] =
    PH_CIRC_LOOPS_NO_LANGEVIN_0[2:L_series_loops_no_langevin]
160             n_nolang = sum(abs.(PH_CIRC_LOOPS_NO_LANGEVIN_1-
    PH_CIRC_LOOPS_NO_LANGEVIN_0))
161             push!(ndefects_no_langevin,n_nolang)
162             push!(wn_total_no_langevin, pop!(
    PH_CIRC_LOOPS_NO_LANGEVIN))
163         end
164         #We compute the mean and standard deviation of the
    number of defects obtained from all the series which start
     at different cores
165         N_defects_binning = [mean(ndefects_binning),std(
    ndefects_binning)]
166         N_defects_no_langevin = [mean(ndefects_no_langevin),
    std(ndefects_no_langevin)]
167         #We set the total winding number of the sample as the
     value of the circulation fo the last loop of the series
```

```
168         WN_total_binning, WN_total_no_langevin = pop!(
    wn_total_binning), pop!(wn_total_no_langevin)
169         return N_defects_binning,N_defects_no_langevin,
    WN_total_binning, WN_total_no_langevin, q_binning_whole,
    q_no_langevin_whole, patch_indices_binning
170 
171     elseif version_algorithm == "circle" #Circles algorithm
172         #We set the arrays to count the number of defects for
     each smoothing method
173         ndefects_binning, ndefects_no_langevin = [], []
174         #Also, we set an array to keep the value of the last
    circulation loop
175         wn_total_binning, wn_total_no_langevin = [], []
176         for cs in core_spirals
177             #Initial loop. Loops start in the southwest (SW)
    point and continue in counterclockwise order.
178             # (W,E), (S,N) are the x and y coordinates
    respectively of the most exterior points of the loop.
179             cs_x, cs_y = cs
180             if (cs_x != Nx) & (cs_y != Ny)
181                 W,S = cs_x, cs_y
182                 E,N = cs_x+1, cs_y+1
183             elseif (cs_x == Nx) & (cs_y != Ny)
184                 W,S = cs_x-1, cs_y
185                 E,N = cs_x, cs_y+1
186             elseif (cs_x != Nx) & (cs_y == Ny)
187                 W,S = cs_x, cs_y-1
188                 E,N = cs_x+1, cs_y
189             else
190                 W,S = cs_x-1, cs_y-1
191                 E,N = cs_x, cs_y
192             end
193             loop = [[W,S],[E,S],[E,N],[W,N],[W,S]]
194 
195             #CIRCULATION OF THE PHASE ON THE FIRST LOOP
196             #Binning_2d
197             L = length(loop)
198             phi_0_binning = [q_binning[i[1],i[2]] for i in
    loop] #Array with the field phase at every site which
    belongs to the loop
199             phi_f_binning = copy(phi_0_binning)
200             phi_f_binning[1:L-1] = phi_0_binning[2:L] #Copy
    the phase at every point of the loop but displaced one
    index
201             phase_circulation_loop_binning = sum(Ph_diff(
    phi_0_binning,phi_f_binning))/(2*pi) #Sum of all the small
     phase differences around the loop
202             #We set an array to save the value of the
    integration of the phase for each loop in the series of
```

```
closed loops
203             PH_CIRC_LOOPS_BINNING = [0.0]
204             push!(PH_CIRC_LOOPS_BINNING,
phase_circulation_loop_binning)
205             #No_langevin
206             phi_0_no_langevin = [q_no_langevin[i[1],i[2]] for
 i in loop] #Array with the field phase at every site
which belongs to the loop
207             phi_f_no_langevin = copy(phi_0_no_langevin)
208             phi_f_no_langevin[1:L-1] = phi_0_no_langevin[2:L]
 #Copy the phase at every point of the loop but displaced
one index
209             phase_circulation_loop_no_langevin = sum(Ph_diff(
phi_0_no_langevin,phi_f_no_langevin))/(2*pi)#Sum of all
the small phase differences around the loop
210             #We set an array to save the value of the
integration of the phase for each loop in the series of
closed loops
211             PH_CIRC_LOOPS_NO_LANGEVIN = [0.0]
212             push!(PH_CIRC_LOOPS_NO_LANGEVIN,
phase_circulation_loop_no_langevin)
213
214             #SERIES OF LOOPS
215             while (N-S) + (E-W) < (Nx+Ny)-2 #The maximum loop
 goes from [1,1] to [Nx,Ny]
216                 S = (S > circle_step) ? S-circle_step : 1 #
Bottom
217                 E = (E < Nx-circle_step) ? E+circle_step : Nx
 #Right
218                 N = (N < Ny-circle_step) ? N+circle_step : Ny
 #Top
219                 W = (W > circle_step) ? W-circle_step : 1 #
Left
220
221                 #Loop
222                 loop = union([[i,S] for i in W:E], [[E,j] for
 j in S:N], [[k,N] for k in E:-1:W], [[W,l] for l in N:-1:
S], [[W,S]])
223                 L = length(loop)
224
225                 #Circulation loops
226                 #We proceed in the same way as with the
circulation of the first loop
227                 #Binning_2d
228                 phi_0_binning = [q_binning[i[1],i[2]] for i
in loop]
229                 phi_f_binning = copy(phi_0_binning)
230                 phi_f_binning[1:L-1] = phi_0_binning[2:L]
231                 phase_circulation_loop_binning = sum(Ph_diff(
```

```
phi_0_binning,phi_f_binning))/(2*pi)
232             push!(PH_CIRC_LOOPS_BINNING,
phase_circulation_loop_binning)
233             #No_langevin
234             phi_0_no_langevin = [q_no_langevin[i[1],i[2]]
 for i in loop]
235             phi_f_no_langevin = copy(phi_0_no_langevin)
236             phi_f_no_langevin[1:L-1] = phi_0_no_langevin
[2:L]
237             phase_circulation_loop_no_langevin = sum(
Ph_diff(phi_0_no_langevin,phi_f_no_langevin))/(2*pi)
238             push!(PH_CIRC_LOOPS_NO_LANGEVIN,
phase_circulation_loop_no_langevin)
239         end
240
241         #We consider now the arrays in capital letters.
Each element of the array consist of the phase circulation
 around one loop. The first element accounts for the first
 loop. The subsequent elements accounts for the loops
which have grown from this first loop. Eventually, the
last element accounts for a loop which includes the whole
sample.
242         #We compute the number of times the difference
between the circulation along two consecutive loops in the
 series has changed sign
243         #Binning_2d
244         PH_CIRC_LOOPS_BINNING_0 = PH_CIRC_LOOPS_BINNING
245         PH_CIRC_LOOPS_BINNING_1 = copy(
PH_CIRC_LOOPS_BINNING_0)
246         L_series_loops_binning = length(
PH_CIRC_LOOPS_BINNING_0)
247         PH_CIRC_LOOPS_BINNING_1[1:L_series_loops_binning
-1] = PH_CIRC_LOOPS_BINNING_0[2:L_series_loops_binning]
248         nbinning = sum(abs.(PH_CIRC_LOOPS_BINNING_1-
PH_CIRC_LOOPS_BINNING_0))
249         push!(ndefects_binning,nbinning)
250         push!(wn_total_binning,pop!(PH_CIRC_LOOPS_BINNING
)) #This array records the circulation of the last loop
251         #No_langevin
252         PH_CIRC_LOOPS_NO_LANGEVIN_0 =
PH_CIRC_LOOPS_NO_LANGEVIN
253         PH_CIRC_LOOPS_NO_LANGEVIN_1 = copy(
PH_CIRC_LOOPS_NO_LANGEVIN_0)
254         L_series_loops_no_langevin = length(
PH_CIRC_LOOPS_NO_LANGEVIN_0)
255         PH_CIRC_LOOPS_NO_LANGEVIN_1[1:
L_series_loops_no_langevin-1] =
PH_CIRC_LOOPS_NO_LANGEVIN_0[2:L_series_loops_no_langevin]
256         n_nolang = sum(abs.(PH_CIRC_LOOPS_NO_LANGEVIN_1-
```

```
    PH_CIRC_LOOPS_NO_LANGEVIN_0))
257             push!(ndefects_no_langevin,n_nolang)
258             push!(wn_total_no_langevin,pop!(
    PH_CIRC_LOOPS_NO_LANGEVIN))
259         end
260         #We compute the mean and standard deviation of the
    number of defects obtained from all the series which start
     at different cores
261         N_defects_binning = [mean(ndefects_binning),std(
    ndefects_binning)]
262         N_defects_no_langevin = [mean(ndefects_no_langevin),
    std(ndefects_no_langevin)]
263         #We set the total winding number of the sample as the
     value of the circulation fo the last loop of the series
264         WN_total_binning, WN_total_no_langevin = pop!(
    wn_total_binning), pop!(wn_total_no_langevin)
265         return N_defects_binning,N_defects_no_langevin,
    WN_total_binning, WN_total_no_langevin, q_binning_whole,
    q_no_langevin_whole, patch_indices_binning
266     end
267 end
```

Two final remarks about this function. The first one is that some of the parameters of this function must be chosen carefully as the final number of defects may be affected by them. In particular, `diameter_patch_mean` and `number_steps`, in the smoothing functions, and `spiral_step` and `circle_step` in the main function. In general, a previous calibration must be performed with the help of one known sample before using this function to measure a series of samples of similar nature.

The second remark is that this algorithm always provides a result, even in a configuration where there are no vortices –for instance, a configuration in the symmetric phase. Besides, measurements from same sample which have been smoothed by different methods are different if the configuration is random. However, it is observed that both values converge when vortices are formed. This constitutes a proof of the consistency of the function, but it also reveals its limitations: their results can only be trusted from the time when we are certain that vortices are formed, not before. Although the convergence

of results from different smoothing methods give us an approximate value of such a time, a more rigorous criterion must be used to determine it.

11.2 Correlation length. Power spectrum

This function are used to obtain the power spectrum of the square fluctuations of the field [64],

$$I(\mathbf{k}) = \lim_{L\to\infty} \frac{L^3}{(2\pi)^3} \langle \left[Q(\mathbf{k}) - \bar{Q}(\mathbf{k}) \right]^2 \rangle \tag{11.1}$$

We can use this spectrum to compute the correlation length of the fluctuations,

$$\xi = \frac{\int d\mathbf{k} \mathbf{k}^2 \, Re(I(\mathbf{k}))}{\int d\mathbf{k} \, Re(I(\mathbf{k}))}. \tag{11.2}$$

```
function power_spectrum(A, Nx, Nz, dx)
    #Computes the power spectrum of the fluctuations of the
   field
    k_values = fftfreq(Nx,2*pi/dx)
    k_values_z = fftfreq(Nz,2*pi/dx)
    k_mod2 = [i^2+j^2+k^2 for k in k_values_z for j in
   k_values for i in k_values] #for loops need to be defined
   in this order
    k_mod2_matrix = reshape(k_mod2,(Nx,Nx,Nz))

    delta_A = A .- mean(A)
    correlation_delta_A = zeros((Nx,Nx,Nz))
    for i in 0:Nx-1, j in 0:Nx-1, k in 0:Nz-1
        delta_A_displaced = zeros((Nx,Nx,Nz))
        delta_A_displaced[1:Nx-i,1:Nx-j,1:Nz-k] = delta_A[1+i
   :Nx,1+j:Nx,1+k:Nz]
        correlation_delta_A[i+1,j+1,k+1] = mean(delta_A.*
   delta_A_displaced) #Correlation of the fluctuations of the
    field
    end

    delta_A_fourier = fft(correlation_delta_A) #Fast Fourier
   Transform
    I_k = delta_A_fourier.*conj(delta_A_fourier) #Power
   spectrum

```

```
    #Correlation length is estimated through different estimators
    #k^2
    k_mod_matrix_A = k_mod2_matrix
    estimator_k2 = sum(real(I_k).*k_mod_matrix_A)/sum(real(I_k))
    #k^-2
    k_mod_matrix_B = k_mod2_matrix.^-1
    k_mod_matrix_B[1,1,1] = 0.0
    estimator_kminus2 = sum(real(I_k).*k_mod_matrix_B)/sum(real(I_k))
    #mod_k
    k_mod_matrix_C = sqrt.(k_mod2_matrix)
    estimator_modk = sum(real(I_k).*k_mod_matrix_C)/sum(real(I_k))

    return k_values, I_k, estimator_k2, estimator_kminus2, estimator_modk
end
```

11.3 Mean-field relaxation time and correlation length

This functions are used to compute the relaxation time and correlation length in the mean field regime of our model. The reason to include them is that they are used as auxiliary functions. Notice that it computes both the radial and the angular contributions in the broken phase. Formulas are derived in section 5.1.

```
#Returns the relaxation times obtained theoretically from the mean field.
function tau(a0,b,c1,gamma,eps)
    tau_q = zeros(Float32,length(eps))
    tau_6 = copy(tau_q)
    index = 1
    for i in eps
        if i<0
            tau_q[index] = gamma / (a0*abs(i))
            tau_6[index] = gamma / (3.0*abs(c1)) *(b/(a0*abs(i)))^2
        elseif i>0
```

```
            tau_q[index] = gamma / abs(a0*i)
        end
        index += 1
    end
    return tau_q,tau_6
end

#Returns the correlation length obtained theoretically from
   the mean field.
function zeta(a0,b,c,c1,gx,gz,eps)
    g_eff = (gz*gx^2)^(1/3)
    zeta_q = zeros(Float32,length(eps))
    zeta_6 = copy(zeta_q)
    index = 1
    for i in eps
        if i<0
            zeta_q[index] = sqrt(g_eff/(4*abs(a0*i)))
            zeta_6[index] = sqrt(g_eff/(3*abs(c1)))*b/(a0*abs
   (i))
        elseif i>0
            zeta_q[index] = sqrt(g_eff/abs(a0*i))
        end
        index += 1
    end
    return zeta_q,zeta_6
end
```

Chapter 12

Main function

Besides integrating the equation of motion from the initial conditions and computing and saving the relevant data, this function set and classify several time intervals during a quench. Specifically, it distinguishes four different time-intervals. The first interval takes into account the time that the system spends evolving before the quench starts. In this first interval, the temperature –or the mass term– remains fixed at some value above the critical temperature. This time is required to ensure that the system is thermalised before it starts cooling. Afterwards, the system begins to cool. The second time-interval spans from this moment to the point when the critical temperature is reached –*i.e.*, it covers the cooling in the symmetric phase. The third time-interval starts at the moment the temperature has passed through the critical temperature and finishes when the temperature gets to its final value –*i.e.*, the time the system spends cooling in the broken phase. Finally, we let the system evolve at the final temperature for some more time. This is the fourth and last time-interval.

```
#We set sample rates to save different observables
NDEFECTS_SAVE = 200; #Number of time steps between two
   consecutive measurements of the number of defects and
   other observables
```

```
PS_SAVE = 1000; #Number of time steps between two consecutive computations of the power spectrum
FIELD_SAVE = 500; #Number of time steps between two consecutive savings of the field.

function main_function(a0, b, c, c1, gx, gz, eps_0, eps_final, Tc, theta_0, gamma, r_q, time_steps, initial_state, boundary, dx, Nx, Nz, dt, seed0=false)
    #=Update the field q 'time_steps' times following the Langevin equation.
    --INPUTS--
    (a0,b,c,c1,gx,gz) are the parameters of the free energy.
    eps_0 is the initial reduced temperature (adimensional).
    eps_final is the final reduced temperature in a quench (adimensional).
    Tc is the critical temperature.
    theta_0 is the initial temperature (not reduced temperature!) of the langevin term. If theta="self_consistent", then is related with eps: Tc*(eps+1) and may vary with time if there is a quench. If theta does not relate with eps, then is a constant number.
    r_q is the quenching rate (in 1/[time])). If r_q = 0, it remains in the same temperature.
    gamma is the damping coefficient.
    'time_steps' is the number of times the equation is updated.
    'initial_state' indicates the initial setup of the mesh. If it is string type, we start from a certain initial conditions described in the function init. If it is a number (let's call it t0), we start the simulation from the final value of other simulation at time t=t0.
    'boundary' indicates the type of boundary conditions imposed on the system.
    (dx, Nx, Nz, dt) are used to define the space and time steps and also the size of the grid.
    seed0 is the seed for the random number generator.=#

    #We seed the program
    seed = (seed0 == false) ?  rand(1:1000)  : seed0
    S_rng =  Xoroshiro128Star(seed)

    #Space_step
    dy, dz = dx, dx

    #Grid dimensions
    Ny = Nx

    #Time array
```

```
33      t0::Int32 = (typeof(initial_state) == String) ? 0 :
    initial_state #Initial time from which we will choose a
    fixed time_steps value
34      time_steps::Int32 = time_steps
35      time = range(t0+1,stop=time_steps+t0)
36      if r_q != 0
37          #If the system quenches, we will also distinghish
    four different regimes
38          time_steps_cool_symmphase = round(Int,eps_0/(r_q*dt))
39          time_steps_cool = round(Int,(eps_0-eps_final)/(r_q*dt
    ))
40
41          t1::Int32 = 1000 #This time needs to be high enough
    to ensure that the system is thermalised
42          t2::Int32 = t1 + round(Int,time_steps_cool_symmphase)
43          t3::Int32 = t2 + round(Int,time_steps_cool)
44          t4::Int32 = time_steps
45
46          time_1 = range(1,stop=t1) #Cooling in the symmetric
    phase before the freezing
47          time_2 = range(t1+1,stop=t2) #Cooling in the
    symmetric phase while freezing
48          time_3 = range(t2+1,stop=t3) #Cooling in the broken
    phase while freezing
49          time_4 = range(t3+1,stop=t4) #Time spend in the
    broken phase at eps_final with no cooling
50      end
51
52      #Directory name
53      if typeof(initial_state) == String
54          directoryname = string("data/quench/a0=",a0,"_b=",b,"
    _c1=",c1,"_g=",gx,"_eps0=",eps_0,"_Tc=",Tc,"_theta0=",
    theta_0,"_rq=",r_q,"_gamma=",gamma,"_Nx=",Nx,"_Nz=",Nz,"
    _dx=",dx,"_dt=",dt,"_BC=",boundary,"_initial_state=",
    initial_state,"_time_steps=",time_steps,"_seed=",seed)
55      else
56          directoryname = string("data/quench/a0=",a0,"_b=",b,"
    _c1=",c1,"_g=",gx,"_eps0=",eps_0,"_Tc=",Tc,"_theta0=",
    theta_0,"_rq=",r_q,"_gamma=",gamma,"_Nx=",Nx,"_Nz=",Nz,"
    _dx=",dx,"_dt=",dt,"_BC=",boundary,"_initial_state=time",
    initial_state,"_time_steps=",time_steps,"_seed=",seed)
57      end
58      #Create a new directory if it is not created
59      ((directoryname in readdir("./")) == false) && mkdir("./"
    *directoryname)
60
61      #= We save the ratio between the space_step and the
    lowest correlation length at a given temperature, as well
    as the ratio between the total length of the sample (dx*Nx
```

```
) and the largest of the correlation lengths=#
 correlation_lengths = zeta(a0, b, c, c1, gx, gz, [eps_0])
 cl_min = (eps_0>0) ? correlation_lengths[1][1] : min(correlation_lengths[1],correlation_lengths[2])[1]
 cl_max = (eps_0>0) ? correlation_lengths[1][1] : max(correlation_lengths[1],correlation_lengths[2])[1]
 space_resolution_factor = cl_min/dx #How many space steps are required to get the lowest correlation length
 grid_factor, grid_factor_z = [Nx,Nz].*(dx/cl_max) #How many largest-correlation length fit into the sample
 writedlm(directoryname*"/0_spaceresolution_gridfactor.txt", [space_resolution_factor, grid_factor, grid_factor_z])

 #Initial_state
 if typeof(initial_state) == String
     q = init(a0,b,c,c1,gx,gz,gamma,eps,Tc,Nx,Ny,Nz,dx,dy,dz, initial_state,amplitude_perturbation,S_rng=Xoroshiro128Star())
 else
     #We define the recovering parameters as the same as the ones we are using in the new simulation.
     #However, we may change if there was need:
     recover_a0 ,recover_b ,recover_c1 ,recover_gx, recover_Tc, recover_gamma = a0, b, c1, gx, Tc, gamma
     recover_eps_0, recover_theta_0, recover_r_q = eps_0, theta_0, r_q
     recover_Nx, recover_Nz, recover_dx, recover_dt = Nx, Nz, dx, dt
     recover_boundary, recover_time_steps, recover_initial_state = boundary, time_steps, "no_perturbation" ########
     recover_seed, recover_t0, recover_eps = seed, t0, eps_0-dt*min(r_q*t0,ceil((eps_0-eps_final)/(dt)))

     #We rebuild the matrix of the field with an auxiliary function
     q = recover_q(recover_a0, recover_b, recover_c1, recover_gx, recover_eps_0, recover_Tc, recover_theta_0, recover_r_q, recover_gamma, recover_Nx, recover_Nz, recover_dx, recover_dt, recover_boundary, recover_initial_state, recover_time_steps, recover_seed, recover_t0, recover_eps)

     #We also need to update the random number calls before we go on with the simulation from the time we left
     eps_aux = (recover_initial_state == "instant_quench") ? abs(eps_0) : eps_0 #eps_sym if recover_initial_state == 'instant_quench' else eps_0
     recover_initial_state_aux = "no_perturbation"
```

```
87          q_init_aux_rd = init(a0,b,c,c1,gx,gz,gamma,eps_aux,Tc
    ,Nx,Ny,Nz,dx,dy,dz,space_resolution_factor,grid_factor,
    recover_initial_state_aux,S_rng)
88          for i in range(1,stop=trunc(Int,t0/5))
89              randn(S_rng,ComplexF64,(Nx,Ny,Nz,5))
90          end
91          randn(S_rng,ComplexF64,(Nx,Ny,Nz,t0%5))
92      end
93
94      #Arrays to record the number of defects and total winding
        number
95      TIME_DEFECTS = []
96      N_DEFECTS_FILTER, N_DEFECTS_FILTER_ERROR, TOTAL_WN_FILTER
        = [], [], []
97      N_DEFECTS_NO_LANG, N_DEFECTS_NO_LANG_ERROR,
    TOTAL_WN_NO_LANG = [], [], []
98
99      #Arrays to record the different force contributions
100     POT_A1, POT_A2, POT_B1, POT_B2, POT_C1, POT_C2, POT_1,
    POT_2, GRAD_1, GRAD_2, LANG_1, LANG_2, MOD_FORCES,
    MOD_FORCES_NOLANG, PHS_FORCES, PHS_FORCES_NOLANG =
    [],[],[],[],[],[],[],[],[],[],[],[],[],[],[]
101
102     #Arrays to record the modulus mean and std
103     MOD_MEAN, MOD_STD = [],[]
104
105     #Arrays to record the varianze of k for several
    observables: q1, q2, abs(q), phs(q), q
106     VAR_K_Q1, VAR_K_Q2, VAR_K_MODQ, VAR_K_PHSQ, VAR_K_Q = [],
        [], [], [], []
107     VAR_Q1, VAR_Q2, VAR_MODQ, VAR_PHSQ, VAR_Q = [], [], [],
    [], []
108
109     #We set the algorithm and the seed for the
    counting_defects function
110     version_algorithm = 1 #Spirals
111     seed_cores0 = 666 #Random choice
112
113     t_old_ndef, t_old_ps = 0, 0 #Label to erase old data
    files
114
115     if r_q == 0.0
116         #We do not include this case, since it is less
    interesting
117     else #Quench rate different from zero
118
119         #If it is a recovered simulation, we distinguish
    between four cases:
120         if 0 <= t0 < t1
```

```
            time_1 = range(t0+1,stop=t1)
            time_2, time_3, time_4 = time_2, time_3, time_4
        elseif t1 <= t0 < t2
            time_1 = []
            time_2 = range(t0+1,stop=t2)
            time_3, time_4 =  time_3, time_4
        elseif t2 <= t0 < t3
            time_1, time_2 = [], []
            time_3 = range(t0+1,stop=t3)
            time_4 = time_4
        elseif t3 <= t0 < t4
            time_1, time_2, time_3 = [], [], []
            time_4 = range(t0+1,stop=t4)
        end
        time_spend_cooling = min(t0,t3)

        #We change the name of eps_0, since now is a dynamic (non-static) variable:
        eps = eps_0 - dt*r_q*time_spend_cooling

        if length(time_1) != 0 #Cooling in the symmetric phase before the freezing.
            for t in time_1
                #Update equation
                q, eps, pot_forces_a1, pot_forces_a2, pot_forces_b1, pot_forces_b2, pot_forces_c1, pot_forces_c2, grad_forces_1, grad_forces_2, langevin_forces_1, langevin_forces_2, mod_forces, phase_forces, mod_forces_withoutlang, phase_forces_withoutlang = step(q, a0, b, c, c1, gx, gz, gamma, eps, Tc, theta_0, 0.0, dt, Nx, Ny, Nz, dx, dy, dz, boundary, S_rng)
                #Save data.
                if t%FIELD_SAVE == 0 ||  (t-t0) == 1.0
                    writedlm("./"*directoryname*"/order_parameter_real_part_time"*string(t)*"_eps"*string(round(eps,digits=3))*".txt",real(q))
                    writedlm("./"*directoryname*"/order_parameter_im_part_time"*string(t)*"_eps"*string(round(eps,digits=3))*".txt",imag(q))
                end

                #Computation of the power spectrum
                if (t-t0)%PS_SAVE == 0
                    #First component of the field
                    k_values,I_k,variance_k = power_spectrum(real(q), Nx, Nz, dx)
                    push!(VAR_K_Q1,variance_k)
                    push!(VAR_Q1,ifft(I_k)[1,1,1])
```

```
156                     #The power spectrum of other quantities
    are also computed
157
158                     #Save the data of the variance_k for all
    observables and remove the old ones
159                     writedlm("./"*directoryname*"/
    ps_q1_variance_k_time"*string(t)*".txt",VAR_K_Q1)
160                     if t_old_ps != 0
161                         rm("./"*directoryname*"/
    ps_wholefield_variance_k_time"*string(t_old_ps)*".txt")
162                     end
163                     t_old_ps = t
164                 end
165
166                 #Number of defects and winding number
167                 if (t-t0)%NDEFECTS_SAVE == 0
168                     N_defects_filter,N_defects_no_langevin,
    total_wn_filter, total_wn_no_langevin, q_filter_whole,
    q_no_langevin_whole, patch_indices_filter =
    counting_defects(q, a0, b, c, c1, gx, gz, gamma, eps, dt,
    Nx, Ny, Nz, dx, dy, dz, boundary,
    diameter_patch_mean_filter, iterations_filter,
    patch_indices_filter, number_steps_no_Langevin,
    spiral_step, circle_step, version_algorithm, seed_cores0)
169
170                     #Filter_2d
171                     push!(N_DEFECTS_FILTER,N_defects_filter
    [1])
172                     push!(N_DEFECTS_FILTER_ERROR,
    N_defects_filter[2])
173                     push!(TOTAL_WN_FILTER,total_wn_filter)
174                     #No_langevin
175                     push!(N_DEFECTS_NO_LANG,
    N_defects_no_langevin[1])
176                     push!(N_DEFECTS_NO_LANG_ERROR,
    N_defects_no_langevin[2])
177                     push!(TOTAL_WN_NO_LANG,
    total_wn_no_langevin)
178
179                     #Modulus mean and std
180                     push!(MOD_MEAN,mean(abs.(q)))
181                     push!(MOD_STD,std(abs.(q)))
182
183                     #Save the data of the number_vortices and
     total_winding_number and remove the old data files
184                 end
185             end
186         end
```

```
187         if length(time_2) != 0 #Cooling in the symmetric
    phase while freezing.
188             for t in time_2
189                 #Idem as time 1
190             end
191         end
192         if length(time_3) != 0 #Cooling in the broken phase
    while freezing.
193             for t in time_3
194                 #Idem as time 1
195                 end
196             end
197         end
198         if length(time_4) != 0 #Time spend in the broken
    phase at eps_broken_freeze with no cooling.
199             r_q = 0.0 #We stop the cooling
200             for t in time_4
201
202                 end
203             end
204         end
205         return q, eps
206     end
207 end
```

Comments and conclusions

In this work, we have performed numeric simulations to reproduce the process of vortex formation after a phase transition takes place. We focus on the case where a global symmetry is broken. Inspired by the structural phase transition which occurs in the hexagonal manganites, we present a theoretical model for a scalar field based on the Landau theory for phase transitions of the second kind. This model reproduces the most characteristic feature of the hexagonal manganites –the non-trivial discrete topology of the vacuum manifold $\mathbb{Z}_6$. We make use of the formalism developed by Langevin [51, 52] to include thermal fluctuations as an stochastic contribution of non-correlated noise in the equations of motion, which we formulate in the over-damped regime.

We discuss the problems which arises in the customary implementations of such formalism, namely the possible double-counting of thermal effects. Indeed, the coefficient of the mass term of the theory is forced to vary as an explicit function of the temperature. Simultaneously, thermal fluctuations are introduced in the dynamics through the already mentioned stochastic contributions. We give arguments to support that the change in the value of the coefficient of the mass term must be only caused by the effective renormalization induced by the thermal fluctuations –the Langevin noise. Thus, no external law must be imposed on the coefficient. We propose a

modification of the usual procedure to avoid this possible issue.

Furthermore, we present different scenarios to test the Kibble-Zurek mechanism. We have performed quenches in three different regimes: ultra-fast quenches; finite quenches varying the temperature of the Langevin term whilst maintaining constant the mass term; and finite quenches varying the bare value of the coefficient of the mass term whilst maintaining constant the noise temperature.

First, we consider the regime of ultra-fast quenches. This regime is achieved when the time that the system spends cooling is much shorter than any other relevant time scale of the problem –in particular, the time of vortex formation. This limit tries and reproduce the regime of experimental set-ups where it has been reported that the Kibble-Zurek prescription is reversed [38] –*i.e.*, faster quenches produce less defects. In our approach to this regime, the dynamics of the system is entirely caused by the final temperature of the system –therefore, independent on the quench rate. In this investigation, we conclude that the vortex formation process involves three distinguishable and complementary mechanisms. Namely, the diffusive dynamics of the order parameter in configuration space as a result of its coupling to the thermal bath; the local relaxation of its phase as a result of the tension forces between adjacent domains; and the global relaxation of the amplitude of the order parameter as it rolls down the effective potential. Each of these effects posses characteristic times, τ_d, τ_0, and τ_1, respectively. The primordial vortex network shows up at τ_0, whereas its consolidation takes place at τ_1. Hence, the spatial distribution of vortices is not determined by their core radius, but by the correlation length of the phase of the order parameter at τ_0, ξ_0. While the alternative choice of τ_1 as the characteristic time for this determination is also possible, it is less physical since then the inter-

twined dynamics of both the phase and the amplitude have an impact on the resulting topological structure. In fact, from a practical perspective, the unambiguous connection between the phase relaxation time and the density of primordial vortices is one of main results of our work. We find that the distance between the primordial vortices increases monotonically with the final temperature of the quench. We explain this behaviour as a result of the persistent thermal fluctuations of the order parameter throughout the transition. Moreover, τ_d as well as the intervals between the times τ_d, τ_0, and τ_1 increase for higher temperatures, which then causes an effective delay of the phase transition together with an increase on the average distance between vortices. In some sense, this can be seen as a sort of ancestor for some intrinsic deviations from the KZ scaling that have been predicted for slow quenches [65]. In the weak-anisotropy regime, once formed, vortices and antivortices annihilate at a rate inversely proportional to time. In turn, all these effects hinder the dissipation of energy, causing a delay in the accomplishment of the thermalization process. Including a six-fold anisotropy we find that, whereas the vortex formation process is unaffected, their annihilation rate slows down, signalling the impact of the $\mathbb{Z}_6$-anisotropy in the short-range vortex-antivortex interaction.

Next, we consider quenches at finite rates. We distinguish two different ways of perform quenches which are compatible with our way of simulating the thermal effects in our model. Though, both can be related if the functional dependence of the bare parameter with the critical temperature of the system is known –see equation (6.9). In one prescription, we decrease the temperature of the Langevin term while maintaining the rest of parameters unchanged. This is in contrast with the usual way to simulate quenches in the literature, which fix the temperature of the Langevin term to a constant free

parameter –*e.g.*, see [61]. In the second prescription, we fix the temperature of the Langevin term while varying the bare value of the coefficient of the mass term. The dynamics reproduced in this two scenarios differs from the quenches in the ultra-fast limit. This is due to the fact that the amplitude of the thermal fluctuations in this case is much larger than in the latter case. Nevertheless, the description of the different regimes during the process of vortices formation is still valid in the essence. In this case, we find that the number of vortices do follow a scaling law with respect the quench rates, as the mechanism of Kibble-Zurek suggests. Though, the scaling coefficients obtained from fitting the data are not in accordance with the mean-field prediction.

In the analysis of our simulations, we do not observe the phenomenology described in the Kibble-Zurek mechanism. Indeed, we do not detect the freezing of domains of correlated phase in a neighbourhood of the transition point, since the thermal fluctuations erase all memory of the system of its previous state during the symmetric phase. The scaling behaviour that we observe is due to causes different to causality and criticality in the transition point.

Lastly, we also present a detailed collection of all the code scripts used to performed this work. In the third part we comment how our model is implemented numerically. It is of special relevance the function used to count the number of vortices, described in section 11.1.

To conclude, let us summarise our findings and relate them with the objectives of our work:

- A new approach to include thermal fluctuations through a Langevin term is proposed. It avoids some of the problems of the customary prescriptions, such as a possible double-counting of thermal effects.

- The process of vortex formation involves three different regimes, each with a characteristic time. First, the order parameter diffuses around the origin due to thermal fluctuations. Second, the complex phase relaxes, leading to the formation of domains of homogeneous phase. Lastly, the modulus of the order parameter relaxes, causing the vortex consolidation.

- The freezing of domains of correlated phase in the symmetric phase predicted by the Kibble-Zurek argument is not detected. Criticality and causality are not the responsible of domain formation in our model.

- The phase relaxation time is the most suitable time to measure the density of primordial vortices. Before this time, no patches of homogeneous phase are formed, so no vortices can be properly defined.

- There exist important differences in the dynamics of the phase transition depending on how the quench is performed. Regardless, the former conclusions are valid in all instances.

Bibliography

[1] T. W. B. Kibble. Topology of cosmic domains and strings. *Journal of Physics A: Mathematical and General*, 9(8):1387, 1976.

[2] W. H. Zurek. Cosmological experiments in condensed matter systems. *Physics Reports*, 276(4):177 – 221, 1996.

[3] A. Rajantie. Formation of topological defects in gauge field theories. *International Journal of Modern Physics A*, 17(01):1–43, 2002.

[4] L. D. Landau and E. M. Lifshitz. *Course of Theoretical Physics*, volume 5. Pergmon Press, New York, 1980.

[5] V. L. Ginzburg. *Soviet Phys. Solid State*, 2:1824, 1960.

[6] N. Manton and P. Sutcliffe. *Topological solitons*. Cambridge University Press, New York, 2004.

[7] S. Coleman. *Aspects of symmetry: selected Erice lectures*. Cambridge University Press, Cambridge, 1988.

[8] R. Rajaraman. *Solitons and instantons*. North Holland Publishing Co., Amsterdam, 1982.

[9] T. W. B. Kibble. Some implications of a cosmological phase transition. *Physics Reports*, 67(1):183 – 199, 1980.

[10] W. H. Zurek. Cosmological experiments in superfluid helium? *Nature*, 317(6037):505–508, 1985.

[11] M. Donaire. Topological defects from first-order gauge theory phase transitions. *Journal of Physics A: Mathematical and General*, 39(48):15013, 2006.

[12] K. Pyka, J. Keller, H. L. Partner, R. Nigmatullin, T. Burgermeister, D. M. Meier, K. Kuhlmann, A. Retzker, M. B. Plenio, W. H. Zurek, A. del Campo, and T. E. Mehlstäubler. Topological defect formation and spontaneous symmetry breaking in ion coulomb crystals. *Nature Communications*, 4(1), August 2013.

[13] S. Ulm, J. Roßnagel, G. Jacob, C. Degünther, S. T. Dawkins, U. G. Poschinger, R. Nigmatullin, A. Retzker, M. B. Plenio, F. Schmidt-Kaler, and K. Singer. Observation of the kibble–zurek scaling law for defect formation in ion crystals. *Nature Communications*, 4(1), August 2013.

[14] C. N. Weiler, T. W. Neely, D. R. Scherer, A. S. Bradley, M. J. Davis, and B. P. Anderson. Spontaneous vortices in the formation of bose–einstein condensates. *Nature*, 455(7215):948–951, October 2008.

[15] D. R. Scherer, C. N. Weiler, T.W. Neely, and B.P. Anderson. Vortex formation by merging of multiple trapped bose-einstein condensates. *Physical Review Letters*, 98:110402, Mar 2007.

[16] G. Lamporesi, S. Donadello, S. Serafini, F. Dalfovo, and G. Ferrari. Spontaneous creation of kibble–zurek solitons in a bose–einstein condensate. *Nature Physics*, 9(10):656–660, September 2013.

[17] I. Chuang, R. Durrer, N. Turok, and B. Yurke. Cosmology in the laboratory: Defect dynamics in liquid crystals. *Science*, 251(4999):1336–1342, March 1991.

[18] A. Maniv, E. Polturak, and G. Koren. Observation of magnetic flux generated spontaneously during a rapid quench of superconducting films. *Physical Review Letters*, 91:197001, Nov 2003.

[19] K. G. Lagoudakis, F. Manni, B. Pietka, M. Wouters, T. C. H. Liew, V. Savona, A. V. Kavokin, R. André, and B. Deveaud-Plédran. Probing the dynamics of spontaneous quantum vortices in polariton superfluids. *Physical Review Letters*, 106:115301, Mar 2011.

[20] R. Carmi, E. Polturak, and G. Koren. Observation of spontaneous flux generation in a multi-josephson-junction loop. *Physical Review Letters*, 84:4966–4969, May 2000.

[21] V. M. H. Ruutu, V. B. Eltsov, A. J. Gill, T. W. B. Kibble, M. Krusius, Yu. G. Makhlin, B. Plaçais, G. E. Volovik, and W. Xu. Vortex formation in neutron-irradiated superfluid 3he as an analogue of cosmological defect formation. *Nature*, 382(6589):334–336, July 1996.

[22] C. Bäuerle, Y. M. Bunkov, S. N. Fisher, H. Godfrin, and G. R. Pickett. Laboratory simulation of cosmic string formation in the early Universe using superfluid ^{3}He. *Nature*, 382(6589):332–334, Jul 1996.

[23] O. V. Lounasmaa and E. Thuneberg. Vortices in rotating superfluid 3he. *Proceedings of the National Academy of Sciences*, 96(14):7760–7767, 1999.

[24] K. W. Madison, F. Chevy, W. Wohlleben, and J. Dalibard. Vortex formation in a stirred bose-einstein condensate. *Physical Review Letters*, 84:806–809, Jan 2000.

[25] M. J. Bowick, L. Chandar, E. A. Schiff, and A. M. Srivastava. The cosmological kibble mechanism in the laboratory: String formation in liquid crystals. *Science*, 263(5149):943–945, 1994.

[26] B. F. de Oliveira, P. P. Avelino, F. Moraes, and J. C. R. E. Oliveira. Nematic liquid crystal dynamics under applied electric fields. *Physical Review E*, 82:041707, Oct 2010.

[27] M. Hindmarsh and A. Rajantie. Defect formation and local gauge invariance. *Physical Review Letters*, 85:4660–4663, Nov 2000.

[28] M. Donaire, T. W. B. Kibble, and A. Rajantie. Spontaneous vortex formation on a superconducting film. *New Journal of Physics*, 9(5):148, 2007.

[29] J. C. R. E. Oliveira, C. J. A. P. Martins, and P. P. Avelino. Cosmological evolution of domain wall networks. *Physical Review D*, 71:083509, Apr 2005.

[30] A. Vilenkin and E. P. S. Shellard. *Cosmic strings and other topological defects*. Cambridge University Press, Cambridge, 2000.

[31] R. K. Bullough, P. M. Jack, P. W. Kitchenside, and R. Saunders. Solitons in laser physics. *Physica Scripta*, 20(3-4):364, 1979.

[32] P. C. Hendry, N. S. Lawson, R. A. M. Lee, P. V. E. McClintock, and C. D. H. Williams. Generation of defects in superfluid ^{4}He as an analogue of the formation of cosmic strings. *Nature*, 368(6469):315–317, Mar 1994.

[33] S. Donadello, S. Serafini, T. Bienaimé, F. Dalfovo, G. Lamporesi, and G. Ferrari. Creation and counting of defects in a temperature-quenched Bose-Einstein condensate. *Physical Review A*, 94(2):023628, Aug 2016.

[34] S. C. Chae, N. Lee, Y. Horibe, M. Tanimura, S. Mori, B. Gao, S. Carr, and S.-W. Cheong. Direct observation of the proliferation of ferroelectric loop domains and vortex-antivortex pairs. *Physical Review Letters*, 108:167603, Apr 2012.

[35] S. Z. Lin, X. Wang, Y. Kamiya, G. W. Chern, F. Fan, D. Fan, B. Casas, Y. Liu, V. Kiryukhin, W. H. Zurek, et al. Topological defects as relics of emergent continuous symmetry and higgs condensation of disorder in ferroelectrics. *Nature Physics*, 10(12):970–977, 2014.

[36] S. Deutschländer, P. Dillmann, G. Maret, and P. Keim. Kibble–zurek mechanism in colloidal monolayers. *PNAS*, 112(22):6925–6930, 2015.

[37] S. M. Griffin, M. Lilienblum, K. T. Delaney, Y. Kumagai, M. Fiebig, and N. A. Spaldin. Scaling behavior and beyond equilibrium in the hexagonal manganites. *Physical Review X*, 2:041022, Dec 2012.

[38] Q. N. Meier, M. Lilienblum, S. M. Griffin, K. Conder, E. Pomjakushina, Z. Yan, E. Bourret, D. Meier, F. Lichtenberg, E. K. H. Salje, N. A. Spaldin, M. Fiebig, and A. Cano. Global formation of topological defects in the multiferroic hexagonal manganites. *Physical Review X*, 7:041014, Oct 2017.

[39] A. Dutta, A. Rahmani, and A. del Campo. Anti-kibble-zurek behavior in crossing the quantum critical point of a thermally isolated system driven by a noisy control field. *Physical Review Letters*, 117:080402, Aug 2016.

[40] M. Gerster, B. Haggenmiller, F. Tschirsich, P. Silvi, and S. Montangero. Dynamical ginzburg criterion for the quantum-classical crossover of the kibble-zurek mechanism. *Physical Review B*, 100:024311, Jul 2019.

[41] T. W. B. Kibble and G. E. Volovik. On phase ordering behind the propagating front of a second-order transition. *Journal of Experimental and Theoretical Physics Letters*, 65(1):102–107, January 1997.

[42] J. Dziarmaga, P. Laguna, and W. H. Zurek. Symmetry breaking with a slant: Topological defects after an inhomogeneous quench. *Physical Review Letters*, 82:4749–4752, Jun 1999.

[43] A. del Campo, A. Retzker, and M. B. Plenio. The inhomogeneous kibble–zurek mechanism: vortex nucleation during bose–einstein condensation. *New Journal of Physics*, 13(8):083022, August 2011.

[44] A. del Campo, T. W. B Kibble, and W. H. Zurek. Causality and non-equilibrium second-order phase transitions in inhomogeneous systems. *Journal of Physics: Condensed Matter*, 25(40):404210, September 2013.

[45] A. del Campo and W. H. Zurek. Universality of phase transition dynamics: Topological defects from symmetry breaking. *Symmetry and Fundamental Physics: Tom Kibble at 80*, pages 31–87, 2014.

[46] M. E. Holtz, K. Shapovalov, J. A. Mundy, C. S. Chang, Z. Yan, E. Bourret, D. A. Muller, D. Meier, and A. Cano. Topological defects in hexagonal manganites: Inner structure and emergent electrostatics. *Nano Letters*, 17(10):5883–5890, 2017. PMID: 28872318.

[47] S. Artyukhin, K. T Delaney, N. A Spaldin, and M. Mostovoy. Landau theory of topological defects in multiferroic hexagonal manganites. *Nature materials*, 13(1):42–49, 2014.

[48] A. Cano. Hidden order in hexagonal $r\mathrm{Mno}_3$ multiferroics (r = Dy–lu, in, y, and sc). *Physical Review B*, 89:214107, Jun 2014.

[49] P. Laguna and W. H. Zurek. Critical dynamics of symmetry breaking: Quenches, dissipation, and cosmology. *Physical Review D*, 58:085021, Sep 1998.

[50] W. H. Zurek. Cosmic strings in laboratory superfluids and the topological remnants of other phase transitions. *Acta physica polonica. B*, 24(7):1301–1311, 1993.

[51] P. Langevin. On the theory of brownian motion. *Compt. Rendus*, 146:530–533, 1908.

[52] A. Schmid. Diamagnetic susceptibility at the transition to the superconducting state. *Physical Review*, 180(2):527, 1969.

[53] M. Karttunen, K. R. Elder, M. B. Tarlie, and M. Grant. Instabilities and resistance fluctuations in thin accelerated superconducting rings. *Physical Review E*, 66(2):026115, 2002.

[54] R. Kato, Y. Enomoto, and S. Maekawa. Effects of the surface boundary on the magnetization process in type-ii superconductors. *Physical Review B*, 47(13):8016, 1993.

[55] R. Kato, Y. Enomoto, and S. Maekawa. Simulation study of the mixed state in inhomogeneous superconductors. *Physica C: Superconductivity*, 227(3-4):387–394, 1994.

[56] P. C. Hohenberg and B. I. Halperin. Theory of dynamic critical phenomena. *Reviews of Modern Physics*, 49(3):435, 1977.

[57] G. D. Lythe. Domain formation in transitions with noise and a time-dependent bifurcation parameter. *Physical Review E*, 53:R4271–R4274, May 1996.

[58] M. Tello-Fraile, A. Cano, and M. Donaire. Topological thermalization via vortex formation in ultrafast quenches. *Physical Review E*, 101(5):052113, 2020.

[59] J. Berger. Ginzburg-landau equations with consistent langevin terms for nonuniform wires. *Physical Review B*, 75:184522, May 2007.

[60] I. E. Graboy, A. A. Bosak, O. Yu. Gorbenko, A. R. Kaul, C. Dubourdieu, J.-P. Sénateur, V. L. Svetchnikov, and H. W. Zandbergen. Hrem study of epitaxially stabilized hexagonal rare earth manganites. *Chemistry of Materials*, 15(13):2632–2637, 2003.

[61] P. Laguna and W. H. Zurek. Density of kinks after a quench: When symmetry breaks, how big are the pieces? *Physical Review Letters*, 78:2519–2522, Mar 1997.

[62] I. S. Aranson, N. B. Kopnin, and V. M. Vinokur. Nucleation of vortices by rapid thermal quench. *Physical Review Letters*, 83(13):2600, 1999.

[63] I. A. Sadovskyy, A. E. Koshelev, C. L. Phillips, D. A. Karpeyev, and A. Glatz. Stable large-scale solver for ginzburg–landau equations for superconductors. *Journal of Computational Physics*, 294:639–654, 2015.

[64] R. Kubo, M. Toda, and N. Hashitsume. *Statistical physics II: nonequilibrium statistical mechanics*, volume 31. Springer Science & Business Media, New York, 2012.

[65] G. Biroli, L. F. Cugliandolo, and A. Sicilia. Kibble-zurek mechanism and infinitely slow annealing through critical points. *Physical Review E*, 81:050101, May 2010.